AN ABSTRACT OF THE THESIS OF

Julie A. Huff for the degree of Master of Science in Water Resources Engineering presented on December 9, 2009.
Title: Monitoring River Restoration using Fiber Optic Temperature Measurements in a Modeling Framework.

Abstract approved:

John S. Selker

The Middle Fork of the John Day River (MFJD) in Northeastern Oregon contains important spawning grounds for spring Chinook and summer steelhead of the Columbia River Basin. In the summer of 2008 phase one of a river restoration project was completed which included the addition of engineered log jams (ELJs) and scour pools. The restoration focuses on increasing habitat diversity and decreasing peak summer temperatures which, perhaps, had been degraded due to anthropogenic activities such as dredge mining, cattle grazing, channelization and deforestation.

This study utilized Distributed Temperature Sensing (DTS) technology to measure the temperature the MFJD study site before and after restoration during the summer of 2008. The temperature data along with other physical and climatic data were modeled using a physically based stream temperature model which incorporated groundwater inflows and an average depth of hyporheic exchange over the entire study reach. The root mean square errors for the pre- and post-restoration model are 0.57°C and 0.47°C, respectively. An average depth of the thermal mass associated with hyporheic exchange was calculated within the model to be 11m for pre-

restoration and 1.6m for post-restoration. It is unclear as to whether the hyporheic exchange increased due to restoration or is an artifact of high flows during the pre-restoration period.

A statistical analysis was completed on the longitudinal temperature profiles of the MFJD to identify lengths of the river whose temperatures are different upstream and downstream. Groundwater inflow was defined as locations with cooler day time and night time temperatures than the surroundings whereas hyporheic discharge was defined as locations with cooler day time temperatures but warmer night time temperature than the surroundings. Statistically significant locations were highlighted for both pre- and post-restoration and equated to an average decrease in local temperature of 0.08°C pre-restoration and 1.18°C post-restoration. This equates to 0.004 m^3/s and 0.012 m^3/s of groundwater inflow for pre- and post-restoration, respectively. Again, these differences could be artifacts of high flows during pre-restoration and cannot conclusively be linked to the restoration efforts. However, the largest groundwater inflow (0.004 m^3/s) can be associated with one ELJ structure and its corresponding scour pool.

Monitoring River Restoration using Fiber Optic Temperature Measurements in a Modeling Framework

by
Julie A. Huff

A THESIS

submitted to

Oregon State University

in partial fulfillment of
the requirements for the
degree of

Master of Science

Presented December 9, 2009
Commencement June 2010

Master of Science thesis of Julie A. Huff presented on December 9, 2009.

APPROVED:

____

Major Professor, representing Water Resources Engineering

____

Director of the Water Resources Graduate Program

____

Dean of the Graduate School

I understand that my thesis will become part of the permanent collection of Oregon State University libraries. My signature below authorizes release of my thesis to any reader upon request.

____

Julie A. Huff, Author

ACKNOWLEDGEMENTS

I would like to thank my faculty advisor, John Selker, whom without I would have never experienced the beautiful Middle Fork of the John Day River. Throughout my time at OSU I have been in awe of the knowledge that John carries in every subject from hydrology to electrical engineering, he has quite an encyclopedia tucked up there. I am also very appreciative of John's excitement and motivation for research because for every meeting we had (which was too many to count) I came out giddy in anticipation to push further into my research.

I would like to thank my committee members, Dr. Desiree Tullos and Dr. Pat McDowell. Desiree has helped me 'think' like a river and Pat has opened my eyes to what lays beneath the water and vegetation of the John Day. Thank you for your support throughout the past two years.

This research would not have been possible without the help of Aida Arik and Kace Fujiwara. I am indebted to you for the many long hours of back braking work and dozens of setbacks we endured through the summer of 2008. Thank you for putting up with my snicker cravings, grocery outlet runs and early wake-up calls. I would like to thank everyone else who came to lend a hand on the Middle Fork of the John Day; Tristan, Travis, Mike, Yutaka, Maria, Jim, Chris, Jeff and Ryan. Nick was a huge help with all of my questions from Cygwin to vicarious calibrations. I would especially like to thank Travis, whom I would go to regularly with questions I was too embarrassed to ask anyone else – Thank you for being such a good friend and putting up with stupid questions.

The people I have meet have been truly inspiring and the friendships forever lasting. Never have I worked and played so hard with such passionate folk, they have been the best support a graduate student could ask for. The natural sciences at OSU are a magnet for wonderfully caring and gifted scientists whom I am proud to have worked side by side.

Lastly, I would like to thank my family. Without my twin brother, Chris, I would have never made it out to OSU – thank you for showing me the way. I'd also like to thank both my mother and father for all of the support they've given me throughout this journey and for letting go of their daughter to the west coast. Furthermore, I'd like to thank my new family, Ray and Sue, for opening their arms to a girl who has been stuck behind a computer for the last 6 months. And of course, I would have never made it this far without the encouragement of my loving husband Tristan. You have always been able to put a smile on my face.

TABLE OF CONTENTS

LIST OF FIGURES

LIST OF FIGURES (continued)

Figure Page

LIST OF FIGURES (continued)

Figure | Page

LIST OF TABLES

LIST OF TABLES (continued)

LIST OF TABLES (continued)

Table Page

Chapter 1: Introduction

Oregon waterways have been adversely affected since the settlement of westerners, by dams, dredge mining, logging, draining fields or filling in wetlands. In 2006 the Clean Water Act 303(d) list of impaired waters reached 1,397 within Oregon, continually increasing year after year (US EPA, 2006). The leading cause of impairment for the past ten years, affecting over 59% of impaired waters within Oregon, has been temperature (US EPA, 2006). With the development and publication of lists such as the 303(d), attention is brought to the condition of species that rely on healthy waters. In many cases, actions to improve watershed health, like conservation or river restoration, have followed. River restoration has become increasingly common throughout the United States and Oregon is second, behind Maryland, in density of restoration projects per river-kilometer (Bernhardt et al., 2005). From 1990-2004 Oregon averaged 65.31 restoration projects per 1000 river-kilometers (Bernhardt et al., 2005). This was made possible by the expenditure of $80 million a year in Oregon on river protection, recovery and restoration (Taylor, 2007). In 1998 the State of Oregon designated an agency, Oregon Watershed Enhancement Board (OWEB), to focus on maintaining and improving watershed health by funding statewide projects. In addition to funding restoration projects, OWEB has selected seven watersheds throughout the state to take part in the Intensively Monitored Watershed program (IMW) (Pacific Northwest Aquatic Monitoring Partnership, 2005). The Middle Fork of the John Day River (MFJD) was selected as an IMW because of the multitude of restoration projects occurring within the MFJD basin.

This IMW study took place on the Forrest property in the upper MFJD basin, where Chinook salmon runs have been steadily decreasing in the MFJD, thought to be largely due to the historical impacts of dredge mining, logging and ditching from the early 1900's (Beschta and Ripple, 2005). The property is owned by the Confederated Tribes of the Warm Springs Reservation (CTWS) and in the summer of 2008 underwent phase one of the restoration plan. There are many parties invested in the restoration projects occurring on the MFJD and they are all curious, is the restoration effective?

Restoration Monitoring

Monitoring of river restoration plays a critical role in the advancement of the restoration field. The most valuable knowledge is gained when monitoring objectives address **why** a characteristic has changed in addition to **if** a characteristic has changed. This includes studying projects that have both failed and succeeded. Effectiveness monitoring is the only way to quantify a positive or negative ecological effect due to restoration (Independent Scientific Advisory Board, 2003; Palmer et al., 2005). Furthermore, previous monitoring results can give insight as to what restoration practice is best suited for the specific site. For example, installing engineered log jams or constructing pools and side channels both protect juvenile salmonids from high flows but monitoring results will help to choose a practice well suited for the site

(Independent Scientific Advisory Board, 2003; Lacey and Millar, 2004). In addition, when a project fails, the monitoring may tell why the project failed, providing a lesson for future designs (Lacey and Millar, 2004; McDonald et al., 2007). As Palmer et al. (2005) states, the importance of monitoring lies in which criteria the restoration is measured by and not simply whether monitoring is completed. Furthermore, the monitoring data can be used as a basis for adaptive management of the restoration site continually improving the project's effectiveness (McDonald et al., 2007; Wohl et al., 2005).

A broad range of tools and methods can be used to carry out restoration monitoring. A simple and inexpensive thermometer can be used effectively to obtain point temperature measurements in a stream (Johnson, 2003) while a complex and expensive forward looking infrared (FLIR) image can address spatial variability (Torgersen et al., 2001; Loheide II and Gorelick, 2006); both methods are acceptable. Determining the most effective strategy for monitoring is becoming increasingly difficult (Palmer et al., 2005). For example, on a small budget monitoring can incorporate point measurements such as temperature loggers, automated water samplers, and stage height recorders. While monitoring of a highly studied restoration site, like an IMW, could include high resolution data such as distributed temperature sensing (DTS), FLIR or LiDAR (Tyler et al., 2009; Selker et al., 2006a; Selker et al., 2006b). The limiting factor for most monitoring projects is a financial constraint (McDonald et al., 2007). Beyond field measurements, monitoring can incorporate a numerical model of the river to use for comparison in subsequent years (Independent

Scientific Advisory Board, 2003) or to run what-if scenarios for future restoration. Modeling will give insight into which processes are dominant in the system and may reveal otherwise hidden processes.

Stream Temperature Modeling

Restoration monitoring can focus on flora, fauna and physical characteristics such as riparian vegetation, salmonid locations, local hydraulics or temperature. This thesis will focus solely on temperature monitoring in keeping with the objectives of the restoration. In the last 20 years the scientific community has developed many diverse stream temperature models (Sinokrot and Stefan, 1993; Bartholow, 1999; Runkel et al. 2003; Boyd and Kasper, 2004; Cox and Bolte, 2007; Allen et al., 2007; Westhoff et al., 2007). The majority of the models present deterministic physically-based representations of the processes that directly influence stream temperature (M. C. Westhoff et al., 2007; Johnson, 2003). There are many advantages to the use of deterministic temperature models as opposed to empirical models. First, the potential impacts of various restoration options can be evaluated directly based on their design characteristics. Further, the model can efficiently be adapted to different river locations. On the other hand, empirical models express temperature through site specific, calibrated coefficients rather than through the major processes. While this can allow for prediction of how the current stream would respond to changed environmental context, it is not possible to simulate “what if” scenarios to evaluate potential restoration efforts.

The basis of the deterministic model relies on mathematical equations that relate energy and mass transport to the change in temperature. According to Caissie (2007), the four factors influencing water temperature are: atmospheric conditions, topography, stream discharge, and the streambed interactions (conduction, hyporheic exchange and groundwater inflow). Atmospheric conditions are the dominant controls on energy delivery affecting water temperature, and are usually the basis for many energy budgets within deterministic models. Few models incorporate groundwater and hyporheic flows (streambed factors) into the mass and energy balance (Loheide II and Gorelick, 2006; Runkel et al., 2003) because determination of these parameters is time intensive and may require tracer tests to obtain accurate values. Groundwater inflow is water from below the surface, typically at a depth where the temperature is close to the average annual air temperature (Anderson, 2005), and originates from hillslopes and meadows rather than from the channel itself. During the warm summer months, groundwater generally cools the surface water throughout the diurnal cycle. Hyporheic exchange is the process of surface water entering the subsurface, then remerging downstream, generally with a different chemical and temperature signature. Similar to groundwater, hyporheic exchange in general will cool peak temperatures during the day but, unlike groundwater, hyporheic will in general warm the lower temperatures seen at night since residence times are typically hours and days, rather than the seasons or years typical of groundwater (Arrigoni et al., 2008; Bencala, 2005; Findlay, 1995; Harvey and Wagner, 2000; Runkel et al., 2003; Wondzell, 2006). Hyporheic exchange therefore creates a dampening effect on the diurnal temperature amplitude without a net offset in temperature. Both of these groundwater interactions can create cool thermal refugia during peak daily temperatures (Torgersen et al., 1999).

Stream temperature is the primary pollutant in the waterways of Oregon and directly affects the health of salmonids (McCullough, 1999). When temperatures rise to between 17.8°C and 22°C cold water fish species experience a decrease in metabolic energy for feeding, spawning and growth, in addition the strength of the immune system decreases. This temperature range, slightly higher than normal but causing a decrease in the functioning of cold water fish is called the sub-lethal limit. The next stage of heat induced illness is the incipient lethal limit, when temperatures range from 22°C to 25°C. Fish will die from a decrease in function of the respiratory and circulatory system within hours to days of exposure to these temperatures. Above 25°C cold water fish species will die essentially immediately due to the denaturing of enzyme systems within the body, this is referred to as the instantaneous lethal limit (Boyd and Kasper, 2004; Brett, 1956, 1952). Increasing temperatures have devastating effects on the salmon population and it is crucial for their survival to reverse some of the anthropogenic activities that have increased temperature (McCullough, 1999).

To successfully decrease the temperature of a stream it is important to know the driving processes of temperature change. A simple energy balance of the stream and its physical surroundings can be written as:

$$\Phi_{stream} = \Phi_{radiation} + \Phi_{longwave} + \Phi_{conduction} + \Phi_{latent} + \Phi_{sensible}$$

Where Φ_{stream} is the heat flux of the stream, $\Phi_{radiation}$ is the solar radiation, $\Phi_{longwave}$ is the net-longwave radiation, $\Phi_{conduction}$ is the heat flux due to the conduction between the water and streambed, Φ_{latent} is the heat flux due to evaporation and $\Phi_{sensible}$ is the heat flux from convection between the air and water interface (Boyd and Kasper, 2004). The energy budget of a stream is complex. Atmospheric conditions change quickly both spatially and temporally, requiring measurements to be taken near the water's edge (Roth et al., 2010 In Press; Westhoff et al., 2007). The quantification of groundwater being gained or lost within a reach or the amount of hyporheic water being exchanged, not included in simple energy budgets, require a tracer (Caissie, 2006). Due to this complex energy budget the deterministic stream temperature models incorporate a range of processes.

SSTEMP was created by the USGS and uses a basic energy balance that does not allow for dynamic inputs, but the energy flux from lateral inflows is included in SSTEMP, whether they are tributaries or groundwater (Bartholow, 1999). SSTEMP is good for basic modeling and what-if scenarios, but lacks the temporal resolution required to predict effects on critical daily maximum stream temperatures by outputting only daily, weekly or monthly mean temperatures.

When coarse-scale modeling is necessary, the BasinTemp model allows for large area assessment with very minimal inputs. This keeps the cost and time of the required field measurements to a minimum, while allowing evaluation of which processes are dominant at the basin scale. The main objective of this model is to describe how much additional vegetative shading is needed to meet temperature requirements for TMDLs (Allen et al., 2007).

A very popular model, Heat Source, incorporates atmospheric conditions, vegetative shading and physical stream characteristics, while allowing inclusion of dynamic atmospheric and tributary data (Boyd and Kasper, 2004). Heat Source is a model that works well both at a reach scale and a larger basin scale due to the detailed energy budget. To achieve this Heat Source requires fine scale spatial resolution of input data which is time intensive (http://www.heatsource.info). An important limitation of this model is the neglect of groundwater inputs and hyporheic exchange to the energy balance.

Westhoff et al. (2007) produced a temperature model based on the Heat Source mass and energy balance equations which goes on to incorporate effects of groundwater inflows. Although the model includes groundwater, it does not identify spatially where the groundwater is entering the system, nor does the model quantify the flow of incoming groundwater. The model also allows dynamic atmospheric conditions both temporally and spatially which incorporates microclimates at the reach scale. A limitation to this model is the lack of heat flux due to hyporheic exchange.

Identifying the hyporheic zone within a river reach is a complex task that has to date required the use of tracers to determine flow and location (Wondzell, 2006). This is challenging primarily because the amount of flow that is entering and leaving the stream water within the hyporheic zone is small compared to the discharge of the stream itself, and further there is the potential for difficult to distinguish interaction of groundwater-surface water (Bencala, 2005). A popular conceptual model for hyporheic exchange is transient storage: the temporary storage of surface water within the stream bed and slower velocity surface water. This is the basis for the one-dimensional OTIS model used for solute transport (Runkel, 1998). The physically-based OTIS model assumes the major processes in the main channel are advection and dispersion moving downstream. In addition, the concentration of the storage zone is only affected by the main channel and not the upstream or downstream storage zones (Runkel, 1998). Building on the OTIS model is the two-dimensional Transient Storage Model which allows for continual solute exchange downstream (Bencala, 2005). Although these two models allow for quantification of hyporheic flows, they are used at a fine spatial scale and typically for solute transport rather than heat transport. Furthermore, transport models like these have not been incorporated into a larger reach-scale temperature model.

The temperature monitoring of the restoration in this project will include a modified Westhoff model to fulfill the IMW requirements. The Westhoff model was chosen for several reasons. First, the model includes a very detailed energy balance. Second, the model is written in Matlab code and can readily be modified to include new processes. Lastly, the model already incorporates lateral inflow whether from groundwater or a tributary. The main modification we made to the Westhoff model is the addition of a hyporheic exchange term. The hyporheic flow is quantified by using a simplified energy balance that Collier (2008) used on the Walla Walla River which accounts for hyporheic flow in terms of a volume of thermal mass below the streambed; the theory will be expanded upon in the subsequent chapters.

In addition to the modeling efforts a statistical analysis will be done on the DTS temperature data to identify areas of groundwater and hyporheic exchange. Similar to the work of Arrigoni et al (2008), a statistical analysis will compare the temperature signals found within the temperature profile. Groundwater inflows can be identified as areas where the maximum and minimum temperatures are lower relative to the rest of the river. Hyporheic flows are identified as areas of the river where the maximum temperature is lower and the minimum temperature is higher than the rest of the river. The use of DTS and this statistical method will give insight into where groundwater and hyporheic exchange occur in the river without the rigorous task of modeling the study site.

Goals and Objectives

The objective of this thesis is to accurately model the stream temperature of the restoration reach within the Forrest Conservation Area on the MFJD. An accurate model will be of great importance in determining what type of temperature effects occurred due to the current restoration. In addition, the model can be used for what-if scenarios to determine when lethal limits of temperature are reached for the Chinook and Steelhead runs. The specific goals and deliverables are:

- Use a deterministic stream temperature model coupled with DTS data to locate any changes in temperature due to restoration, both reach and run scale (Chapter 2)
- Add a supplemental section in the model to identify locations of hyporheic exchange and quantify the amount of hyporheic exchange in terms of thermal mass (Chapter 2)
- Use the DTS temperature measurements without a model to identify groundwater inputs and hyporheic exchange locations (Chapter 3)
- Use the DTS temperature measurements without a model to quantify the amount of groundwater gained in the Forrest reach (Chapter 3)
- Compare the two methods of locating zones of hyporheic exchange (Chapter 4)

Chapter 2: Application of a Physically Based Stream Temperature Model for Monitoring of River Restoration

Introduction

Stream temperature is an important part of a healthy river ecosystem and has been modeled extensively in the past two decades (Runkel 1998; Bartholow 1999; Evans et al., 1998; Fernald et al., 2001; Gooseff et al. 2003; Boyd and Kasper 2004; Loheide II and Gorelick 2006; Cox and Bolte 2007; Allen et al. 2007; Westhoff et al. 2007; Kasahara and Hill 2008; Kulongoski and Izbicki 2008). Much of the recent increase in studies focused on stream temperature in the Pacific Northwest can be attributed to the negative impacts of high temperatures on salmonids (Brett, 1956). The Pacific Northwest relies on salmon both as a commodity harvested by commercial fisheries and as a symbol and sustenance to local Native American tribes. Dam construction in the Columbia River basin started in the late 1800's and subsequently decreased the amount of suitable salmonid river habitat by half (Smith, 1998). Moreover, the effects are magnified because the majority of lost habitat was in the cooler headwaters (Smith, 1998; McCullough, 1999). To improve and maintain salmon habitat throughout Oregon, over $80 million a year are spent on recovering or protecting the health of Oregon waterways (Taylor, 2007). This includes river restoration to improve habitat complexity, allow fish passage, enhance riparian vegetation and decrease daily maximum temperatures. Effectiveness monitoring of restoration projects is key to understanding the outcome of the project and assisting in adaptive management (Palmer et al., 2005; Independent Scientific Advisory Board, 2003). A useful monitoring strategy employs a deterministic stream temperature model, which is based on the driving factors of temperature. With this strategy, the pre-restoration processes are identified and quantified and a change in the magnitude of processes due to restoration is identifiable.

The majority of the stream temperature models available are deterministic and based on simple energy budgets (Caissie, 2006; Poole and Berman, 2001). They include the processes that directly influence temperature such as solar radiation, stream bed conduction, evaporation and convection but also include indirect factors such as vegetative shading and cloud cover (Poole and Berman, 2001; Boyd and Kasper, 2004; Cox and Bolte, 2007; Westhoff et al., 2007). Deterministic models are made for different scales, with the majority at the reach and basin scale and only a few at the meander bend scale. Unfortunately, even with such a broad base of models there is still a dearth of models that incorporate heat flux due to groundwater inputs and hyporheic exchange (Caissie, 2006). Groundwater and hyporheic flows are important components controlling stream temperature, particularly during summertime periods of low flows. Groundwater inflows are typically colder than the stream water during the summer, thus decreasing the river's daily maximum, minimum and mean temperatures. Hyporheic zones act differently than groundwater inflows due to a lagged diel cycle; hyporheic exchange shrinks the daily temperature amplitude by decreasing the daily maximum and increasing the daily minimum temperature (providing an averaging mechanism for temperature). Most often groundwater interactions (both groundwater inflows and hyporheic exchange) do not significantly change the overall mean reach temperatures, but do create pockets of cool thermal refugia that are important for cold water fish and can reduce peak temperatures (Torgersen et al., 1999; Fernald et al., 2006).

Hyporheic exchange models typically operate at very fine scales because they require high resolution data spatially and temporally. Furthermore, most hyporheic models focus solely on hyporheic processes and are not part of a larger stream temperature model (Runkel, 1998; Gooseff et al., 2003). Loheide II and Gorelick, (2006) successfully used a combination of forward looking infrared (FLIR) temperature data, temperature loggers and a modified Heat Source model which incorporates groundwater inflow and hyporheic exchange. Upon closer examination, it can be seen that the modified Heat Source model did not model groundwater and hyporheic processes; rather, it used both the spatial distribution and flow as calibration parameters that were varied manually until a best-fit was found.

The driving forces of groundwater inflows and hyporheic exchange at a reach scale are preferential flow paths, topography of the streambed, underlying geology, channel geomorphology and stream depth, velocity, and hydraulic conductivity (Runkel et al., 2003). Modeling groundwater interactions at a reach scale is difficult because measuring the heterogeneity of the driving factors, mentioned above, is a time intensive, methodologically uncertain task (e.g., requiring complex geophysical analyses).

Hyporheic zone models are usually empirical and have relied on tracer tests to describe the movement of surface and subsurface water (Bencala and Walters, 1983;

Wondzell and Swanson, 1996). Empirical models use simple relationships between characteristics, such as temperature and flow, which do not attempt to describe the underlying physical processes. Many studies in recent years have empirically modeled hyporheic and groundwater activity using measurements from buried temperature probes or minipiezometers installed within the stream subsurface (Silliman and Booth, 1993; Baxter et al., 2003; Conant, 2004; Neilson et al., 2009). However, modeling hyporheic discharge and groundwater activity deterministically is possible with an intensive field and analysis campaign; such as was done on the Umatilla River by Poole et al. (2008).

Heat as a tracer to examine groundwater-surface water interactions is growing in popularity (Conant, 2004; Anderson, 2005; Arrigoni et al., 2008). There are many benefits to using heat as a tracer. For one, heat is conservative therefore a tracer test can always be performed because heat exchange is continuous between water and the surroundings. Also, temperature measurements are inexpensive to perform, as there are no costs for the tracer (using natural fluctuations) and measurement devices are cheap and easily accessible. On the downside, energy and mass transfer of a river system interacting with groundwater is very complex and requires considerable climatic, geologic and geographic data to close the energy budget. This can become quite expensive depending on the equipment and personnel needs. Finally, the background ‘concentration’ of heat changes diurnally and is difficult to control, except in those situations where mixing occurs with either ice or snow.

Westhoff Model Theory

A stream energy budget must include heat flux arising from advection, convection, radiation and conduction (Boyd and Kasper, 2004; Evans et al., 1998; Westhoff et al., 2007). The modified deterministic Westhoff model that will be used in this study incorporates all four modes of energy flux in the terms of solar radiation, longwave radiation, streambed conduction, latent heat, sensible heat and lateral inflow from either tributaries or groundwater inflows. The model is based on a fully mixed reservoir theory (where the system is modeled as a series of fully mixed reservoirs). Below is an abbreviated explanation of the equations used in the stream temperature model; for a comprehensive justification of the model equations see Westhoff et al. (2007).

Net solar radiation results from a combination of direct and diffuse radiation, with the former being influenced by shadows.

$$\Phi_{solar} = (1 - Df) \cdot (\Phi_{direct} + \Phi_{diffuse}) \qquad \text{(eq. 2.1)}$$

Where Φ_{direct} is the direct solar radiation (W/m^2) accounting for shadow effect, $\Phi_{diffuse}$ is the diffuse solar radiation (W/m^2) and Df is the fraction of solar radiation (-) which reaches the stream bed. Solar radiation was measured at the study site and these data are assumed to accurately portray cloudiness within the data. Therefore, for this study direct radiation was calculated without a cloud shadow variable.

Net longwave radiation is a combination of atmospheric longwave radiation, back radiation and land cover radiation. Atmospheric longwave radiation is the longwave radiation emitted from the atmosphere onto the water and is calculated using the Stefan-Boltzman law.

$$\Phi_{atm} = 0.96 \cdot \varepsilon_{atm} \cdot \sigma_{sb} \cdot (T_{air} + 273.2)^4 \qquad \text{(eq. 2.2)}$$

where Φ_{atm} is the atmospheric longwave radiation (W/m^2), ε_{atm} is the emissivity of the atmosphere (-), σ_{sb} is the Stefan-Boltzman constant (W/m^2 °C^4) and T_{air} is the air temperature (°C). Unlike Westhoff et al. (2007), the emissivity of the atmosphere was calculated using Brutsaert's equation (2005) for clear skies, with a standard error of 20-25 W/m^2 for cloudy conditions (eq. 2.3).

$$\varepsilon_{atm} = a\left(\frac{e_a}{T_{air}}\right)^b \qquad \text{(eq. 2.3)}$$

Where e_a is the vapor pressure of air (hPa), a and b are empirical constants with values of 1.24 and 1/7, respectively. The emissivity equation cited by Westhoff et al. (2007) is in Dutch which makes the equation difficult to use, therefore, Brutsaert's emissivity equation was used.

Back radiation is the radiation emitted from the water into the atmosphere and is also computed using the Stefan-Boltzman law.

$$\Phi_{back} = -0.96 \cdot \sigma_{sb} \cdot (T_{air} + 273.2)^4 \qquad \text{(eq. 2.4)}$$

Land cover longwave radiation is the longwave radiation emitted by the riparian vegetation onto the water and has a positive relationship with increasing vegetation density.

$$\Phi_{landcover} = 0.96 \cdot (1 - VTS) \cdot 0.96 \cdot \sigma_{sb} \cdot (T_{air} + 273.2)^4 \qquad \text{(eq. 2.5)}$$

where VTS is the "view to sky coefficient". When there is 100% riparian vegetation covering the stream VTS is 0.

Streambed conduction is the heat flux due to the temperature difference between the water column and the streambed material. It is assumed that there are two layers of streambed material, a deeper layer that does not fluctuate in temperature and is consistent with the groundwater temperature and a shallower layer that has a diel temperature fluctuation altered by the surrounding heat fluxes.

$$\Phi_{net} = \Phi_{solar} \cdot \frac{D_f}{1-D_f} - \Phi_{conduction} + \Phi_{alluv\_cond} \qquad \text{(eq. 2.6)}$$

$$\Phi_{conduction} = -K_{soil} \cdot \frac{T-T_{soil}}{d_{soil}} \qquad \text{(eq. 2.7)}$$

$$\Phi_{alluv\_cond} = -K_{soil} \cdot \frac{T_{soil} - T_{alluvium}}{d_{soil}} \qquad \text{(eq. 2.8)}$$

where T is the water temperature (°C), K_{soil} is the volumetric weighted thermal conductivity (J/m s °C) of the soil, T_{soil} and d_{soil} are the temperature (°C) and depth of soil (m) and $T_{alluvium}$ is the temperature of the deeper alluvium (°C). These equations are valid with the assumption that the stream bed is saturated and that $T_{alluvium}$ is equal to the groundwater temperature.

The energy transfer due to evaporation is called latent heat flux. The Penman equations for open water are used to quantify the heat flux.

$$\Phi_{evaporation} = -\rho_w L_e E \qquad \text{(eq. 2.9)}$$

$$L_e = 1000(2501.4 + T) \qquad \text{(eq. 2.10)}$$

$$E = \frac{s \cdot \Phi_r}{\rho_w \cdot L_e \cdot (s+\gamma)} + \frac{c_{air} \cdot \rho_{air} \cdot (e_s - e_a)}{\rho_w \cdot L_e \cdot r_a \cdot (s+\gamma)} \qquad \text{(eq. 2.11)}$$

where L_e is the latent heat of evaporation (J/kg), E is the Penman open water evaporation rate (m/s), ρ_w is the density of water (kg/m^3), Φ_r is the net (solar and longwave) radiation (W/m^2), s is the saturated vapor pressure curve slope at a given air temperature (kPa/°C), γ is the psychrometric constant (kPa/°C), r_a is the aerodynamic resistance (s/m) and c_{air} and ρ_{air} are the specific heat capacity and density of air.

The heat exchange between air and water surface due to a temperature difference is sensible heat.

$$\Phi_{sensible} = B_r \cdot \Phi_{evaporation} \quad \text{(eq. 2.12)}$$

$$B_r = 6.1 \cdot 10^{-4} \cdot P_A \cdot \frac{T - T_{air}}{e_s^w - e_a^w} \quad \text{(eq. 2.13)}$$

where B_r is the Bowen Ratio (-), P_A is the adiabatic atmospheric pressure (kPa), e_s^w and e_a^w are the saturated and actual vapor pressure (kPa) at the water-air boundary.

Lateral inflow, whether by groundwater inflows or tributaries, is included in the model by adding an additional energy term into the energy balance of the specific "reservoir". Thus the additional term which only includes the energy flux due to lateral inflow is:

$$\frac{dT}{dt} = \frac{Q_L \cdot (T_L - T)}{V} \quad \text{(eq. 2.14)}$$

where Q_L and T_L are the flow (m^3/s) and temperature (°C) of the lateral inflow and V is the volume of the reservoir (m^3).

Hyporheic Exchange Component Theory

Hyporheic exchange was not included in the original Westhoff model. The "HyZo" module described here does not try to determine the particular length of hyporheic flow paths but rather calculates how much hyporheic exchange occurs in terms of a thermal mass. This representation will lump all heat flux due to hyporheic exchange together for a certain length of stream taken to act as an average exchange per length. The main assumption is that the terms of the Westhoff model capture all other energy fluxes within the system and that the discrepancy seen between simulated and observed is due solely to hyporheic exchange. To make this an accurate assumption, the model is calibrated prior to the addition of HyZo, such that the only error can be attributed to measurement error. The equations used for HyZo are from the work of Collier (2008) and are based on an energy budget around the control volume or "reservoir" of water. This energy budget is similar to the Westhoff model, with the following terms: the energy gained from the incoming water, the energy lost due to the outgoing water, the energy gained from incoming groundwater or tributaries, the lumped energy term for radiation, streambed conduction, latent heat and sensible heat, the stored energy of the reservoir and sediment volumes, and the energy term due to hyporheic exchange. However, temperature effects due to streambed conduction act similarly to those of hyporheic exchange, therefore the hyporheic energy term may include an otherwise underestimated streambed conduction. This model has two assumptions – that there is no loss of groundwater and that flow is steady-state – which negate the need for other energy flux terms.

Based on the law of conservation of mass and energy, the rate of the stored energy term is equal to the total outgoing energy subtracted from the total incoming energy (eq. 2.15).

$$E_c = E_i + E_{gw} + E_l - E_o \qquad \text{(eq. 2.15)}$$

where E_c is the rate of change of stored energy (J/s), E_i is the incoming water energy (J/s), E_{gw} is the incoming groundwater energy (J/s), E_l is the lumped energy term (J/s) and E_o is the outgoing water energy (J/s).

All of the terms are computed from either the inputs or outputs of the Westhoff model and follow the same spatial resolution. The incoming water energy is computed by using the temperature and flow at the upstream point of entry into the reservoir (eq. 2.16).

$$E_i = C_{vw} \cdot T_u \cdot Q_u \qquad \text{(eq. 2.16)}$$

where C_{vw} is the volumetric heat capacity of water (J/°C m^3), and T_u and Q_u are the temperature (°C) and flow (m^3/s), respectively, of the upstream point of entry into the reservoir.

The incoming groundwater energy is calculated using the temperature of groundwater and the quantity entering the reservoir (eq. 2.17). The quantity and locations of groundwater input for the study site are calculated in Chapter 3. Groundwater inflows are typically diffuse rather than discrete and range in length from 2m to 100m.

$$E_{gw} = C_{vw} \cdot T_{gw} \cdot Q_{gw} \qquad \text{(eq. 2.17)}$$

where T_{gw} and Q_{gw} are the temperature (°C) and flow (m^3/s), respectively, of the groundwater entering the reservoir.

The lumped energy term is the sum of net radiation, latent heat flux and sensible heat flux from the calibrated Westhoff model multiplied by the surface area of the reservoir (eq. 2.18).

$$E_l = L \cdot R \qquad \text{(eq. 2.18)}$$

where L is the lumped energy term (J/s m^2) and R is the surface area of the reservoir (m^2).

The energy flux due to the outgoing water is calculated the same way as the incoming water (eq. 2.19).

$$E_o = C_{vw} \cdot T_o \cdot Q_o \qquad \text{(eq. 2.19)}$$

where T_o and Q_o are the temperature (°C) and flow (m^3/s), respectively, of the downstream point of departure from the reservoir.

If the reservoir is assumed to be the entire study reach (~1800m) we can find the average depth of hyporheic exchange by dividing the reservoir volume into its separate parts. Of the three terms in the rate of change of stored energy equation - stored energy of the reservoir volume, sediment volume, and hyporheic exchange - only the hyporheic exchange component is unknown. By then combining these energy terms with the volumetric heat capacities of both the water and sediment, C_{vw} and C_{vs}, and the porosity of the streambed, η, we can calculate the average volume of hyporheic exchange within the reservoir. The depth then can easily be calculated by dividing the volume of hyporheic exchange by the surface area of the streambed. We assume that the surface area of the streambed and river are the same and that hyporheic exchange occurs only below the streambed. Both of these assumptions are valid when the river is wide and shallow, which is an accurate depiction of the MFJD. The calculations for the stored energy term of the reservoir are:

$$E_c = \left(\frac{dT}{dt}\right) C_r \cdot V_r \qquad \text{(eq. 2.20)}$$

Integrated as:

$$\int dT = \frac{E_c}{C_r \cdot V_r} \int dt \qquad \text{(eq. 2.21)}$$

Resulting in:

$$\Delta T = \frac{E_c}{C_r \cdot V_r} \cdot \Delta t \qquad \text{(eq. 2.22)}$$

where C_r and V_r are the volumetric heat capacity of the reservoir (J/m^3°C) and volume of the reservoir (m^3), respectively. Separating the reservoir terms to include the surface water, hyporheic water and sediment, we can express the reservoir as:

$$C_r \cdot V_r = C_{vw} (V_w + \eta \cdot V_h) + C_{vs} \cdot (1 - \eta) \cdot V_h \qquad \text{(eq. 2.23)}$$

(eq. 2.23) can be substituted into (eq. 2.22) to get:

$$\Delta T = \frac{E_c}{C_{vw} (V_w + \eta \cdot V_h) + C_{vs} \cdot (1 - \eta) \cdot V_h} \cdot \Delta t \qquad \text{(eq. 2.24)}$$

(eq. 2.24) can be rewritten to express the volume of hyporheic exchange as:

$$V_h = \frac{\frac{\Delta t \cdot E_c}{\Delta T} - C_{vw} V_w}{\eta \cdot C_{vw} + (1 - \eta) \cdot C_{vs}} \qquad \text{(eq. 2.25)}$$

The volume of hyporheic exchange can be used to determine the average depth of hyporheic, D_h (m), across the entire river when it is assumed to be constant for the entire length and width of the river. The volume of thermal mass associated with hyporheic exchange is expected to be mainly constant on a daily scale but vary moderately at a seasonal scale.

$$D_h = \frac{V_h}{R} \qquad \text{(eq. 2.26)}$$

where R is the surface area of the streambed (m^2), assumed to be the same as the surface area of the river. The thermal mass associated with hyporheic exchange is then added to the Westhoff model for the validation of post-restoration data and the pre-restoration data.

Distributed Temperature Sensing

Distributed temperature sensing (DTS) technology was used in this study to capture a high resolution representation of the MFJD's temperature profile which is used for boundary conditions of the Westhoff Model. DTS technology has improved temperature sampling resolution in both time and space with resolutions as fine as 30 seconds and 1 meter for lengths up to ten km. Until the DTS was extended from oil and gas exploration to ecological systems, FLIR was the only stream temperature measurement instrumentation capable of such high resolution data (Torgersen et al., 2001). Although FLIR gives extremely high spatial resolution, it is typically only a snapshot in time and not continuous. Both FLIR and DTS allow insights into the spatial variability of stream temperatures but with DTS temperature fluctuations can be examined continually in time. For example, hyporheic flows can be distinguished from groundwater inflows by examining the temperature characteristics during the day and night (Collier, 2008).

In the last 5 years DTS and fiber optic technology have been implemented in a wide range of ecological systems. In 2006, the work of Selker et al. made a significant impact on temperature instrumentation by exploring the possibilities of the DTS in small headwater streams, on the lake bed of Lake Geneva, at the air-snow interface of a glacier and at the air-water interface of lakes. Since then, fiber optics and DTS have been used to characterize cold-air drainage in valleys (J. S. Selker et al., 2008), the soil moisture of agricultural fields and groundwater flow through wetlands (Lowry et al., 2007), as well as to help understand snow hydrology (Tyler et al., 2009) and the changes experienced by stream temperature due to global climate change (T. R Roth et al., 2008).

The technology that allows for the acquisition of such high resolution data relies on the Raman-backscatter theory of light. When a pulse of light is sent down a fiber optic cable part of the incident light is sent backwards due to scattering of the light when it comes in contact with the optical atoms. Two types of backscatter occur: Rayleigh-backscatter, which scatters the light at the same frequency of the incident light pulse, and Raman-backscatter, which scatters the light at a frequency just above and below the incident light pulse. The Raman backscattering that is at a wavelength greater than the incident spectrum is called Stokes scattering and is temperature independent. The Raman backscatter which gains energy and therefore is at a lower wavelength is called Anti-Stokes scattering and is temperature dependent. For the

DTS to calculate temperature a pulse of light is sent down the fiber optic cable at a given wavelength and the DTS records the time and wavelength of the backscatter. From the ratio of Stokes to Anti-Stokes, a temperature can be calculated, and the location of this temperature can be calculated by the time it takes for the backscatter to reach the DTS. This temperature point is then averaged at the given spatial scale (typically 1m) and temporal scale (30s-1hr) along the entire cable (Selker et al., 2006b).

Methods

Site Description

The 520 km John Day River is the second longest unregulated river in the US, only a few miles shorter than the Yellowstone. The Middle Fork of the John Day is situated within Grant County in northeastern Oregon which tends to have hot dry summers and cold wet winters (Figure 2.1). At an elevation of over 1200m and receiving a mere 63 cm of rain a year, the MFJD provides spawning grounds to many spring Chinook salmon and summer steelhead. Unfortunately in the hot summer of 2007 over 120 salmon (about half of those present) died due to water temperatures above the instantaneous lethal limit (25 °C). Temperatures within the MFJD are high, perhaps due to anthropogenic activities occurring in the past two centuries. Gold was first discovered in the region during the 1860’s, which left the MFJD river channel and floodplain dredged and sluiced. Around the time gold mining ended in the early

1900's, a small railroad was built through the entire valley. At different locations throughout the valley, the railroad company restrained the river from meandering. This left the river channelized between the railroad grade and County Road 20. Throughout these two distinct time periods, heavy grazing was occurring on the floodplains while deforestation was occurring in the valleys and hills (Beschta and Ripple, 2005). Today, the MFJD is still riddled with dredge tailings, channelization, bank stabilizing structures and grazing.

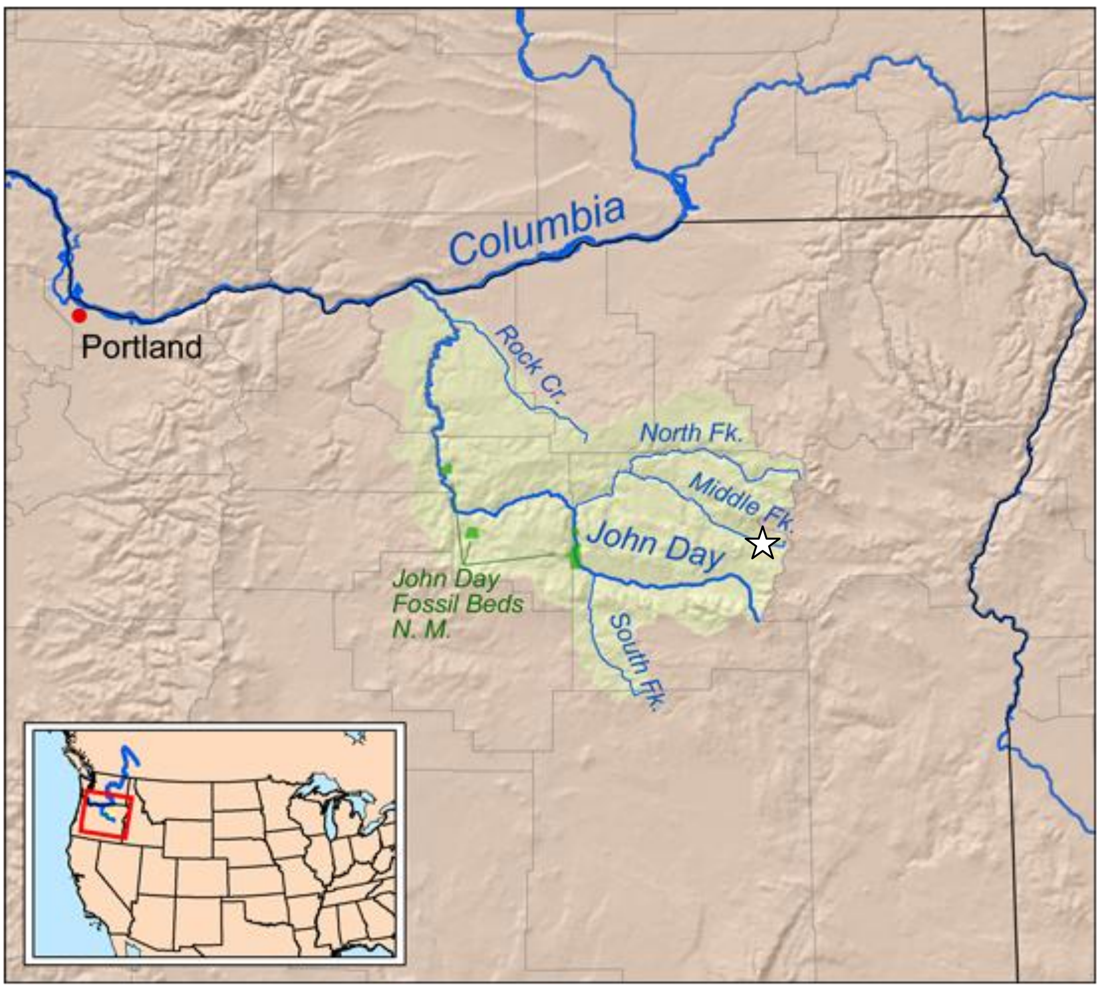

Figure 2.1 The study site is located on the upper Middle Fork of the John Day River represented by the star on the map. (en.wikipedia.org)

Our study site is the 1.8 km upper section of the Forrest property on the MFJD and drains approximately 175 km^2 (Beschta and Ripple, 2005). The Forrest property is in an unconfined alluvial valley of the Greenhorn range within the Blue Mountains. There is little riparian vegetation due to the heavy grazing and what little there is exists mostly as sedges, with a few scattered willows or hawthorns. The Confederated Tribes of the Warm Springs Reservation (CTWS) purchased the property in 2002 and shortly afterwards fenced the cows out of the river and riparian area. In 2005 CTWS enrolled the Forrest property in the Conservation Reserve Enhancement Program (CREP) and over 72,000 trees were planted on the Forrest and another CWTS property downstream. Unfortunately, the survival rate of the CREP plantings was low because of heavy grazing by wildlife such as black-tailed deer and elk (personal communication, Brian Cochran, July 2008). The MFJD at the study site has a mild slope of 0.0043, with an average width of 5.2m.

The Bureau of Reclamation has teamed up with CTWS to design a multi-phased restoration project on their two Middle Fork properties, Forrest and Oxbow. The two main objectives of restoration are to increase fish habitat and to decrease peak summer temperatures. Phase one on the Forrest property included removal of 33 rock barbs and the installation of 18 engineered log jam structures (ELJs). The 18 ELJs included 12 excavated scour pools.

The restoration was carried out in July of 2008. The pre-restoration data sampling was carried out June 26th to July 5th, 2008. The post-restoration data sampling occurred from Aug 28th to Sept 3rd, 2008. Each installation was instrumented with two fiber optic cables, one parallel to each bank, to capture the local micro-habitats found on the inside and outside portions of the channel bends.

Field Measurements and instrumentation

At the heart of our methods is the use of the DTS. A 2006 Agilent N4386A was used to measure temperature, and a Fujitsu Stylistic ST5000 tablet PC was used to run the necessary software, DTS Configurator version 3.0, for measurement taking and saving. The Agilent DTS was used for its superior handling of the harsh field conditions. The air temperature regularly exceeds 35°C and there is no power at the site. A DTS was needed that can handle high ambient temperatures while keeping power requirements to a minimum and the Agilent N4386A fit the bill (Table 2.1).

Table 2.1 Agilent N4386A environment and measurement specifications.

Operating Temperature	-10 to 60
Distance Range	8 km
Minimum Spatial Resolution	1 m
Minimum Temporal Resolution	30 s
Temperature Resolution	0.01 °C
Temperature Repeatability	0.1 °C
Voltage Requirements	10 to 30 V (DC)
Power Requirements	15 to 40 W

Two different types of fiber optic cable were used for the study: the pre-restoration cable was a black mini-flat manufactured by OFS of Furukawa Inc. and the post-restoration was a white stainless steel loose tube manufactured by AFL Telecommunications. The mini-flat cable is a heavy duty multimode cable that incorporates 2 fibers with a 50μm core and 125μm cladding within 2mm gel-filled buffer tubing. Two fiber glass rods provide a strength element to the buffer tube and improve crush resistance. A polyethylene jacket encases the buffer tube and fiberglass rods to provide protection during installation. The mini-flat cable weighs roughly 32 kg/km. The stainless steel loose tube consists of two multimode fibers with a 50μm core and 125μm cladding within 1mm diameter stainless steel tubing coated with 2mm of white polyvinylidene fluoride for protection and weighed roughly 7 kg/km. The length of the cable was marked every meter on the protective coating. This aided in documentation of cable placement. E2000 connectors were used to connect the cable to the DTS; these were spliced onto the cable using a Fujiwara Fitel splicer.

Installation of the fiber optic cables was a physically demanding task due to the length and weight of the cables. The pre-restoration installation required seven individuals. The reel of cable was situated at the upstream end of the study site near the DTS on a steel rod placed upon two saw horses. Two people were stationed at the reel to ensure proper feeding of the cable downstream. One person, holding onto the end of the cable, walked downstream pulling the cable with him/her. Typically, the first 500m was relatively easy and then, due to the friction and meandering, additional help was required: four people were stationed equidistance downstream and helped pull the cable. Hand-held radios were instrumental for a smooth installation because of the need for simultaneous pulling at all five locations. Once the cable was fully stretched out, two people walked back upstream placing the cable roughly one meter from the respective bank and securing it with large rocks from the streambed. The same process was repeated for the second cable parallel to the opposite bank of the stream.

The installation for the post-restoration measurements only required three people due to the difference in cable size and weight. The stainless steel loose tube cable is much lighter and therefore could be carried on a steel rod down the stream. Two people carried the reel making sure the cable did not unwind prematurely while the third person placed the cable roughly one meter from the respective bank. This person would simultaneously place the cable and secure it using rocks from the stream bed.

For both pre- and post-restoration, three people documented the location of the cable in the river after the cables had been deployed. Starting from upstream and working downstream meter marks of both river right and left cable were recorded and photographed. Depending on the changing river characteristics GPS points were taken every 20-50m with a Garmin Geko 301 GPS. During the documentation process, feautres such as deep slow sections, pools, irrigation structures and tributary confluences were marked in the field notebook. The next step was to place ice baths at both ends of the cable and a water bath at one end for post-collection calibration purposes. An ice bath consisted of 15-25m of coiled cable at the bottom of a Coleman five-day Extreme cooler filled to the top with crushed ice. Lastly, enough water was added to make an ice slurry mixture ensuring a bath of 0°C. A single water bath was set up at the upstream end and consisted of a submerged 15-25m coil of cable in a

Coleman Extreme cooler filled with river water. To keep the bath from stratifying, a small pump and car battery were used to circulate water to ensure a fully mixed bath.

Onset HOBO tidbit and Pro v2 temperature loggers were placed within all of the baths, in the tributaries and on the cable submerged in the river. The loggers recorded temperature at 10 min intervals. In addition to the loggers, point temperature measurements were taken using a digital thermometer, VWR model 61220-601, which was accurate to ±0.05 °C. Unfortunately, the pre-restoration tidbit data were lost due to a computer malfunction, but the point measurements were sufficient for calibration.

The Forrest property is in a remote location without power; therefore, a power source was needed to run the DTS. A ‘solar trailer’ was built to accommodate the Agilent and Fujitsu power demands. Three Mitsubishi 100W solar panels were attached to a standard flatbed trailer with rails, which were then connected to four 12V deep cycle batteries in two series sets that in parallel produced 24V. The DTS was hooked up directly to the 24V source while a Samlex model PST-30S-24A inverter was used for the Fujitsu tablet.

In this study, two weather stations were installed to capture the microclimates occurring near the river. Average air temperature, relative humidity, solar radiation, wind speed and wind direction were recorded every 10 minutes with the following instrumentation: Campbell Scientific HMP45C Temperature and Relative Humidity Probe, Li-Cor Pyranometer (LI-200), and Campbell Scientific 03001 R.M. Young Wind Sentry Set. A Campbell Scientific 10X data logger, SC32A connector cable and software (short cut and PC 200W) were used to store, program and download the data.

The instrumentation was attached to a T-post at a height of approximately one meter above the ground; the T-post was secured with three guy-wires to prevent swaying in the wind. The resistance of the pyranometer was too low for the Campbell data logger, causing the solar radiation to be doubled. Thus, the solar radiation reached the maximum limit of 1600W/m^2 by 10 am every morning. To account for the missing periods of data the incoming solar radiation was interpolated from the Prairie City Agrimet station (PCYO). The PCYO weather station is 20 km southeast of the Forrest property and about 100 m lower in elevation.

The flow of the river is an important part of a stream temperature model: if the modeled flow is too low, the modeled stream will heat faster, while if the modeled flow is too high then the modeled stream will not heat fast enough. The CTWS maintains six staff gauges on the MFJD, although there was a misunderstanding about where the gauges were located: all of the staff gauges are on the Oxbow site, downstream 12 km of the Forrest site. To obtain flows for both the pre- and post-restoration timeframes a relationship between flows of the Oxbow and Forrest property were made. There is flow data from 2008 and 2009 for the oxbow property. There is no flow data for the Forrest property from 2008 but in early 2009 a stage height logger with no rating curve became available for this cross section. In addition, three flow measurements were taken 2km upstream of the stage height logger in the summer of 2009. The steps to determine flow on the Forrest property for the summer of 2008 were as follows:

1. Determine flows at the Oxbow property for 2008 installations.

2. Find time periods in 2009 when flow on the Oxbow is similar to the 2008 Oxbow data.
3. Make a rating curve of the Forrest stage height recorder using flows 2km upstream and calculate 2009 Forrest discharges.
4. Approximate 2008 Forrest flows from the Forrest 2009 data during the time periods in step two.

Like most Oregon streams, the MFJD has a very consistent summertime flow due to a lack of rain; for example, the flows in 2009 that match up with the post-restoration timeframe have a standard deviation of 0.018 m^3/s. Therefore, the post-restoration flows are fairly accurate. This, however, was not true for the pre-restoration flows due to the large snow pack of 2008 producing large flows during installation. The flow associated with the upstream boundary of the study site was estimated to be 0.538-0.765 m^3/s for pre-restoration and 0.340 m^3/s for post-restoration (Table 2.2 and 2.3).

Table 2.2 MFJD flows for the Oxbow and Forrest properties for summer of 2008 and 2009. The flows at the Oxbow property were calculated using a rating curve. The flows at the Forrest property are downstream of Vinegar Creek.

Oxbow 2008 Flows		Oxbow 2009 Dates & Flows (m^3/s)		Forrest 2009 Dates & Flows (m^3/s)	
5/17/2008	8.822	5/3/09 23:00	8.817	5/3/09 23:00	3.333
6/30/2008	1.490	6/25/09 13:00	1.463	6/25/09 13:00	0.872
7/8/2008	1.053	7/2/09 18:00	1.055	7/2/09 18:00	0.700
7/15/2008	0.826	7/8/09 18:00	0.832	7/8/09 18:00	0.577
7/23/2008	0.760	7/12/09 16:00	0.758	7/12/09 16:00	0.520
8/26/2008	0.494	8/23/09 10:00	0.493	8/23/09 10:00	0.402
9/8/2008	0.453	8/27/09 0:00	0.455	8/27/09 0:00	0.357

Table 2.3 The estimated flows used for Forrest property during the pre- and post-restoration installations.

Estimated 2008 Forrest Flows (m^3/s)		
	Pre (6/25-7/5)	Post(8/28-9/3)
US of Reach	0.793-0.566	0.340
US of Vinegar	0.850-0.623	0.368
Vinegar	0.170-0.085	0.042
DS of Vinegar	1.019-0.708	0.382
DS of Reach	1.019-0.708	0.439

Data Analysis

Post-Data Collection Calibration

Temperature measurements for all of the installations were collected using the DTS Configurator software version 3.09 for the Agilent DTS. The DTS was set up in single-ended mode, which means light was sent through the cable in only one direction. The Agilent DTS has an internal calibration that uses reference coils to correct for temperature offset but not gain or attenuation ratio. Many factors affect the calibration gain, attenuation ratio and offset, including: the quality of connections and splices, the physical stresses on the cable and the quality of the cable itself. Therefore, post-collection calibration needs to be completed to increase accuracy; this can be done using the Calibration Wizard within the DTS Configurator software or in a separate program such as MATLAB or Microsoft Excel. All data analysis was performed in MATLAB and the scripts can be found in Appendix A.

A typical calibration requires a minimum of two known temperatures which are obtained by the ice and water baths described above. The installation was set up assuming the calibration factors are constant with time; therefore the ice and water baths were not maintained for the entire collection period. This was not true for the Agilent DTS during the experiments and was only discovered after the completion of data collection. The instrument performance was far below those specified by the manufacturer, and at the time of this writing the instrument is in Germany where APSensings (the company spun off of Agilent to support this technology) is still investigating the instrument employed in these studies. Further analysis of the raw data from the August 28th-Sepetmebr 2nd installation shows two types of errors: a random error and a systematic error (Figure 2.2). The random error, referred to as jitter, affects the entire cable and causes offsets as large as 2.3 °C, whereas the systematic error occurs slowly over time and is most likely caused by high temperatures.

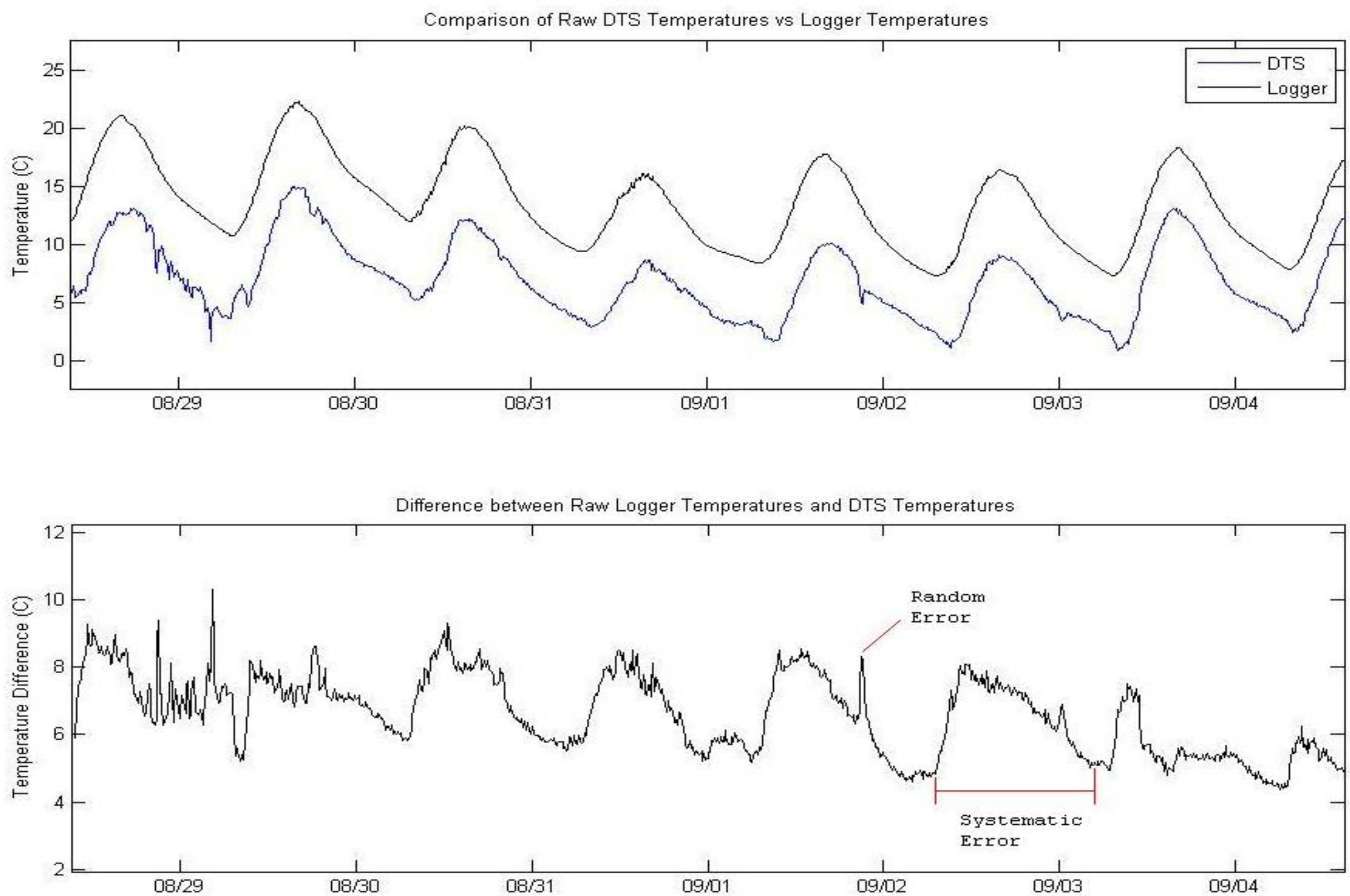

Figure 2.2 (a) Comparison of the raw DTS temperature versus the temperature logger for cable meter 94. (b) The temperature difference between the raw DTS temperature and the temperature logger, accentuating the random error (jitter) and systematic error.

The jitter can be removed from the data set during periods of true ice bath and circulating water bath through a simple offset calculation.

$$T(t) = T_{raw}(t) - (T_{raw,ice\ bath}(t) - T_{logger,ice\ bath}(t)) \qquad \text{(eq. 2.27)}$$

Throughout the remaining traces the jitter cannot easily be accounted for and therefore requires rigorous analysis. The offset seen at each meter along the cable due to a jitter event is not constant, nor is there a pattern to the magnitude (such as increasing with distance from the DTS). To account for this randomness the relative jitter magnitude, $\bar{J}$, was calculated for each meter along the entire cable. Simply stated, the amount of jitter found through a given meter must be compared relative to the jitter at a known point on the cable. The seven largest and most pronounced jitter events within the data set were handpicked; these were considered to be large offsets, in time and not space, surrounded by traces minimally affected by jitter. The offset of the seven jitter traces was found at each meter by comparing the raw temperature to an adjusted two-hour moving average temperature of the trace. The adjusted two-hour moving average uses a dataset where the largest jitter events were flagged and removed so they would not affect the local moving average. The jitter events were flagged by comparing the raw DTS value with the two-hour moving average value; all raw DTS values outside of a 0.75 °C buffer were flagged. Again, skewing of the moving average was seen due to the longer-lasting jitter events and subsequently, temperature traces were wrongly flagged. This required a final screen of the data where jitter events were hand-flagged. The seven traces were then averaged and normalized giving a mean of 1 for the 2122 meters, which can be thought of as the normalized individual jitter magnitude, J. To calculate the relative jitter magnitude, a known temperature is needed at a specific meter along the cable. Since the ice and water baths had stratified during the measurement period, the only known temperature came from a temperature logger placed in the river at a distance of $x = 98$, which was protected from solar radiation by the shadow of a bridge. The relative jitter magnitude, $\bar{J}$, was then calculated for each meter (eq. 2.28).

$$\bar{J}(x) = \frac{J(x)}{J(98)} \qquad \text{(eq. 2.28)}$$

The actual jitter at the logger, $\tilde{O}$, is calculated by subtracting the raw DTS temperature at that meter from the adjusted two-hour moving average, $\tilde{T}$ (eq. 2.29).

$$\tilde{O}(t) = \tilde{T}_{DTS}(98, t) - T_{DTS}(98, t) \qquad \text{(eq. 2.29)}$$

The relative jitter magnitude is then used with the jitter offset at the temperature logger location to get a jitter offset at each meter for all time traces.

The systematic error can be best seen in the comparison between temperatures from a temperature logger to the cable meters representative of the logger, Figure 2.2. Two main assumptions underlie the calculation of the systematic error: first, the error is independent of location and that, consequently, there is only one offset value for each time trace and, second, a two-hour moving average of the data set with the flagged data removed is an accurate representation of the overall trend of the temperature data. From these assumptions, the systematic error, $\hat{O}$, was calculated by subtracting the adjusted two-hour moving average from the logger temperature data (eq. 2.30).

$$\hat{O}(t) = \tilde{T}_{DTS}(98, t) - T_{logger}\ (t) \qquad \text{(eq. 2.30)}$$

An offset, OS, that corrects for both random and systematic error was calculated (eq. 2.31).

$$OS(x, t) = \hat{O}(t) + \tilde{O}(t) * \bar{J}(x, t) \qquad \text{(eq. 2.31)}$$

Not every data set needed this lengthy calibration, so the process was only used as necessary.

The gain calibration factor affects the slope of the trace and can be measured using two known temperatures. Two ice baths, each containing a 20-30m coil of cable, were used to measure the gain at both the upstream and downstream end of the cable. Due to the gain being time dependent for the installations, an average value was found for the time period of constant ice bath and applied to the remaining traces.

The noise in the data set after calibration is due to measurement error and is assumed to be space and time independent. Therefore, to calculate accuracy, the measurement error must be examined during a time period of constant temperature, such as an ice bath. The ice bath for each installation contains at least 20m of cable and stays at a constant temperature, 0°C, for at least three hours, giving more than 360 data points. The measurement noise for the 360 data points is considered to be the temperature difference between the ice bath, 0°C, and the temperature reading of the cable, with the mean being 0°C. The standard deviation was calculated from the absolute measurement error and used as a measure of accuracy.

Post-Calibration Processing

Once the temperature has been calibrated it is necessary to parse out all of the areas which correspond to sections of cable which were not placed in the river during the time of measurement. This includes the cable on land, in intermittent water or in shallow, stagnant water. A simple characteristic of all areas that are either out of water or close to the surface is an increase of the daily temperature amplitude producing a larger standard deviation with respect to time. During the study period, the air ranged in temperature four times as much as the water; therefore, areas influenced by air temperature are easily identifiable. During the ten days of pre-restoration installation, the flow decreased a significant amount, which left much of the cable exposed to air by the end. This caused a significant increase in the amount of data parsed out. For both the pre- and post-restoration data, the standard deviation of a single trace was calculated. Then, through visual inspection, areas with abnormally large standard deviations were removed. MATLAB functions do not work with blank fields (NaNs) so the areas out of water were linearly interpolated from the two edge points. In addition to areas out of water, the sections of cable in side pools and side channels were parsed out. This was done by using the meter marks associated with such features, as recorded during field documentation.

Tributary Flows and Temperatures

Due to problems with the temperature loggers placed at the confluences, tributary temperatures needed to be determined for both pre- and post-restoration. As seen in Figure 2.3, there are distinct spikes due to the tributaries and it is assumed that the spikes are the actual tributary temperatures. This is an accurate assumption because there are cables one meter from each bank and the flow from the tributary will reach the cable before significant mixing occurs. To quantify the flow of both Davis and Vinegar Creek a simple conservation of mass and energy is completed at the confluence (M. C. Westhoff et al., 2007; J. S. Selker et al., 2006; Kobayashi, 1985).

Mass Balance: $$Q_d = Q_u + Q_t \quad \text{(eq. 2.32)}$$

Energy Balance: $$T_d\, Q_d = T_u Q_u + T_t Q_t \quad \text{(eq. 2.33)}$$

where Q is flow (m^3/s), T is temperature (°C) and d, u and t stand for downstream, upstream and tributary, respectively. The mass and energy balance can be solved because there are two equations and two unknowns, Q_d and Q_t (eq. 2.34).

$$Q_t = Q_u \left(\frac{T_u - T_d}{T_d - T_t}\right) \quad \text{(eq. 2.34)}$$

Tributary flow can be found from this method only when the downstream temperature, T_d, has been fully mixed; otherwise the calculated flow will be artificially high. The four hours with the largest difference in temperature were used to find the tributary flows because as the three temperatures converge (in the evening) the validity of these equations decrease. It is assumed the flow of the tributaries is constant throughout the study period even though the flow of the MFJD varied during pre-restoration.

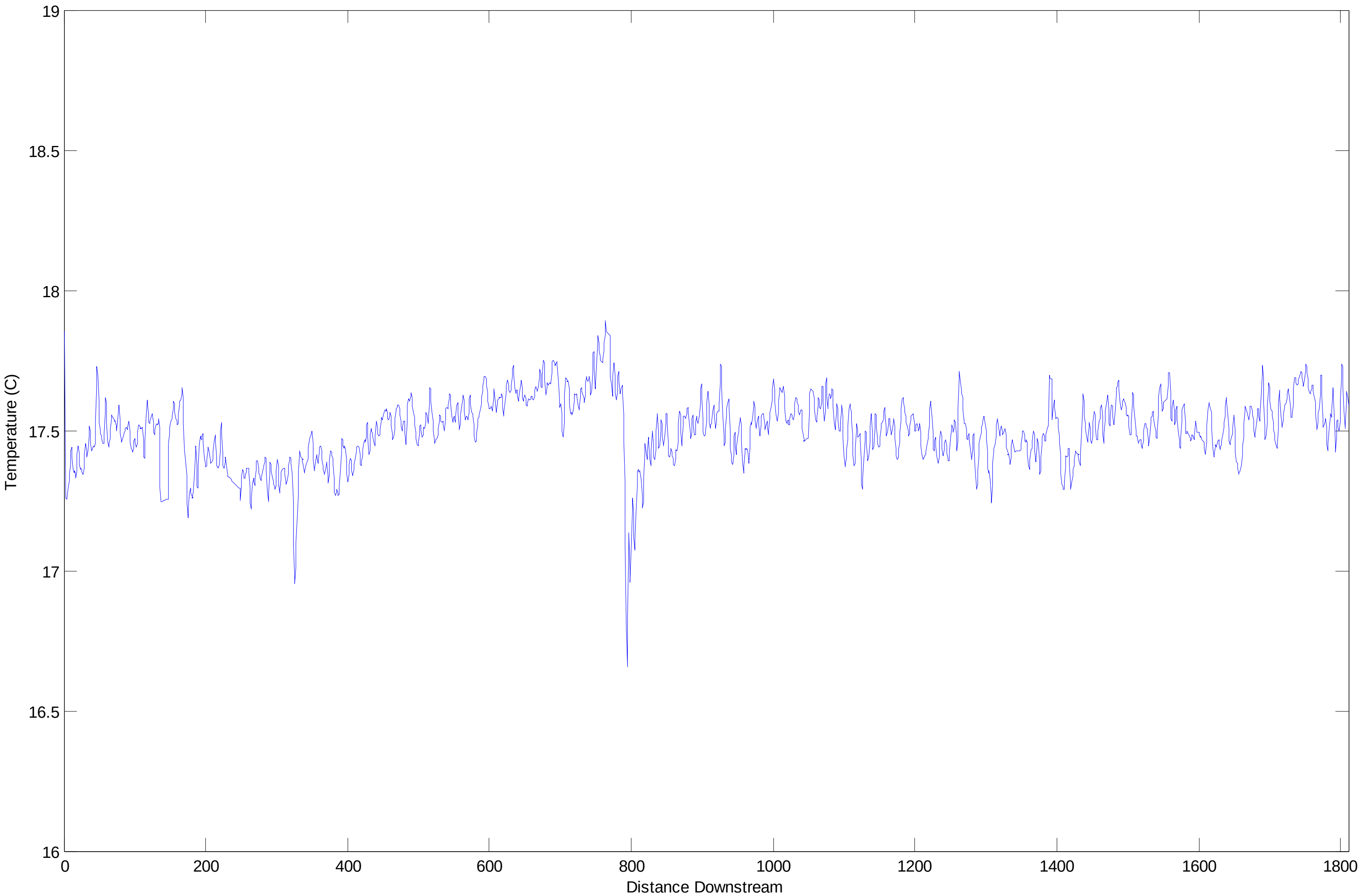

Figure 2.3 An example of the temperature spike due to Davis Creek at meter 794 for the river left post-restoration data.

TTools Extension

The TTools extension within ArcGIS was used for the geospatial data requirements of the Westhoff model. The inputs of TTools are a digital elevation model (DEM), a riparian vegetation map and either an aerial photograph or a digitized stream polyline (Boyd and Kasper, 2004). A fine resolution DEM of the MFJD basin was used from a light detection and ranging (LiDAR) study completed during the summer of 2008. To make the DEM compatible with TTools the DEM had to be mosaiced and projected into the same coordinate system as TTools. These operations were all performed in ArcGIS. A digitized stream polyline was made with a 2006 stream survey conducted by the Bureau of Reclamation. We are assuming that the channel has not changed in the past two years. To create the polylines for the river geometry, the 'water toe' data were used from the stream survey. This assumes that the water level during the stream survey was similar to water level at the time of the installation. The stream polyline was also projected to the correct coordinate system with ArcGIS. A vegetation map was not necessary because there was no significant vegetation to create shading on the Forrest property.

The geospatial data that TTools derives for the stream is aspect, width, gradient and elevation. TTools also calculates the topographic shading angles at each point down the stream. The Westhoff model uses the topographic angle to determine when the sun creates a shadow on the river due to the local topography (M. C. Westhoff et al., 2007).

Westhoff Stream Temperature Model

The Westhoff model is essentially the HeatSource model rewritten from Excel to MATLAB. The main benefit for using the MATLAB software is the ability to handle large data sets and compute at faster rates than Excel. Second, if a researcher is fluent in MATLAB, the model can be modified for his or her specific study site. All of the MATLAB code used for the modeling can be found in Appendix A.

The initial concept was to model the pre-restoration data and compare it against the post-restoration data to see if there are any reach scale changes in temperature. However, due to extremely high flows during the pre-restoration study, we are apprehensive about using the pre-restoration data to calibrate the model since we are interested in the high temperatures seen during low summer flows. Additionally, because there was not significant channel reconstruction we do not believe there will be reach scale changes in temperature, but we do expect to see changes in localized temperatures. For this reason, the temperature model was calibrated using post-restoration conditions and described in detail below. The pre-restoration data will then be run in the calibrated model to evaluate restoration impacts on thermal behavior. This will also show if the process magnitudes are similar at higher flows.

The necessary items for the model to run are the TTools output, climatic data, stream temperature, stream discharge and geometry, tributary discharge and temperature, and groundwater inflow locations and quantities. As noted above, there is minimal riparian vegetation at the study site so the values of the inputs view to sky and land cover longwave radiation are both zero. The groundwater inflow locations and quantities are derived using the DTS temperature profile, for an in-depth explanation see Chapter 3.

The first step is to determine the time and distance step the model will use for calculations, which is based on the Courant number. If the Courant number, CN, is greater than one, the model will not converge.

$$CN = v\frac{dt}{dx} \qquad \text{(eq. 2.35)}$$

where v is velocity (m/s) and dt and dx are the time (s) and distance (m) steps, respectively. The maximum velocity is used in this equation to calculate the Courant number.

The next step is to interpolate all of the inputs in the model to have the same dt and dx as specified from the Courant number. This is done with the use of the interpolate function in MATLAB. MATLAB is able to perform both one-dimension and two-dimension interpolations. A linear interpolation was used for the inputs creating a matrix of over 22 million data points for each variable for the full seven day post-restoration study. Due to the small time step, the amount of memory needed to compute all seven days at once is greater than our computing capacity. Therefore the model was broken up into sections of two and a half days. This was also a natural break in the data because the initial two and a half days were used for calibration of the model and the following two and a half days for validation of the model.

Calibration parameters were used to more accurately model the river. The calibration parameters are the five constants that are difficult to measure in the field.

The first, groundwater temperature, is the temperature assumed of the deeper alluvium in the equations of streambed conduction. It is also used to determine the amount of energy groundwater inflow adds to the system. Typically groundwater is the year-round average air temperature (Anderson, 2005). The second constant is the fraction of solar radiation that reaches the streambed, which is dependent on water depth. However, for our modeling purposes we held this value constant, imposing the fraction of solar radiation not to change with depth. This assumption is satisfactory when the river has a consistent depth, but becomes unsatisfactory when the depth varies significantly. Here we believe this accurately represents the river. The third constant is the fraction of diffuse solar radiation, which is dependent on the particles in the air to deflect the direct solar radiation. The fourth constant is the porosity of the streambed, which is used in the streambed conduction and hyporheic exchange calculations. The last constant used for calibration is the depth of the upper layer of sediment. This layer does not have a temperature equal to the deeper alluvium and groundwater. These five constants were taken as fitting parameters, with the values manually adjusted until the root mean square error was minimized.

The pre-restoration discharge, groundwater inflow and climatic data were modeled using the calibrated model. The RMSE and maximum temperature difference between observed and simulated temperatures was calculated. The pre-restoration run was then visually compared to the post-restoration run looking for anomalies.

Hyporheic Exchange component

Once the model has been calibrated to minimize the RMSE, the hyporheic exchange component (HyZo) was run. It is necessary for the Westhoff model to be fully calibrated since the main assumption in HyZo is a complete energy balance excluding only the hyporheic exchange process. Again, HyZo calculates hyporheic exchange not in terms of flow but effective thermal mass. The thermal mass is averaged across the entire reservoir length and width. Because the temperature of hyporheic exchange fluctuates both diurnally and with varying residence times, we calculated thermal mass based on a residence time of six hours because this is when the largest temperature change will be seen between the hyporheic flow and the surface water. The HyZo calculations were computed every hour from 7am until 1pm on Aug 29-30th of the post-restoration calibration period. The warming up time period was used because this is when the energy flux associated with hyporheic is largest. The energy flux associated with the thermal mass of hyporheic exchange is reintroduced to the Westhoff model equally along the distance of the river. To begin the entire length of the study, ~1800m, was used as the reservoir size of HyZo to give an average depth of hyporheic across the reach. Then the reach is broken up into two segments of ~900m, and the depth of hyporheic exchange is found for both the upper and lower sections. The HyZo calculations were incorporated into the post-restoration validation Westhoff model and pre-restoration Westhoff model for reservoir lengths of 900 and 1800m.

Results

Post-Collection Calibration

Calibration of temperature data is typically an easy task but, unfortunately, the DTS performed far below its specifications. Addressing this complex problem required a time-dependent calibration procedure, and even then introduced more uncertainty in the temperature data than would be expected with this system. Only post-restoration data experienced significant jitter and systematic errors requiring additional offset calibration. The pre-restoration data sets used the traditional calibration techniques for gain and offset (Table 2.4).

Table 2.4 The calibration factors, gain and offset, for river right (RR) and left (RL) cables of pre- and post-restoration. The accuracy associated with each cable is expressed as the standard deviation of the measurement error.

	Pre-restoration		Post-restoration	
	RL	RR	RL	RR
Offset (°C)	4.01	4.12	4.08-8.91	2.20-11.88
Gain (-)	0.0008	0.0060	0.0005	0.0010
Accuracy (°C)	0.38	0.42	0.25	0.46

Measurement error was calculated from the calibrated data by comparing the actual temperatures of the ice bath to the observed temperatures. The standard deviation of the absolute temperature differences was calculated and portrays the accuracy of the DTS measurements (Table 2.4).

Post-Calibration Processing

After the data sets were calibrated the cable was divided into two groups. The first group contained all of the cable that was in the main channel of the river. The second group consisted of all the cable that was out of water, in shallow stagnant water or in side pools or side channels. To distinguish the difference between these two groups the standard deviation of the entire cable was computed for the last 24 hrs of installation. Through visual inspection of the standard deviation data, locations with large standard deviations were omitted from the data sets; these are due to areas out of water. Next, the areas within side pools or side channels as well as locations of cable on land were parsed out of the data set. The pre-restoration data has twice as many ‘out of water’ areas because the flow dropped significantly from June 25th to July 5th (Table 2.5).

Table 2.5 Areas that were removed from the dataset due to being out of the water, in side pools or side channels.

	Pre-restoration		Post-restoration	
	RL	RR	RL	RR
# of areas omitted	20	18	8	10
length of areas omitted (m)	259	217	57	53

Tributary Flows and Temperatures

Two tributaries enter the MFJD within the study site: Davis Creek and Vinegar Creek. Temperature loggers were placed at the mouth of the creeks but, due to problems in the field, no temperature data was recorded. Therefore, tributary temperatures were taken from the DTS temperature profiles (Figure 2.4).

The conservation of mass and energy was applied to the confluences and equation (2.34) was used to determine the tributary flow. The flow was calculated for the four hours of the day with the largest difference and then averaged. This assumes that the flow of the tributaries does not change throughout installation, a valid assumption for post-restoration due to consistent low summer flows but slightly less accurate for pre-restoration. The flows calculated (Table 2.6) are similar to the flows measured in the summer of 2009 (personal communication, Tara O'Donnell, September 2009).

Table 2.6 Calculated flows of the tributaries, Vinegar and Davis creek, for the pre- and post-restoration installations. The calculations are based on energy and mass conservation and use the temperature readings from the DTS.

	Pre-Restoration	Post-restoration
Davis Creek (m^3/s)	0.061	0.016
Vinegar Creek (m^3/s)	0.156	0.054

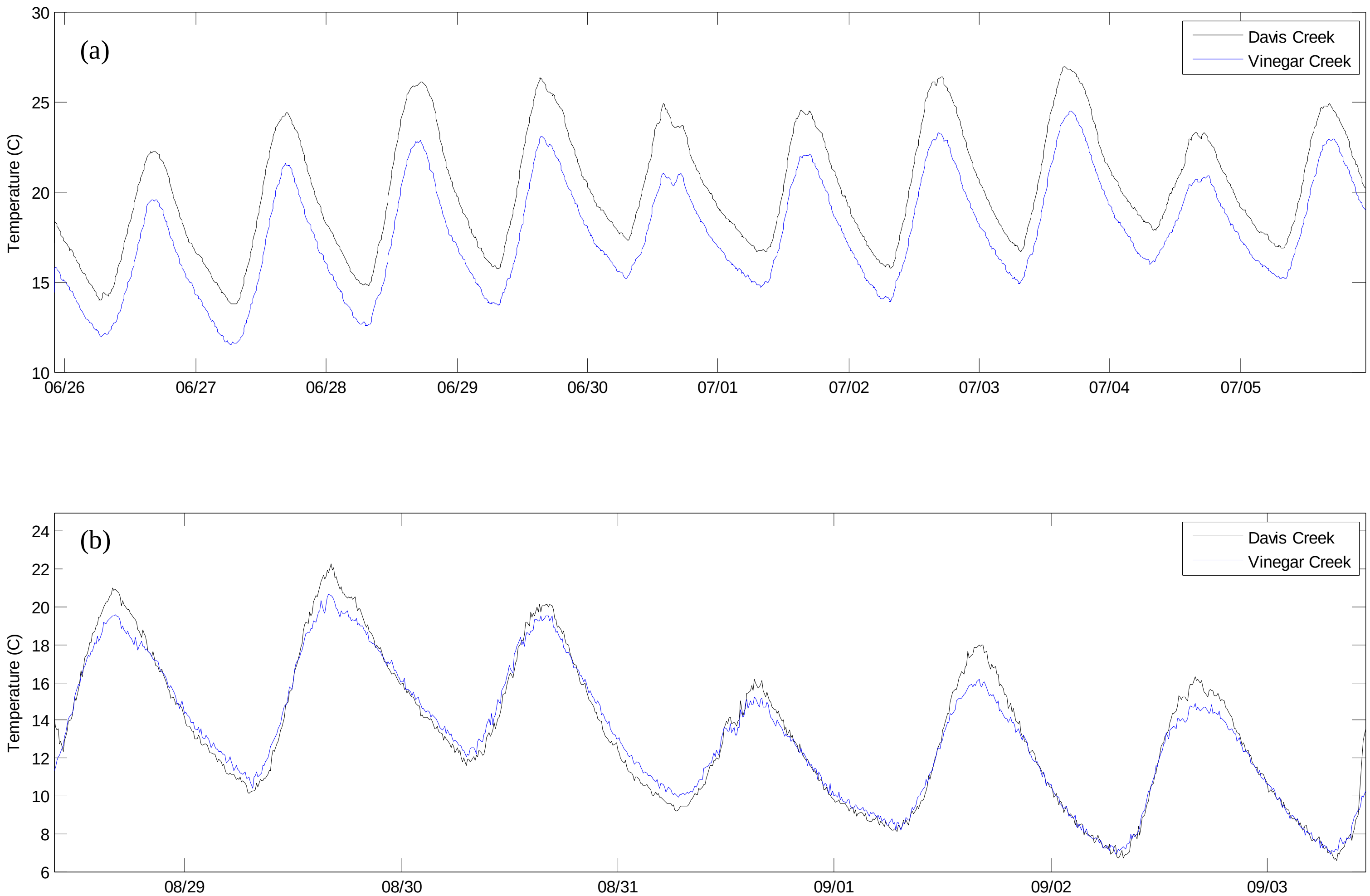

Figure 2.4 Temperature of the tributaries, Davis and Vinegar Creek, entering the study site during (a) pre-restoration and (b) post-restoration.

TTools Extension

TTools was used to calculate aspect, width, gradient and elevation at five meter spacing. Average values for aspect, width, gradient and elevation are 138°, 5.2m, 0.0043 and 1230m, respectively.

Westhoff Stream Temperature Model

The observed temperature profiles are affected largely by the two tributaries, Davis Creek and Vinegar Creek, entering at river meter 794 and 1503 respectively. The 2007-2008 winter at the study site was a heavy snow year and left snowpacks in the headwaters late into June. This created cold tributaries within the study site for the pre-restoration installation and an overall temperature decrease from the upstream boundary to the downstream boundary. Davis Creek runs through the open valley before it meets with the MFJD and warms up considerably during the heat of the day. In contrast, Vinegar Creek is well shaded and emerges directly from the valley edge before it enters the MFJD keeping the creek significantly colder. These two characteristics are evident by the tributary temperature profiles (Figure 2.4). On average, the change in temperature from the upstream boundary to the downstream boundary of the study site is -0.86°C and 0.87°C for pre- and post-restoration.

The first two and a half days, August 28th to August 30th 2008, of the post-restoration study period were used to calibrate the Westhoff model. The Courant Number dictates the time and space steps needed for the partial differential advection equations to converge. Based on the maximum observed stream velocity during the calibration period, a time step of eight seconds and a space step of five meters were calculated. Once the time and space step were set, the input data, including weather station data, flow data, and TTools data, were interpolated to reflect the same step size. To calibrate the model, the tuning parameters (groundwater temperature, fraction of solar radiation that reaches the streambed, fraction of diffuse solar radiation, porosity of the streambed and depth of the upper layer of sediment that varies diurnally in temperature) were manually adjusted until the RMSE was minimized. The resulting minimum RMSE was 0.567°C (Table 2.7).

Table 2.7 The five calibration parameters used to calibrate the Westhoff model for the post-restoration calibration run, Aug 28th-30th, 2008. The 5 parameters were adjusted until a minimum RMSE was met. A RMSE of 0.567 °C is associated with the below values. A sensitivity analysis was completed on the parameters, the sensitivity value represents the relative change in RMSE per 10% change in parameter.

Calibration Parameter	Value	Sensitivity
Groundwater Temperature	6 °C	0.02
Fraction of Solar Radiation reaching streambed	0.25	0.09
Fraction of Diffuse Radiation	0.6	0.10
Porosity of streambed	0.3	0.03
Depth of stream sediment (where $T \neq T_{gw}$)	0.30m	0.05

The two and a half day period from August 31st to September 2nd 2009 of post-restoration was used to validate the calibration of the model. The RMSE of the validation run is larger than the calibration run for post-restoration (Table 2.8). A digital animation of the temperature profile changing with respect to time was made for the calibration and validation runs (Appendix B). These movies allow a different look at how the simulated temperature profiles react compared to the observed temperature profile. A plot of the river temperature averaged over the entire length with respect to time shows the same trends that the movie demonstrates but with less details (Figure 2.5 and 2.6). The movies show the cooling down period for both runs to be more accurate then the heating up period. The heating up period has two characteristics that differ from the observed data – this can only be seen in the movie and not Figures 2.5 and 2.6. First, there is a heat pulse characteristic that creates a downstream wave-like feature in the profile. Second, the downstream half of the observed data has a greater margin of error than the upstream half. A significant difference between the simulated and observed temperatures is present during the warmest timeframe (Figure 2.7). The observed temperature shows that throughout the study site, the temperature increases from upstream to downstream, while the simulation shows the opposite. In addition, the simulated temperatures are consistently too hot during the peaks and too cool during the minimums (Figure 2.5 and 2.6).

Table 2.8 The RMSE and maximum temperature difference between simulated and observed temperature for the Westhoff model and Westhoff-HyZo Model.

	RMSE (°C)	Maximum ΔT (°C)
Pre-Restoration: Westhoff	0.470	2.58
Pre-Restoration: Westhoff-HyZo 900	0.481	2.86
Pre-Restoration: Westhoff-HyZo 1800	0.545	3.04
Post-Calibration: Westhoff	0.567	2.30
Post-Calibration: Westhoff-HyZo 900	0.671	2.96
Post-Calibration: Westhoff-HyZo 1800	1.022	3.73
Post-Validation: Westhoff	0.974	4.13
Post-Validation: Westhoff-HyZo 900	0.714	3.12
Post-Validation: Westhoff-HyZo 1800	0.886	3.81

The energy sources change considerably in magnitude from the calibration run to the validation run. The validation run is cooler, cloudier and less windy than the calibration run. Nonetheless, radiation is the largest driver for temperature increases during the day for both runs. Atmospheric longwave radiation is a consistent cooling mechanism while evaporation cools mostly during the day (Figure 2.8 and Figure 2.9).

The pre-restoration conditions were run in the calibrated model for the first five days of the study. The model simulated the pre-restoration temperatures reasonably well with a RMSE of 0.470°C and a maximum temperature difference of 2.58°C. As suspected, the model calibrated with the post-restoration data fits the pre-restoration data well. Similar to post-restoration, the pre-restoration simulated temperatures have peaks that are too high and minimums that are too low (Figure 2.10).

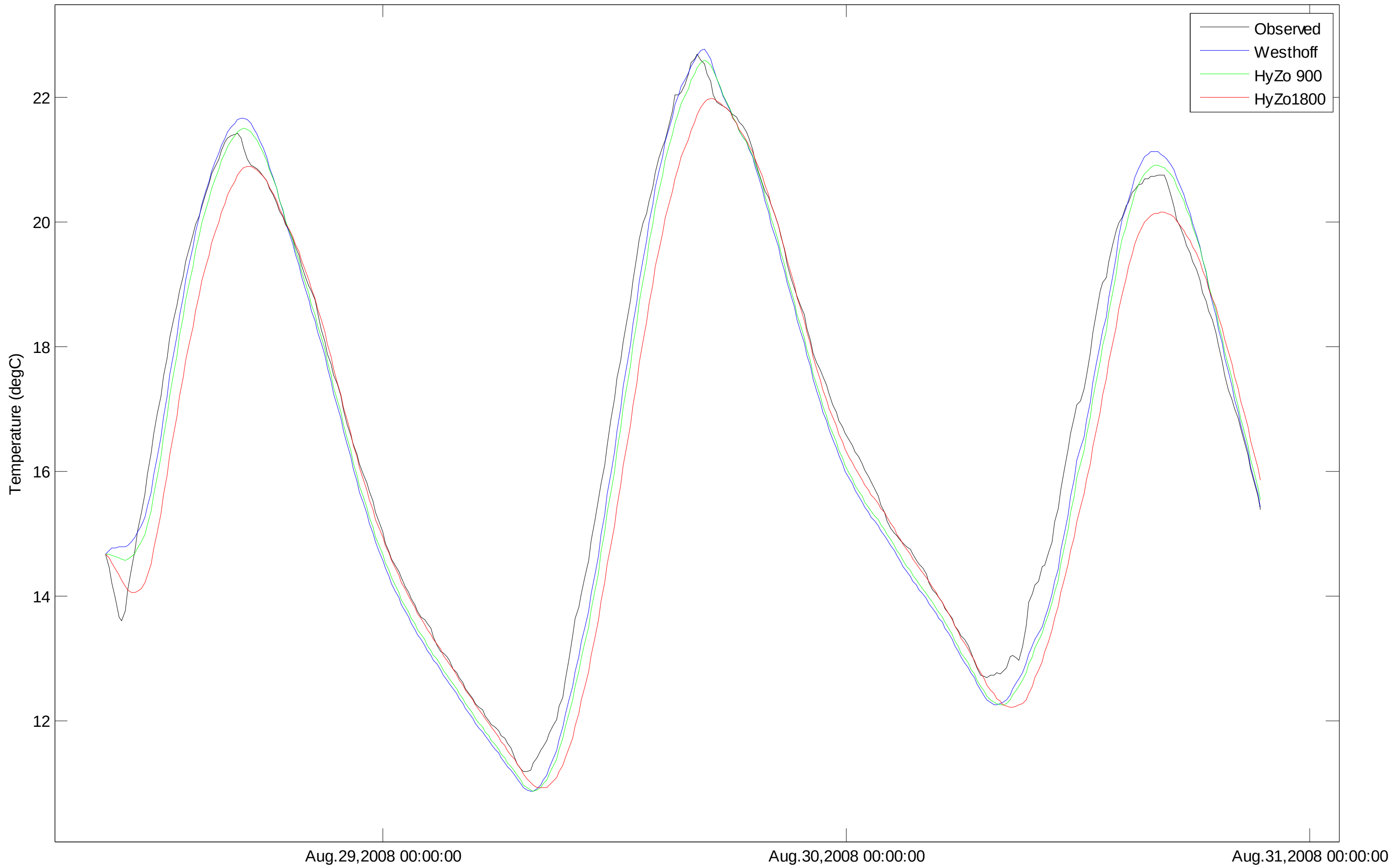

Figure 2.5 The mean temperature of the river with respect to time for the post-restoration calibration period. This plot highlights how the Westhoff model over and under predicts the peaks and minimum temperatures. The Westhoff-Hyzo 900 model is a better predictor of the peak temperatures but does not predict accurate minimum temperatures.

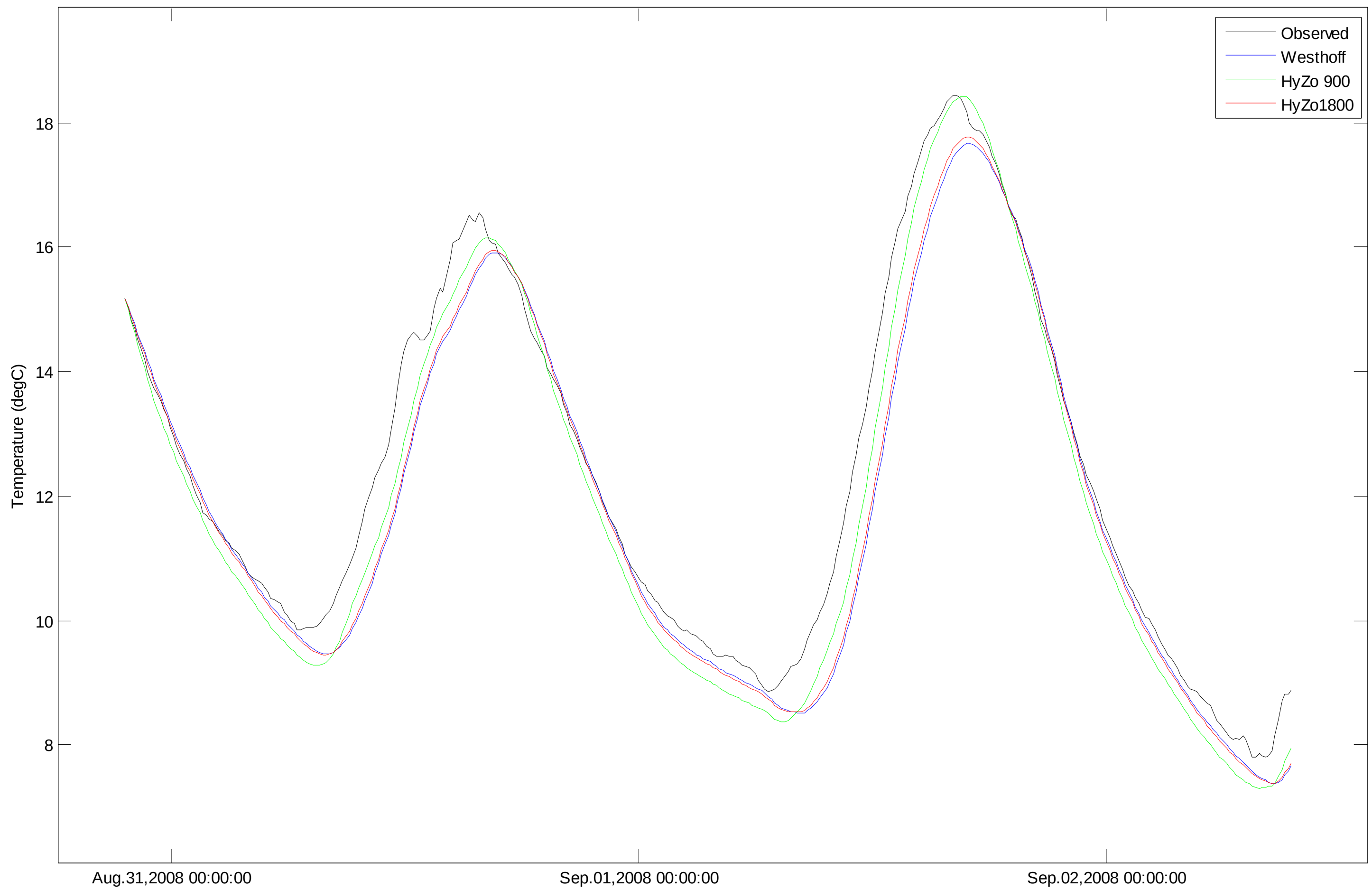

Figure 2.6 The mean temperature of the river with respect to time for the post-restoration validation period. This plot highlights how the Westhoff model over and under predicts the peaks and minimum temperatures. The Westhoff-Hyzo models are a better predictor of the peak temperatures but do not predict accurate minimum temperatures.

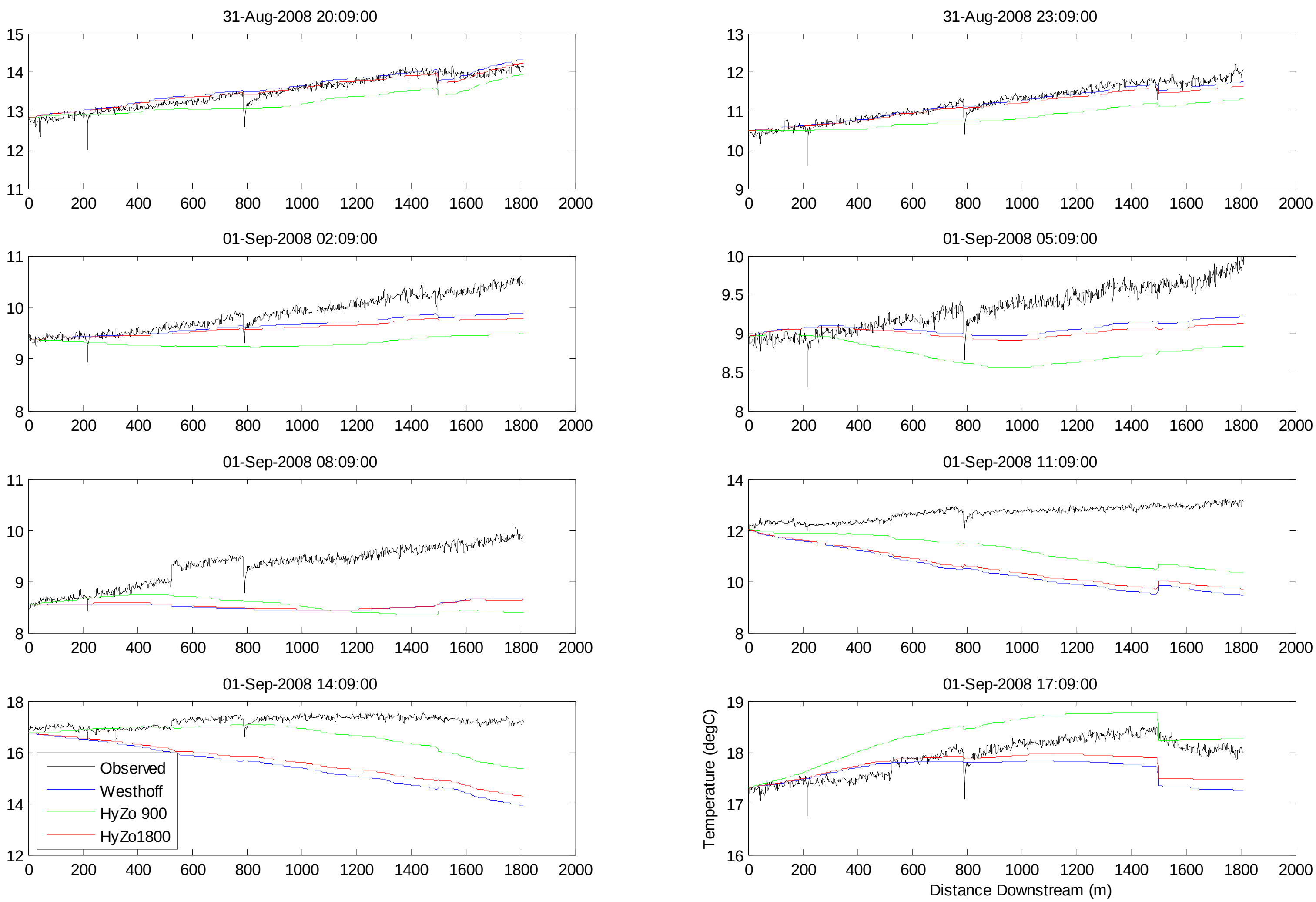

Figure 2.7 Temperatures from the validation run of the post-restoration Westhoff model and Westhoff-HyZo model. The Westhoff-Hyzo model is more accurate during the slower cooling down period than the faster warming up period.

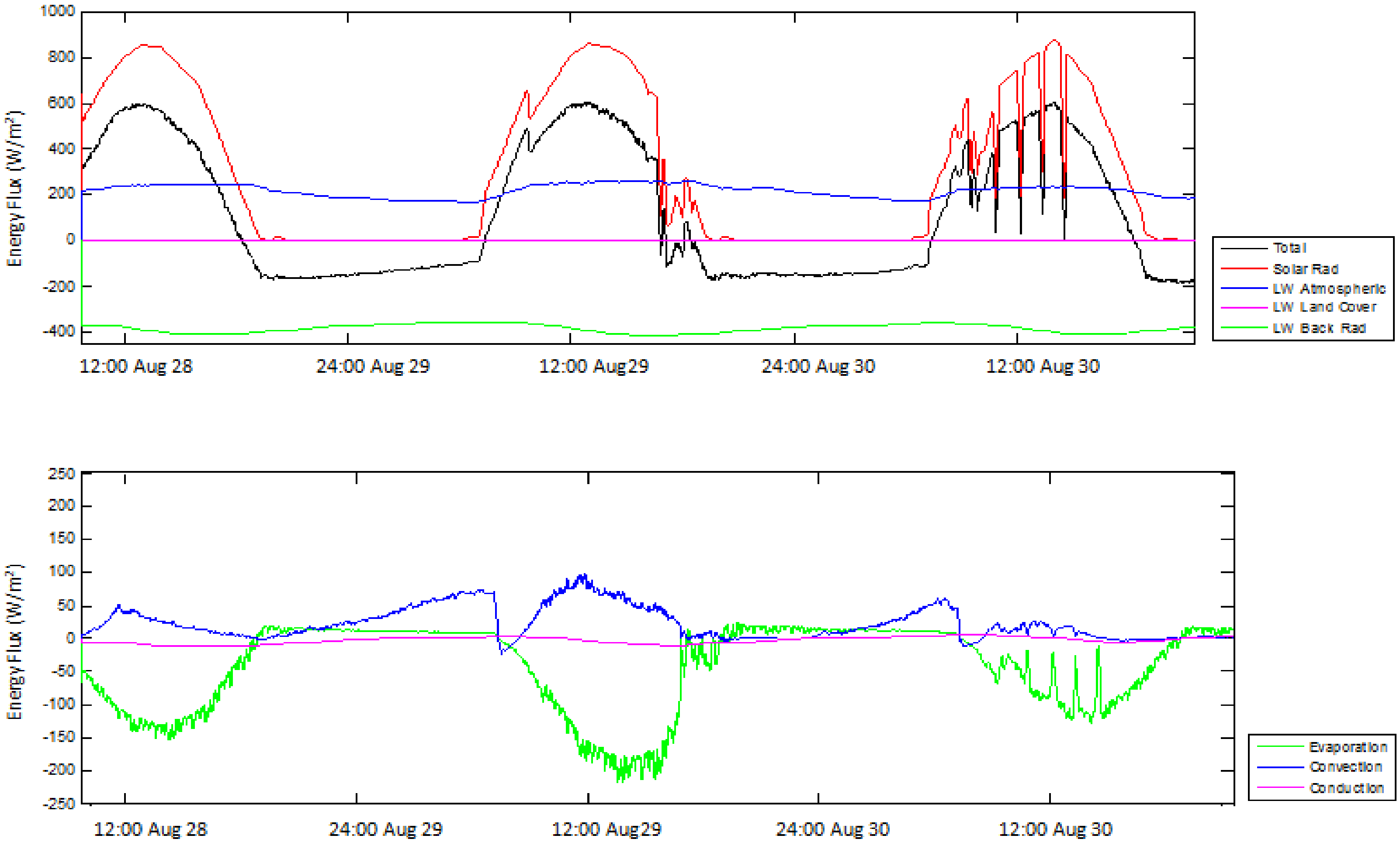

Figure 2.8 Energy fluxes for post-restoration calibration period

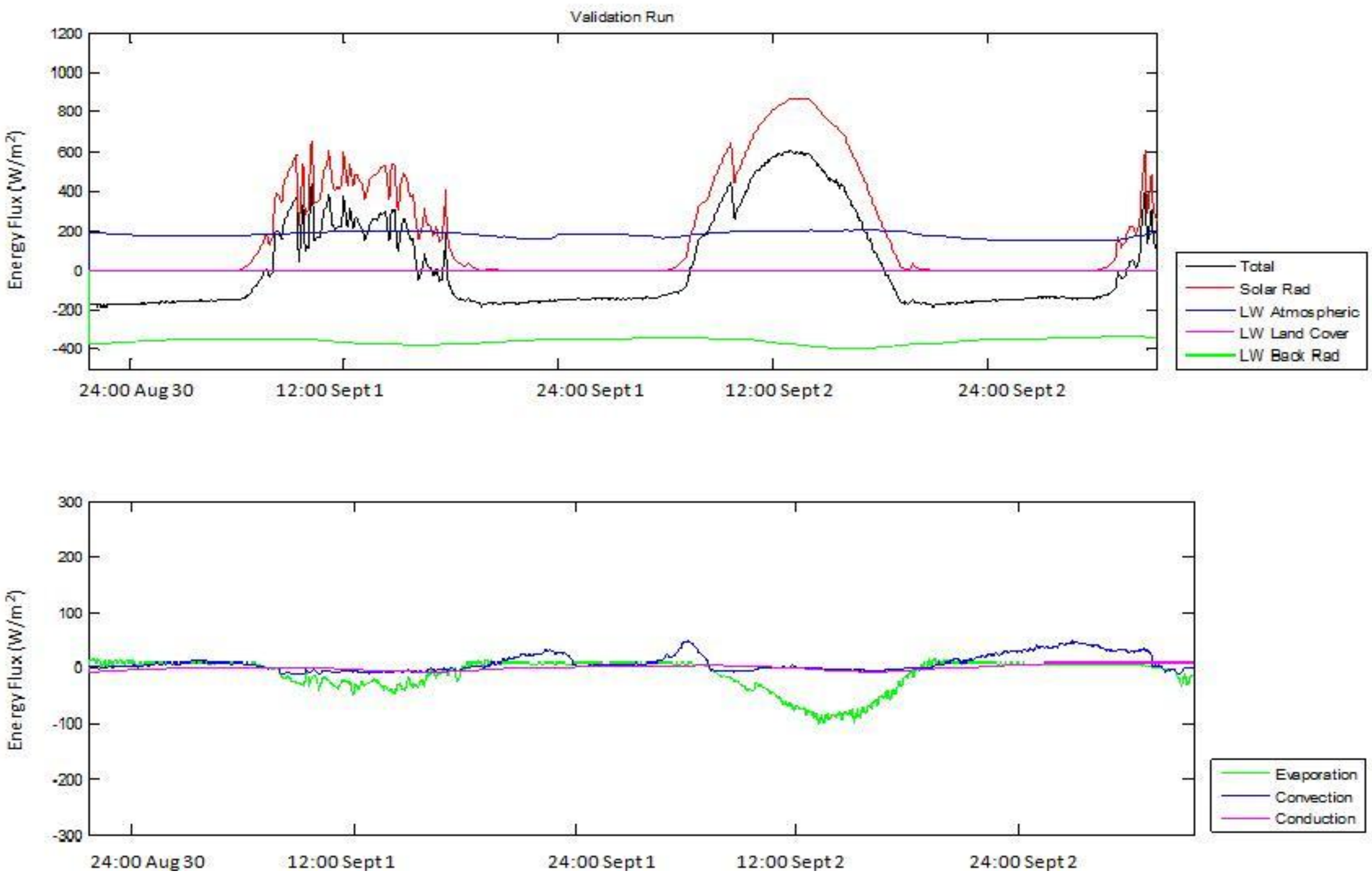

Figure 2.9 Energy fluxes for post-restoration validation period.

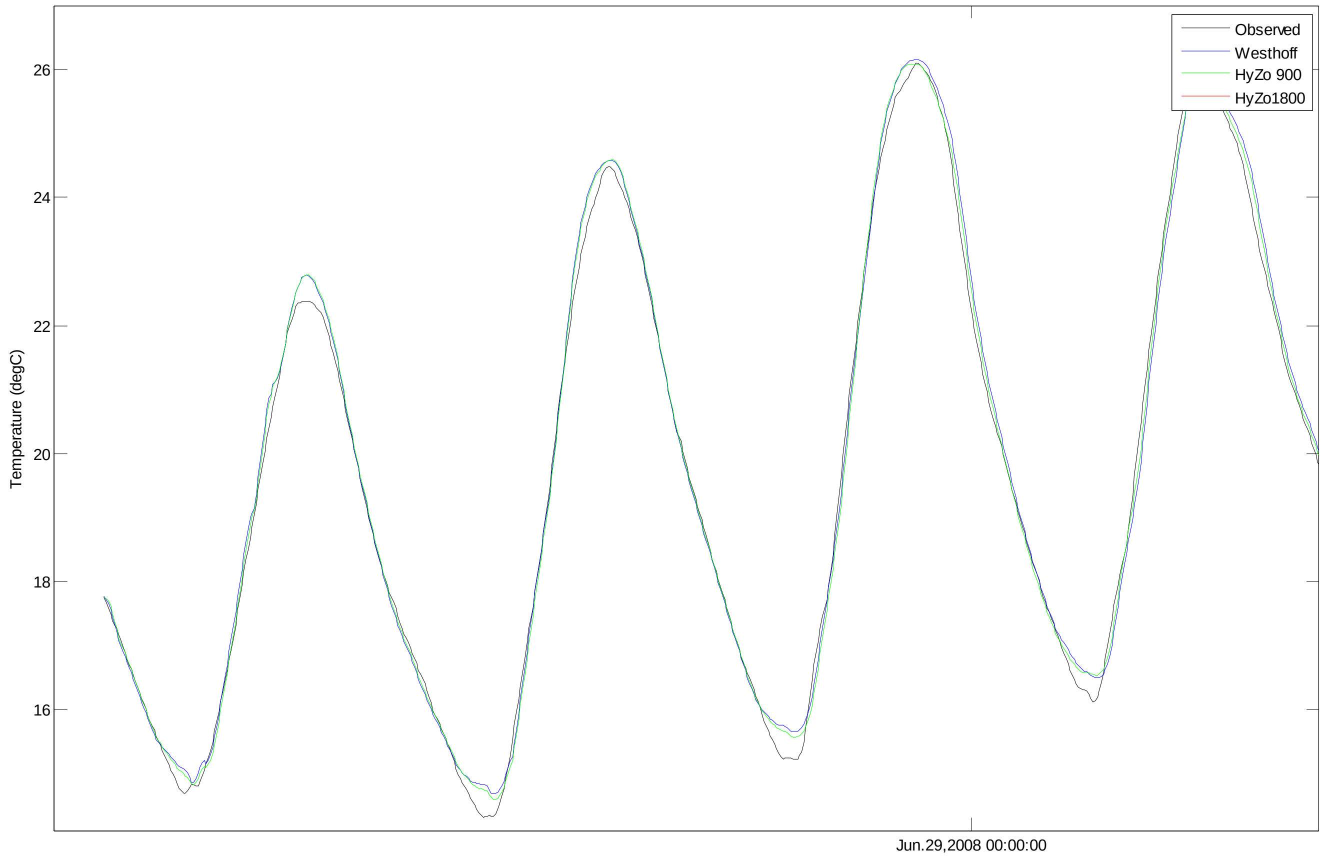

Figure 2.10 The mean temperature of the river with respect to time for the pre-restoration period. This plot highlights how the Westhoff model over and under predicts the peaks and minimum temperatures. The Westhoff-Hyzo models are a better predictor of the temperatures but the calibrated depth of hyporheic exchange (1.6m) does not fully account for the temperature discrepancies.

Hyporheic Exchange component

The HyZo module was run on the three models, pre-restoration, post-restoration calibration and post-restoration validation. Two reservoir lengths were used for each run, 900m and 1800m. When the reservoir was assumed to be the entire length of the study reach, the average depth of the hyporheic thermal mass was 1.61m and 1.66m for post-restoration calibration and validation runs, respectively (Table 2.9). The depth is equivalent to the depth that the surface water would need to occupy in the subsurface (hyporheic zone) to produce the energy flux in order to close the energy budget of the reservoir. When the study site is divided into 900m reservoirs all of the runs show no hyporheic in the upstream half and increased hyporheic in the downstream half. The hyporheic depths of the pre-restoration results are larger than the post-restoration results. The average depth of hyporheic exchange across the entire study site pre-treatment was calculated to be 11.00 m. It is uncertain as to whether hyporheic exchange increased due to higher flows or model error.

Table 2.9 The depth of the hyporheic zone (m) consists of 70% sediment and 30% hyporheic water.

Hyzo Analysis Length (m)	Calculated Depth of Hyporheic Exchange(m)		
	Pre-Restoration	Post-Restoration	
		Calibration	Validation
1800	11.00	1.61	1.66
900	0	0	0
900	7.31	2.60	2.96

The depth of hyporheic exchange calculated for the calibration time-period was added as an additional thermal mass to the Westhoff model to account for hyporheic exchange. The validation period data and pre-restoration data were then inputted into the Westhoff-HyZo model. The depth of hyporheic used in the model was the reach average (1800m) and then the upstream and downstream depths (900m). The RMSE for all of the Westhoff-HyZo model runs was varied whether they increased or decreased as seen in Table 2.8. The model did not adequately account for hyporheic exchange during the cooler time periods (Figure 2.5 and 2.6). However, the Westhoff-HyZo model was successful in decreasing peak temperatures similar to the observed peak temperatures.

Discussion

Limitations with respect to the timeframe of data collection resulted in an inadequate pre-restoration dataset. It would have been preferable to collect pre-restoration data during low flow situations similar to the post-restoration collection period. Low flows would have allowed us to identify the temperature signals of groundwater interactions more confidently.

Due to this major study limitation we were unable to detect a difference in reach scale temperature resulting from restoration activities. However, the construction and testing of this model provides a useful framework for monitoring temperature changes from future restoration projects on this site.

While our truncated time period of data collection did not allow strong inferences regarding temperature changes our analysis still yielded several interesting findings about the model. An interesting characteristic of both model runs is the increased amplitude of daily temperature relative to the observed temperatures (Figure 2.5 and 2.6). Two stream processes have a dampening effect on temperature amplitude: hyporheic exchange and streambed conduction. Hyporheic exchange is known to decrease the daily temperature amplitude by discharging cool water during the day and warm water during the evenings (Arrigoni et al., 2008). Streambed conduction results when sediment warmed by the afternoon sun releases heat into the cooler evening surface water and, once cool, acts as a heat sink, absorbing heat from the warmer surface water. It is highly unlikely that the dampening effect was due to streambed conduction. This is because the variables that comprise the streambed conduction equations were either known or set as calibration parameters. Therefore, the dampening of the daily temperature amplitude is assumed to be caused by hyporheic exchange and is supported by the findings of Torgerson et al. (1999).

In addition, the downstream temperatures of the model seem to be highly dependent on the boundary conditions. The movie (Appendix B), illustrates how the boundary conditions pulls the modeled temperatures to warm up and cool down. Future investigation of this characteristic can be made by running the model in an infinite loop with only an initial boundary condition. This will demonstrate whether the model will either reach equilibrium or continually heat up explaining the underlying processes that might not be fully explained with the current model.

The HyZo model did not accurately reflect the energy flux due to hyporheic exchange during the warming period. The rate at which the MFJD warms is much faster than the rate at which it cools causing the HyZo model to lag behind. This lag in heating can be attributed to how the hyporheic zone was modeled. HyZo assumes the hyporheic zone to act as a homogenous mass requiring full cooling and heating of the water and sediment. However, hyporheic zones actually have a time-dependent heating and cooling within the respect to depth therefore, the hyporheic zone is actually heterogeneous with regards to temperature.

The model created through this study incorporates a few large uncertainties that lead to model limitations. First, a few datasets used for this model were estimated and therefore are not completely accurate of the conditions used for the model calibration; mainly stream flow, time periods of solar radiation and depth of river. Furthermore, the model should only be used during low flow conditions when solar radiation is at its maximum. As seen in the results, the model is also not as accurate during the warming up period even though it does predict peak temperatures well.

While timing of the pre-restoration data collection did not allow a robust simulation of reach- scale temperature effects due to restoration, several insights into the modeling of stream temperature were gained. Our study highlighted the importance of good flow data of the river and its tributaries. Additionally, this study shows how DTS can be used with a deterministic stream temperature model to quantify the thermal mass associated with hyporheic exchange.

Chapter 3: Detecting Groundwater Inflows and Hyporheic Discharge through DTS Temperature Analysis for Restoration Monitoring

Introduction

Watershed health is becoming a large industry in the Pacific Northwest. From 1999-2008 over $680 million was spent on salmon recovery on the Pacific coast (NOAA, 2009) and, on average, over $1 billion was spent annually on river restoration in the nation (Bernhardt et al., 2005). Restoring salmon habitat is the main objective for watershed funds used in Oregon. Much of the historical salmon habitat in Oregon was negatively affected due to anthropogenic activities occurring in the past 150 yrs. For example, miles of habitat for migrating fish have been blocked off by dams, mining and splash dams have altered the channel geometry and bed material, and grazing and logging have greatly decreased the amount of riparian vegetation around the streams and rivers. The effects of human activity have caused the salmon population to plunge to roughly six percent of historical numbers within the Columbia River basin (McCullough, 1999). To revitalize the salmon population, restoration efforts have focused on in-stream habitat improvement, riparian vegetation management, fish passage and water quality management (Taylor, 2007).

To be effective, restoration practices should be designed to permanently re-establish degraded or lost processes and not just provide a band-aid to give short-term improvement. This leads to two questions: 1) exactly which processes should be focused on? And, 2) how do you restore these processes? The EPA Clean Water Act has listed temperature, oxygen depletion, and sediment as three of the top five quality impairments of waterways within Oregon (US EPA, 2006). For example, to decrease temperature, should riparian vegetation be planted, or should the sinuosity be increased to promote hyporheic exchange? Are all secondary effects of restoration practices known? For example, improving salmonid habitat is the main objective for using engineered log jams, but recent studies show hyporheic exchange as another effect of in-stream structures (Hester and Doyle, 2008; Crispell et al., 2009). These questions will not be answered within this study, but are the motivation for the study, which is to monitor the temperature effects of restoration and determine what processes, if any, have been altered.

Monitoring of restoration is underfunded and underutilized in the US with only 10% of projects being monitored or evaluated (Wohl et al., 2005; Bernhardt et al., 2005), although its importance is being recognized more and more with books such as Roni and Quimby's *Monitoring Stream and Watershed Restoration* and Wohl's (2005) review of the subject. Yet, it's unfortunate that Roni and Quimby don't address temperature when it is such an important factor in salmonid heath. For temperature modeling there are a handful of strategies ranging from simple, such as recording temperature year after year, to complex, such as modeling the river using a process based temperature model (Independent Scientific Advisory Board, 2003). Monitoring data should be a tool for adaptive management and scientific advancement; therefore, a physically based temperature model calibrated with high resolution data, such as forward looking infrared thermal imaging (FLIR) or distributed temperature sensing (DTS), is an excellent strategy (Torgersen et al., 2001; Westhoff et al., 2007).

Unfortunately this modeling strategy is very consuming in both time and money; therefore the objective of this study is to determine what cooling processes can be identified with only high resolution data from DTS technology.

The use of DTS and fiber optics to measure temperature was introduced to the ecological field in 2006 (Selker et al., 2006b). It excels in acquiring high resolution temperature data both temporally and spatially with time and distance steps on the order of 30 sec and 1m, respectively (Tufillaro et al., 2008). The DTS system has been used to determine points of groundwater inflow in headwater streams (Selker et al., 2006a), to observe cool air drainage in mountain valleys (J. S. Selker et al., 2008) and to watch the building and melting of snowpacks (Tyler et al., 2009). DTS is a powerful tool that, when paired with statistical analysis like the work of Arrigoni et al. (2008), can provide a new look into how rivers work.

Temperature Signature

Riparian vegetation lowers the incidence of solar radiation, the main driver of peak river temperatures, but as the width of the river increases, the efficacy of riparian shading decreases. In reaches without riparian vegetation, or in larger rivers, the groundwater inflows and hyporheic exchange become more important in lowering peak summer temperatures. Groundwater inflow consists of areas on the streambed where there is direct or diffuse inflow from a groundwater source. The distinction between groundwater and hyporheic flows is controversial and somewhat subjective, but here the thermally-based definition of a groundwater: a source of lateral inflow with a temperature that is largely constant on a daily time-scale (potentially variable seasonally). In particular, groundwater inflow will be lower in temperature than the summer river temperature due to residence times of months to years. The temperature signal seen at areas of groundwater inflows will have an overall cooling effect in summer, both during the day and night (Arrigoni et al., 2008).

Hyporheic exchange is defined here as areas where surface water leaves the channel (hyporheic recharge) and enters the subsurface material (hyporheic zone). In the hyporheic zone, water typically changes both its temperature and chemical signature. After emerging from the hyporheic zone, the water re-enters the stream (hyporheic discharge) further downstream from where it entered. The distance the hyporheic water travels, the new temperature, and chemical signature depend on the particular flow path and are highly variable. This flow path is driven by hydraulic gradient, hydraulic conductivity and the topography of streambed and floodplain (Arrigoni et al., 2008; Gooseff et al., 2006; Wondzell, 2006; Wondzell et al., 2007). The temperature of hyporheic discharge varies depending on the length and depth of the flow path; a longer flow path typically means a longer residence time. Since the hyporheic zone in general involves shorter residence times than groundwater (hours to days), averaging diurnal temperatures rather than carrying seasonal history, the hyporheic discharge will be cooler than surface water during the day and warmer than surface water in the evening (e.g. Figure 3.1, Collier, 2008). In addition, streamlines of hyporheic and groundwater cannot cross therefore there is no groundwater mixing with hyporheic water in the hyporheic zone. Areas of groundwater inflow and hyporheic discharge cannot occur simultaneously (Figure 3.2).

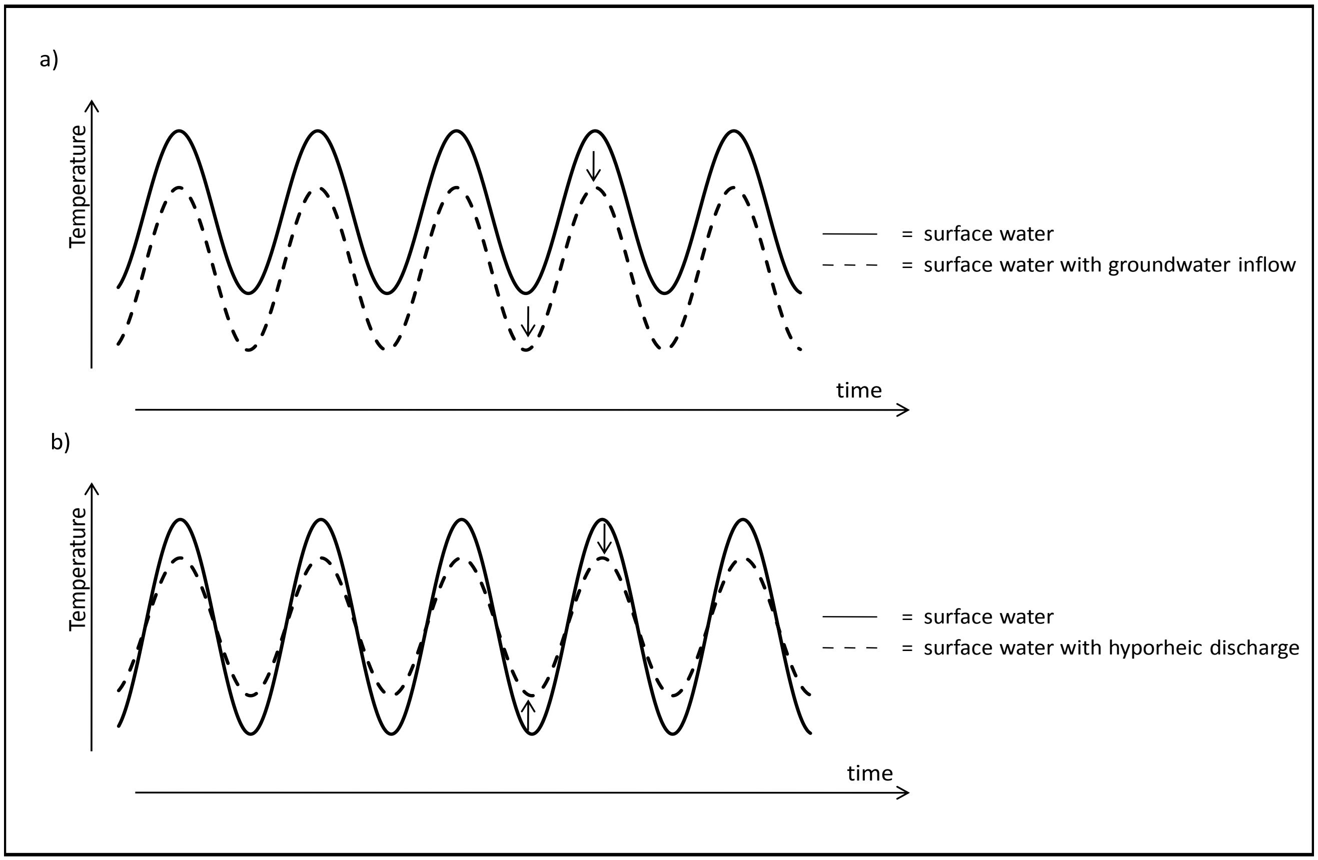

Figure 3.1 A conceptual model of how temperature of surface water reacts to the mixing of a) groundwater inflows and b) hyporheic exchange during baseflows of summer.

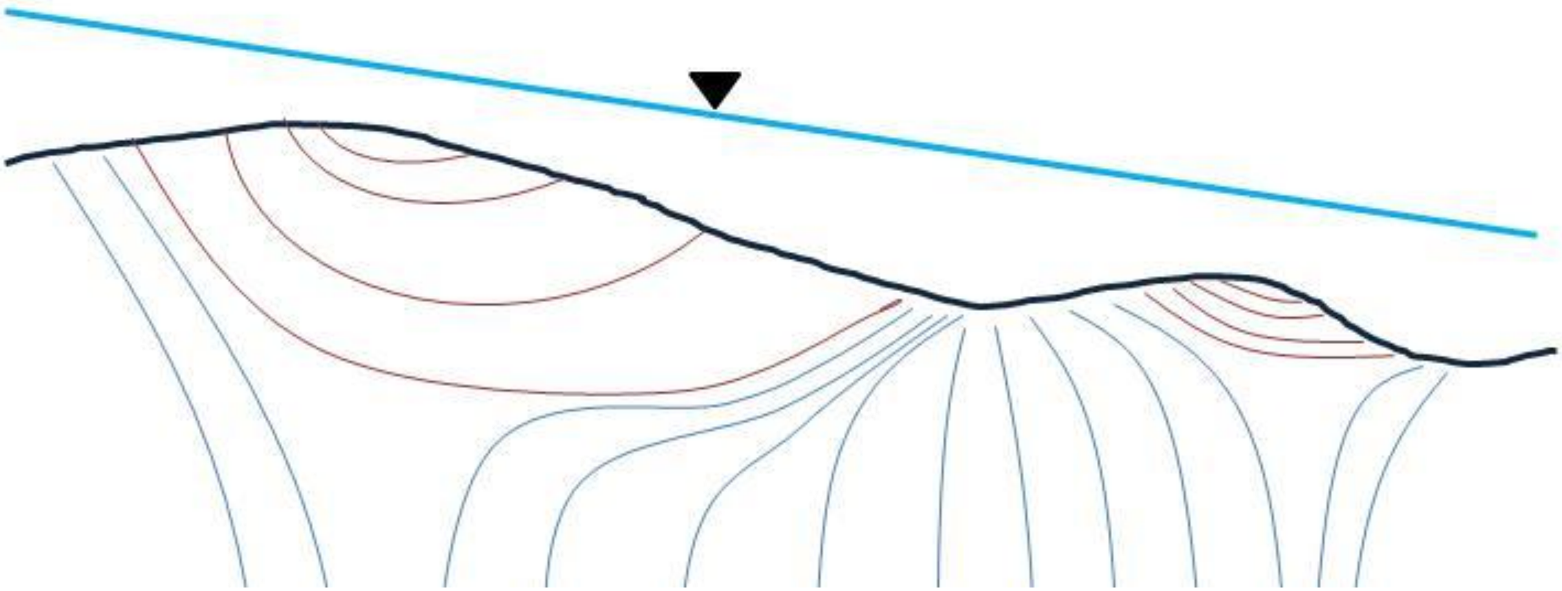

Figure 3.2 A conceptual model of subsurface streamlines below a river viewed as a longitudinal cross-section. The red streamlines represent hyporheic flow while the blue streamlines represent groundwater flow. Streamlines do not converge therefore groundwater and hyporheic discharge occurs at different locations.

We seek to detect and quantify the temperature signatures of groundwater inflow and hyporheic discharge along the course of a river. Traditional point measurements of temperature are not conducive to locating areas of groundwater and hyporheic discharge. FLIR, a newer technology, gives higher spatial resolution than DTS data but is costly to carry-out, and thus involves only 2 or 3 temporal snap shots of the top-surface of a river. The low temporal resolution and inability to penetrate the surface creates difficulty in distinguishing groundwater inflows from hyporheic discharge within the river. The DTS provides excellent resolution, both temporally and spatially, and measures directly on the stream bed, making it the optimum technology for temperature measurements used to identify groundwater inflows and hyporheic exchange.

Methods

Site Description

For a full site description see Chapter 2: Site Description. The first phase of the restoration design for the Forrest property was completed during the in-stream work window of July 14th to Aug 14th, 2008. During this time period, 33 rock barbs were removed from the stream channel. At some of the locations, rock barbs were replaced with engineered log jams (ELJs). A total of 17 ELJs were installed ranging from small structures to large multi-log structures with scour pools dug out around 12 of the 17 ELJ structures. The objective of the restoration was to increase habitat for both adult and juvenile salmonids by adding ELJs. The 2008 results indicate an increased use of the ELJ scour pools by salmonids following treatment (Table 3.1) (Turo, 2009). Although the salmonid use of the scour pools increased, we seek to discover if the temperature profile changed. Did the use of the scour pools increase due to the slower velocities and cover of the ELJ or did the temperature characteristic of the site change, thus drawing more fish?

Table 3.1 Fish use of the study site before and after restoration (Turo, 2009)

	Aug 29, 2006 - All pools in restoration reach	Aug 1, 2008 - 17 constructed ELJ sites
Chinook salmon parr	13	39
Steelhead/trout parr (<6")	9	28
Redband trout (>6")	4	10

The motivation behind restoration of the Forrest reach is lack of habitat complexity created by the unnatural rock barbs. Although the rock barbs lack habitat complexity maybe they provide unknown benefits to the river. Increased hydraulic gradients due to in-stream structures, such as rock barbs or ELJs, can induce hyporheic exchange providing cool thermal refugia (Hester et al., 2009). The addition of ELJs are to increase habitat complexity and depending on their placement during low flow they could create a secondary effect and promote hyporheic exchange (Crispell et al., 2009; Hester et al., 2009; Hester and Doyle, 2008). Rivers are a conglomerate of complex processes that are difficult to predict, monitoring of restoration can be a great learning tool for new insights into river processes.

Field Measurements and Instrumentation

This study utilized the high resolution temperature data that DTS technology produces. An Agilent N4386A instrument was used with a pair of two kilometers fiber optic cables. The two cables were placed in the river about1meter from each bank and recorded temperatures every 10 minutes with one meter spatial resolution. For a more detailed account of how the DTS was installed see Chapter 2: Field Measurements and Instrumentation.

Analysis

Here we build on the calibration and processing work presented in Chapter 2 to employ these prepared data specifically to quantify stream-subsurface interactions.

Groundwater inflow and Hyporheic Exchange Identification

In our framework, groundwater has a distinct temperature signal that is nearly constant year-round and, absent flow to very great depths or contact with geothermal heat sources, can often be assumed to equal the average annual air temperature (Anderson, 2005). When groundwater emerges into surface water, it can produce a cooling effect during high summer-time temperatures or a warming effect during cold winter temperatures. The groundwater will have the greatest effect on surface water temperature during a combination of large temperature differences and low stream flow; this tends to occur in the late summer. The amount of groundwater entering a stream is not constant and depends on the hydraulic gradient of the groundwater table to the stream. During winter there is a steeper hydraulic gradient due to higher groundwater tables. Figure 3.1 demonstrates how cold groundwater affects summer temperatures, both during the day and at night.

The temperature signal of hyporheic exchange is dependent on residence time and its flow path through the hyporheic zone. Both the residence time and flow path reflect local river characteristics, mainly topography and the hydraulic conductivity of the streambed (Arrigoni et al., 2008; Gooseff et al., 2006; S. M Wondzell, 2006; S. M Wondzell et al., 2007). Due to the timing of the start of this study, we must compare data that span some significant changes in river stage. The pre-restoration analysis was completed in early July 2008 when the flows were abnormally high. Typically, temperature signals are weakened during high flows because the diurnal temperature range and the ratio of hyporheic to surface water are smaller. Luckily in this case, even with the high flows, the diurnal water temperature range was still large due to a heat wave, fluctuating at most 10 °C from day to night. The post-restoration analysis was done in late August 2008 to early September 2008 and had flows a third to a half as large as pre-restoration analysis. Similar to pre-restoration conditions, the diurnal water temperature range was up to 10°C. The main differences between pre- and post-restoration conditions are air temperature, surface water flow and groundwater height. There is conflicting evidence in literature whether hyporheic exchange increases or decreases during higher flows (S. M Wondzell, 2006). If hyporheic discharge has the largest signal during the months of higher daily peak temperatures and is not influenced by the change in flow, comparison of pre- and post-restoration is possible.

It is our hypothesis that analysis of the DTS temperature profile of the Forrest property can identify locations of distinct temporal patterns that are associated with groundwater inflows and hyporheic discharge. In this study the term “profile” means a temperature fluctuation with distance along the river. The identified areas will be located at one meter resolution. A key assumption is that both groundwater and hyporheic discharge create localized temperature differences large enough to be detected by the DTS. To aid in detection of signals, the fiber optic cable is placed directly on the streambed. Therefore, when the cooler or warmer water emerges from the subsurface the DTS will register the temperature before it becomes fully mixed within the river. Temperature profiles of the river should be sufficient to identify areas whose temperatures are significantly different upstream and downstream. A conceptual model of these localized temperature differences using the DTS data is presented in Figure 3.3, illustrating three strategies to quantify spatial changes in temperature.

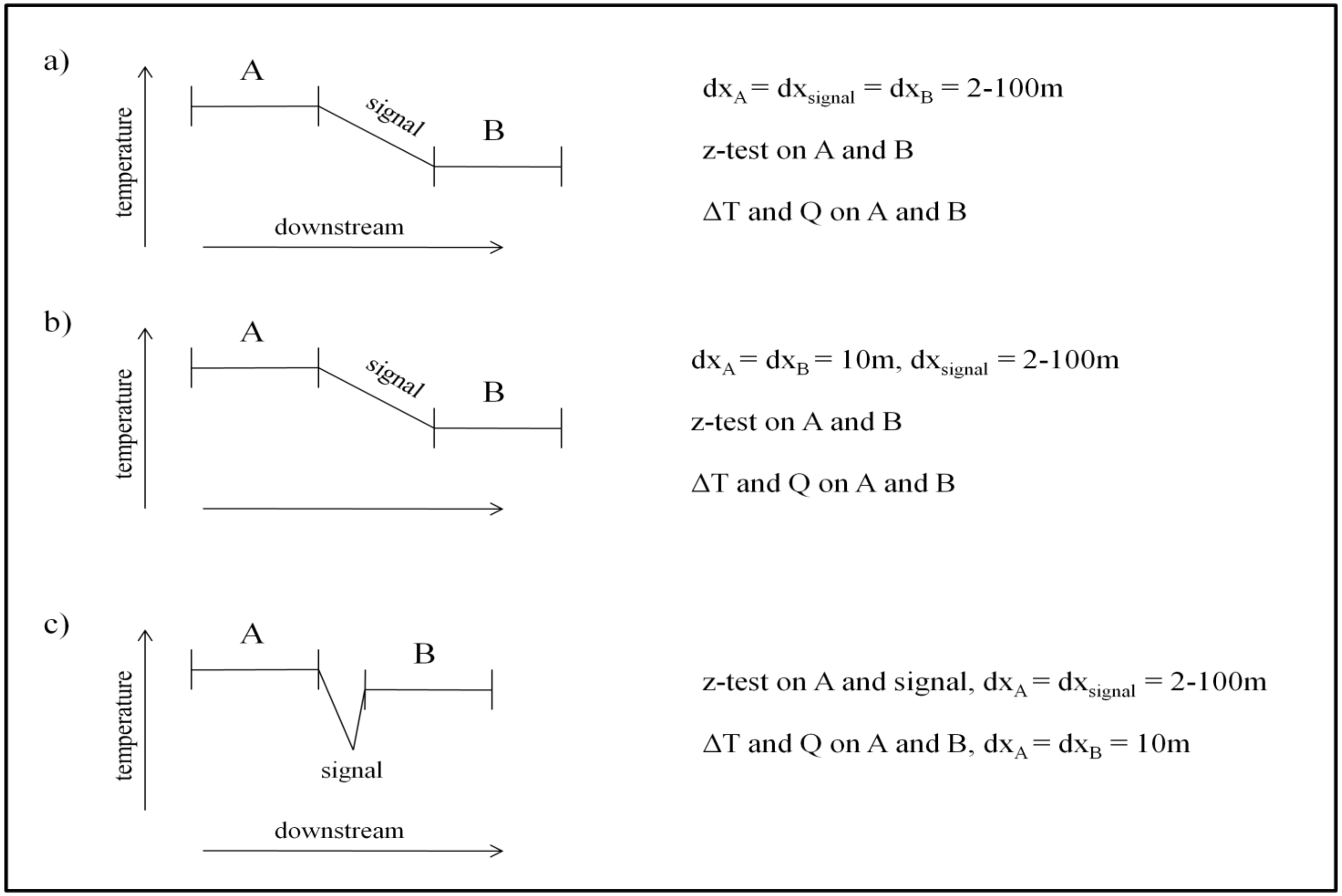

Figure 3.3 Summary of the 3 different strategies used to determine signal locations.

This thesis focuses on identifying the effects of river restoration on stream-subsurface interactions by comparing computed groundwater inflow and hyporheic discharge from before and after restoration. The pre-restoration analysis will also give some insight as to how these two processes change with higher flows for the Middle Fork of the John Day River (MFJD). A statistical analysis of the temperature profile during the hottest four hours and coldest four hours of each day will be utilized.

To obtain a data set with the required temporal resolution, each data set, river right (RR) and river left (RL) of pre-restoration (pre) and post-restoration (post), was temporally averaged using a 60 minute moving average filter. This minimized the noise seen within the data which were collected every 10 minutes. This is a standard technique in DTS data collection wherein the basic computation is one of photon counting, so the instrument is set to the highest temporal resolution one can envision needing, and lower resolution higher precision data is then obtained by post-processing to obtain the specific temporal resolution required. The same analysis was used for all four data sets but the following description will be only for RL-post (Aug 28 -Sept 3 2008). The hottest four hours of the water temperature for RL-post were averaged for every meter of cable within the river, resulting in six temperature profiles. These profiles of the hottest water temperature will be referred to as “Hot”. The same was done with the four coolest hours of water temperature and will be referred to as “Cold”. The hours associated with Hot and Cold are 3:00-7:00 pm and 5:30-9:30 am, respectively.

The following analysis uses the Hot and Cold profiles to determine if there are areas, referred to as signals, with temperatures that are significantly different from areas directly upstream and downstream. The two common types of signals that occur from groundwater inflows and hyporheic discharge are a gradual change in temperature and an abrupt change in temperature. The gradual change in temperature can be associated with a diffuse groundwater inflow and would typically be found in the fully mixed surface water. The second signal is a distinct localized change in temperature that could be caused by direct groundwater inflows. The signal length of groundwater or hyporheic can range anywhere from less than a meter to over hundreds of meters (G. C. Poole et al., 2008). Therefore, analysis was completed to identify signals at 11 different lengths: 2, 4, 6, 10, 16, 20, 30, 40, 60, 80 and 100 meters.

Three different strategies could be used to compare the change in temperature of these two signals. First, the upstream (US) could be compared to the downstream (DS) with US and DS having the same lengths as the signal. Through visual inspection this method misses signals that have a distinct spike but a small overall change in temperature from US to DS. Also when the signal length becomes large (100m) this strategy misses the upstream and downstream 150m of the reach. The second strategy is similar to the first but instead, uses lengths of 10m for US and DS. Again, through visual inspection the temperature spikes are missed. Even though the spikes do not create a large temperature difference in the overall reach they are important because they provide localized thermal refugia for fish during peak summer temperatures. The third strategy compares the signal with US, where the US and signal have a length of 2-100m. Then overall temperature change is calculated between the US and DS, both with lengths of 10m. Although this method misses the upstream and downstream 100m it does not miss the spikes seen within the profile and therefore it was chosen for use in our analysis. In addition, the cable is in direct contact with the river sediment therefore it will measure the discharge temperature before it has been fully mixed with the surface water causing a localized change in temperature. A summary of these three strategies can be found in Figure 3.3.

To determine whether or not the signal had a significantly different mean than the upstream section, a z-test was used ("Hypothesis Test Assumptions," 2009). The z-test was chosen over a t-test to compare the mean temperature because the measurement error (standard deviation) of the dataset is known. The difference in temperature was significantly different if the ΔT was larger than the noise of the data set. The following analysis was done for every signal length from 2-100m and a signal length of 6m will be used for the example calculations. The standard deviation of the noise was calculated for RL-post with no averaging in Chapter 2: Data Analysis. The standard deviation used for this analysis will be different because the data set was averaged using a 60 minute moving average and then averaged again to get the Hot and Cold temperatures. Therefore, equation (3.1) was used to determine the new standard deviation of the dataset, σ_{mav} .

$$\sigma_{mav} = \frac{\sigma}{\sqrt{N}} \tag{3.1}$$

where σ is the standard deviation of the noise and N is the number of data points used to average. N is calculated using equation (3.2).

$$N = signal\ length \cdot (30) \tag{3.2}$$

where signal length is in meters. The number 30 is derived by adding the six data points from the moving average and the 24 data points from the four hottest or coldest hours of the day.

The z-test tests the null hypothesis that the mean of the signal with standard deviation, σ_{mav}, is equal to the mean of the upstream section against the alternative that that the two are not equal. The z-test was performed at the 1% significance level and was run on all 12 Hot and Cold temperature profiles. A groundwater inflow was identified when the temperature of the signal was cooler than the upstream temperature during the Hot and Cold profile of all 6 days. A hyporheic discharge signal was identified when the temperature of the signal was cooler than the US temperature during the Hot profile but warmer than US during the Cold profile. This analysis was performed for every signal length from 2-100m.

The results of the analysis gave overlapping signal lengths at every groundwater inflow and hyporheic discharge location. The signal length that corresponds with the greatest temperature difference was selected as the correct signal length. This will prevent a large temperature difference from being identified as a 100m signal when it is actually only a 16m signal. The greatest temperature difference is expressed as the sum of the absolute temperature difference between the upstream and signal temperatures for all 12 Hot and Cold profiles.

Visual comparison of groundwater and hyporheic locations was completed using photographs and LiDAR of the study reach. The photographs were taken during documentation of the cable installation and are spaced out every 20 to 50m. The LiDAR was completed in 2006 by the firm Watershed Sciences and overlaid onto a Google Earth image of the site. The results of the groundwater and hyporheic analysis were also added to the Google Earth image for easy visual comparison.

Groundwater Inflow Quantification

The quantity of groundwater inflow can be established by applying the mass and energy conservation equations of Kobayashi (1985). This assumes that the entire temperature difference from above and below the groundwater inflow is due solely to the emergence of groundwater.

$$\text{Mass Balance:} \qquad Q_d = Q_u + Q_g \tag{3.3}$$

$$\text{Energy Balance:} \qquad T_d\, Q_d = T_u Q_u + T_g Q_g \tag{3.4}$$

where Q is flow (m^3/s), T is temperature (°C) and d, u and g stand for downstream flow, upstream flow and groundwater flow, respectively. The mass and energy balance can be solved because there are two equations and two unknowns, Q_d and Q_g, giving equation (3.5).

$$Q_g = Q_u \left(\frac{T_u - T_d}{T_d - T_g} \right) \tag{3.5}$$

These equations are correct when the groundwater inflow is large enough to influence the temperature of the mixed river. The flow was calculated at all groundwater inflow signals for the six Hot and six Cold periods. The 12 flows are then averaged together and distributed across the signal length equally.

Results

Groundwater inflow and Hyporheic Exchange Identification

The 60 minute moving-average performed on all data sets greatly minimized the noise seen in the data (Figure 3.4). The Hot and Cold profiles were calculated giving 20 temperature profiles for pre-restoration and 12 temperature profiles for post-restoration. By visual inspection, multiple areas along the temperature profile can be seen in which temperature decreases during both Hot and Cold time periods (Figure 3.5). To strengthen the analysis beyond visual inspection, a statistical analysis was performed. The following results will focus on the river left post-restoration data set and the lengths of river 205-225m and 315-335m to demonstrate areas of groundwater inflow and hyporheic discharge, see Figure 3.6.

The standard deviation of the measurement noise was calculated using the ice baths as outlined in Chapter 2: Data Analysis and can be found in Table 3.2. For RL-post the standard deviation of noise for each signal length analysis can be found in Table 3.3.

For each signal length and temperature profile, a z-test was performed on the temperature of the signal and the temperature directly upstream. This amounts to 132 z-tests for each meter of cable with the lengths of both the signal and the upstream section being equal. The difference in mean temperature of the upstream segment compared to the signal used for the z-test can be found in Table 3.4 for meters 205-

225 and Table 3.5 for meters 315-335. The z-test results for the meters above can be found in Table 3.6 and Table 3.7.

Table 3.2 standard deviation of measurement noise for each DTS data set. The measurement noise was calculated for the hours of complete ice bath where the temperature was assumed to be 0 °C.

	Standard Deviation (°C)
Pre-RL	0.253
Pre-RR	0.458
Post-RL	0.376
Post-RR	0.421

Table 3.3 Standard deviation of measurement noise in the river left post-restoration data for different signal length analyses. The standard deviation decreases with increasing signal length because the number of data points used for averaging increases with signal length.

Signal Length (m)	Std Dev (°C)
2	0.033
4	0.023
6	0.019
10	0.015
16	0.012
20	0.010
30	0.008
40	0.007
60	0.006
80	0.005
100	0.005

Table 3.4 The calculated difference in mean temperature of the signal and the upstream section for the 6 Hot and 6 Cold temperature profiles at a signal length analysis of 2m. The values in bold represent possible groundwater inflows because the signal is colder than the upstream section for the 12 profiles.

	Distance Downstream of Signal Length (m)										
	215	216	217	218	219	220	221	222	223	224	225
Hot Day 1	-0.015	*-0.011*	0.007	**-0.068**	**-0.266**	**-0.346**	**-0.346**	**-0.170**	0.271	0.441	0.408
Hot Day 2	-0.033	*-0.033*	-0.013	**-0.040**	**-0.151**	**-0.209**	**-0.204**	**-0.091**	0.171	0.280	0.250
Hot Day 3	-0.028	*-0.028*	-0.022	**-0.122**	**-0.394**	**-0.497**	**-0.479**	**-0.249**	0.333	0.555	0.527
Hot Day 4	-0.052	*-0.041*	-0.006	**-0.119**	**-0.570**	**-0.737**	**-0.740**	**-0.460**	0.479	0.821	0.783
Hot Day 5	-0.042	*-0.054*	-0.041	**-0.108**	**-0.329**	**-0.415**	**-0.393**	**-0.185**	0.321	0.520	0.478
Hot Day 6	-0.043	*-0.033*	-0.012	**-0.049**	**-0.155**	**-0.206**	**-0.198**	**-0.087**	0.150	0.258	0.243
Cold Day 1	-0.051	*-0.039*	-0.009	**-0.086**	**-0.364**	**-0.492**	**-0.507**	**-0.304**	0.288	0.547	0.546
Cold Day 2	-0.019	*-0.023*	-0.017	**-0.107**	**-0.376**	**-0.485**	**-0.479**	**-0.276**	0.285	0.523	0.504
Cold Day 3	-0.022	*-0.030*	-0.031	**-0.114**	**-0.379**	**-0.492**	**-0.489**	**-0.295**	0.269	0.522	0.517
Cold Day 4	-0.003	*-0.014*	-0.025	**-0.100**	**-0.289**	**-0.363**	**-0.343**	**-0.189**	0.199	0.365	0.343
Cold Day 5	0.010	*-0.006*	-0.011	**-0.089**	**-0.289**	**-0.384**	**-0.398**	**-0.248**	0.176	0.388	0.398
Cold Day 6	-0.024	*-0.031*	-0.019	**-0.066**	**-0.221**	**-0.310**	**-0.326**	**-0.198**	0.136	0.313	0.319

Table 3.5 The calculated difference in mean temperature of the signal and the upstream section for the 6 Hot and 6 Cold temperature profiles at a signal length analysis of 6m. The values in bold represent possible hyporheic discharge locations because the signal is colder than the upstream section for the 6 Hot profiles and warmer for the 6 Cold profiles.

River Meter Associated with Signal Analysis (m)											
	320	321	322	323	324	325	326	327	328	329	330
Hot Day 1	-0.051	**-0.077**	**-0.121**	**-0.162**	**-0.179**	**-0.167**	**-0.132**	**-0.066**	0.026	0.107	0.165
Hot Day 2	-0.035	**-0.060**	**-0.099**	**-0.135**	**-0.156**	**-0.157**	**-0.132**	**-0.075**	0.006	0.090	0.165
Hot Day 3	-0.052	**-0.071**	**-0.099**	**-0.126**	**-0.145**	**-0.139**	**-0.105**	**-0.047**	0.026	0.094	0.153
Hot Day 4	-0.038	**-0.037**	**-0.043**	**-0.060**	**-0.072**	**-0.064**	**-0.046**	**-0.026**	0.003	0.041	0.076
Hot Day 5	-0.058	**-0.083**	**-0.127**	**-0.176**	**-0.200**	**-0.184**	**-0.137**	**-0.066**	0.029	0.125	0.195
Hot Day 6	-0.002	**-0.021**	**-0.047**	**-0.071**	**-0.086**	**-0.089**	**-0.075**	**-0.041**	0.011	0.058	0.089
Cold Day 1	0.006	**0.008**	**0.017**	**0.038**	**0.058**	**0.065**	**0.061**	**0.052**	0.031	-0.002	-0.030
Cold Day 2	0.034	**0.036**	**0.035**	**0.041**	**0.058**	**0.068**	**0.060**	**0.041**	0.020	-0.003	-0.028
Cold Day 3	0.014	**0.019**	**0.026**	**0.040**	**0.056**	**0.063**	**0.058**	**0.049**	0.035	0.018	0.002
Cold Day 4	-0.010	**0.003**	**0.014**	**0.026**	**0.045**	**0.059**	**0.064**	**0.066**	0.059	0.041	0.020
Cold Day 5	0.004	**0.025**	**0.042**	**0.052**	**0.063**	**0.076**	**0.076**	**0.057**	0.031	0.008	-0.013
Cold Day 6	0.043	**0.037**	**0.030**	**0.031**	**0.039**	**0.048**	**0.053**	**0.052**	0.041	0.020	-0.004

Table 3.6 The results of the z-test for the 6 Hot and 6 Cold temperature profiles at a signal length analysis of 2m for river meters 215-225. A value of 1 indicates the mean of the upstream section is different than the mean of the signal at a 99% significance level. The values in bolds are to highlight the six signal analyses that have significantly different means during all Hot and Cold periods.

	River Meter Associated with Signal Analysis (m)										
	215	216	217	218	219	220	221	222	223	224	225
Hot Day 1	0	0	0	0	**1**	**1**	**1**	**1**	**1**	**1**	0
Hot Day 2	0	0	0	0	**1**	**1**	**1**	**1**	**1**	**1**	0
Hot Day 3	0	0	0	0	**1**	**1**	**1**	**1**	**1**	**1**	0
Hot Day 4	0	0	0	1	**1**	**1**	**1**	**1**	**1**	**1**	0
Hot Day 5	0	0	0	0	**1**	**1**	**1**	**1**	**1**	**1**	1
Hot Day 6	0	0	0	0	**1**	**1**	**1**	**1**	**1**	**1**	0
Cold Day 1	0	0	0	0	**1**	**1**	**1**	**1**	**1**	**1**	0
Cold Day 2	0	0	0	0	**1**	**1**	**1**	**1**	**1**	**1**	0
Cold Day 3	0	0	0	0	**1**	**1**	**1**	**1**	**1**	**1**	0
Cold Day 4	0	0	0	0	**1**	**1**	**1**	**1**	**1**	**1**	0
Cold Day 5	0	0	0	0	**1**	**1**	**1**	**1**	**1**	**1**	0
Cold Day 6	0	0	0	0	**1**	**1**	**1**	**1**	**1**	**1**	0

Table 3.7 The results of the z-test for the 6 Hot and 6 Cold temperature profiles at a signal length analysis of 6m for river meters 320-330. A value of 1 indicates the mean of the upstream section is different than the mean of the signal at a 99% significance level. The values in bold are to highlight the three signal analyses that have significantly different means during all Hot and Cold periods.

	River Meter Associated with Signal Analysis (m)										
	320	321	322	323	324	325	326	327	328	329	330
Hot Day 1	1	1	1	1	**1**	**1**	**1**	1	0	1	1
Hot Day 2	0	1	1	1	**1**	**1**	**1**	1	0	1	1
Hot Day 3	1	1	1	1	**1**	**1**	**1**	1	0	1	1
Hot Day 4	1	0	1	1	**1**	**1**	**1**	0	0	1	1
Hot Day 5	1	1	1	1	**1**	**1**	**1**	1	0	1	1
Hot Day 6	0	0	1	1	**1**	**1**	**1**	1	0	1	1
Cold Day 1	0	0	0	1	**1**	**1**	**1**	1	0	0	0
Cold Day 2	0	0	0	1	**1**	**1**	**1**	1	0	0	0
Cold Day 3	0	0	0	1	**1**	**1**	**1**	1	0	0	0
Cold Day 4	0	0	0	0	**1**	**1**	**1**	1	1	1	0
Cold Day 5	0	0	1	1	**1**	**1**	**1**	1	0	0	0
Cold Day 6	1	1	0	0	**1**	**1**	**1**	1	1	0	0

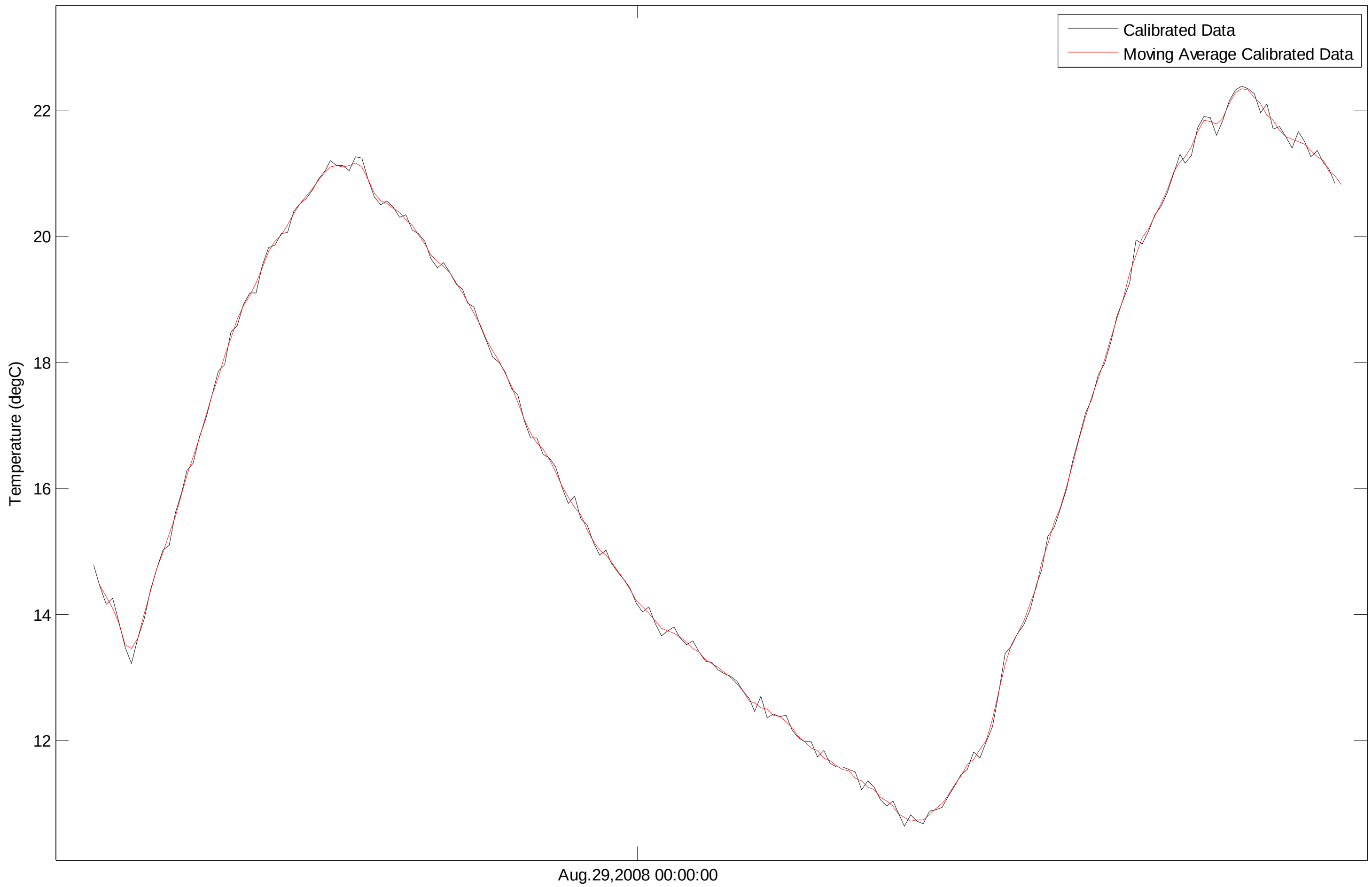

Figure 3.4 Comparison of calibrated temperature data with 60 min-moving average calibrated temperature data for post-restoration river left cable. Applying the moving average minimizes the noise.

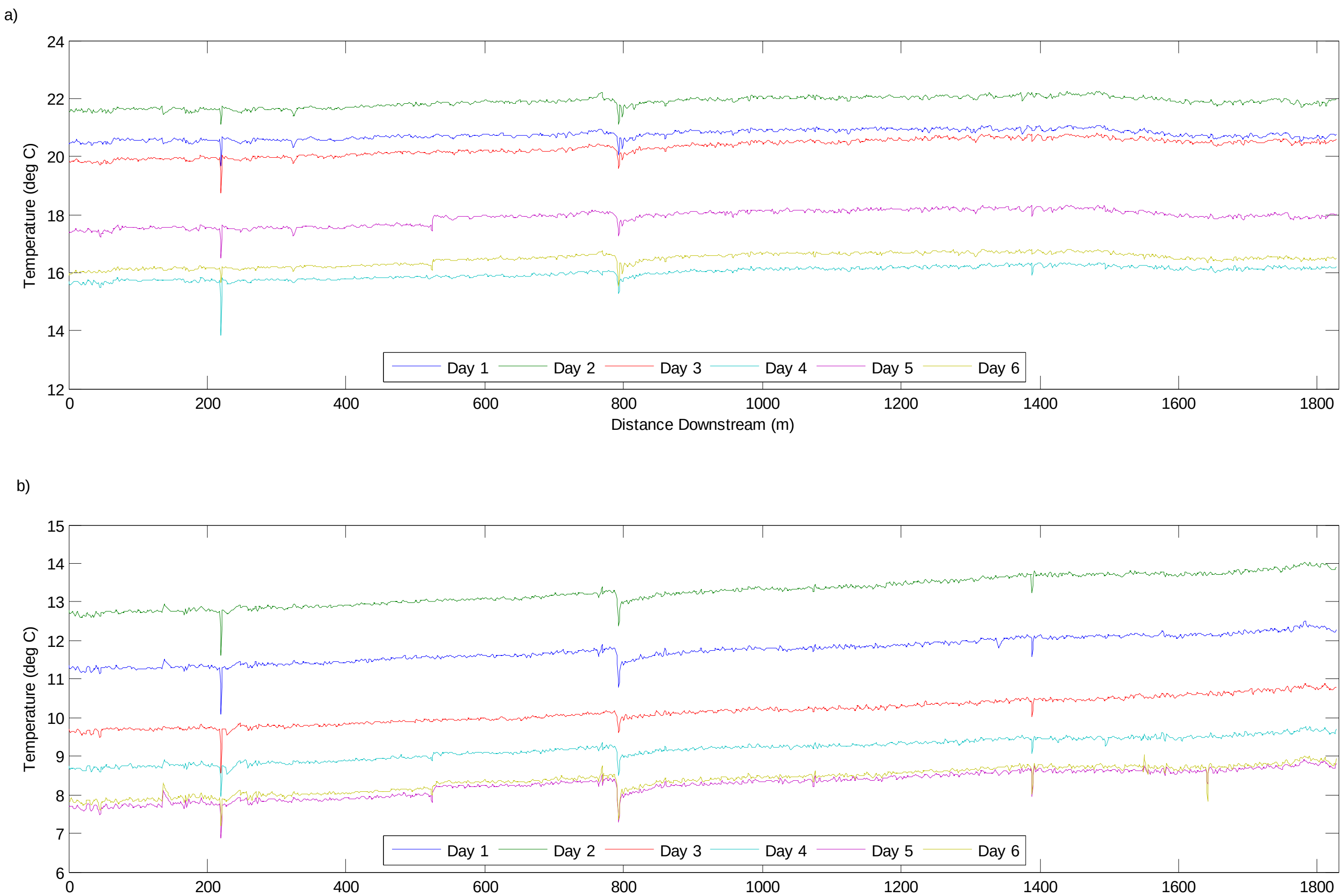

Figure 3.5 The profiles associated with the hottest 4 hours of the day a), "Hot" and coldest 4 hours of the day b) "Cold" for post-restoration river left cable.

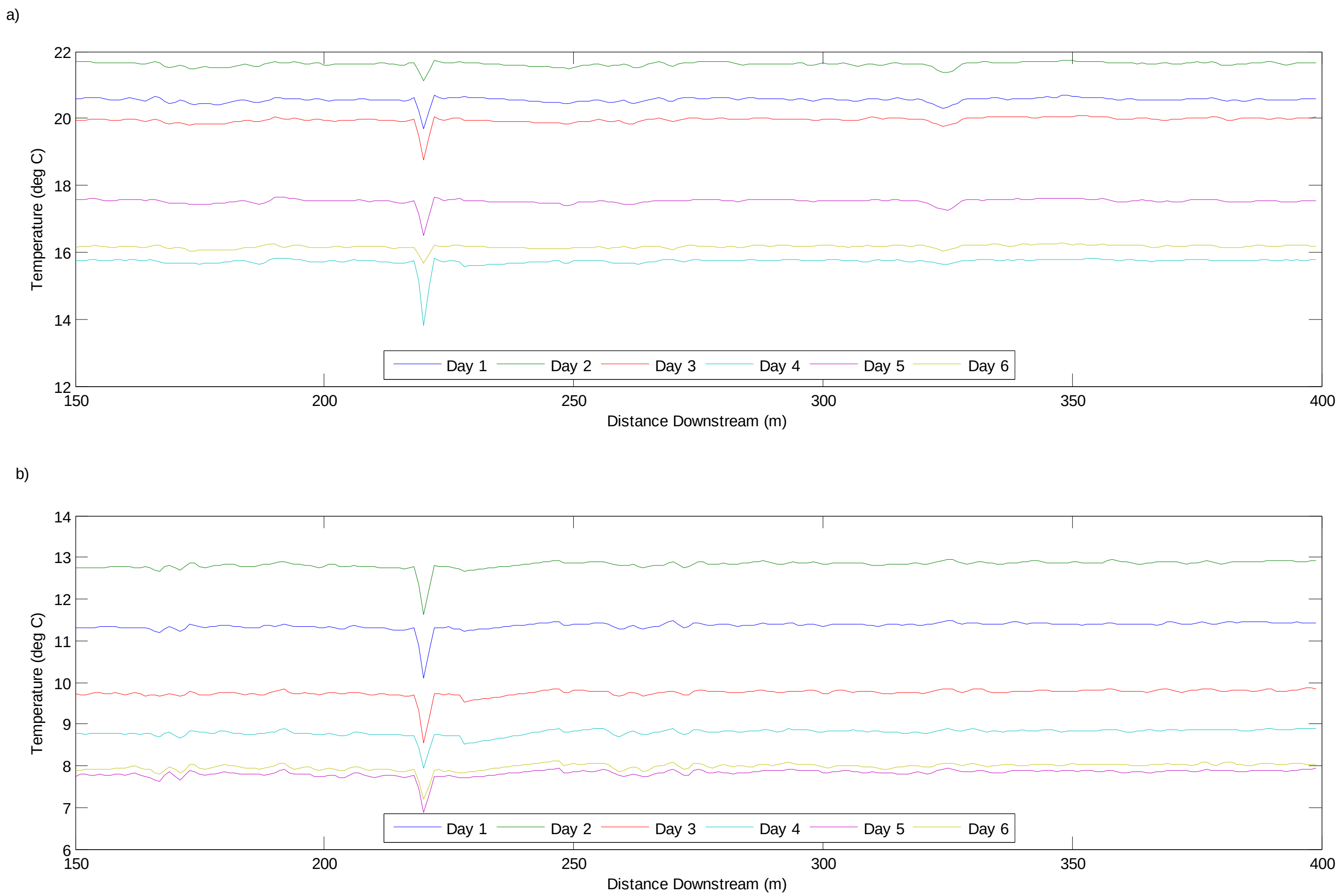

Figure 3.6 Hot, a), and Cold, b), profiles of river meter 205-225 and 315-335 which will be focused on for example calculations.

Next, the signals were separated into two groupings. The first is classified as groundwater inflow and includes all areas where the mean signal temperature is lower than the mean upstream temperature both for the Hot and Cold profiles. All 12 Hot and Cold temperature differences must pass the z-test at a 99% significance level to be considered groundwater inflow. The second group is classified as hyporheic discharge and is defined as areas where the mean signal temperature is cooler than the mean upstream temperature during for the Hot profiles but warmer than the mean upstream temperature for the Cold profiles. Again, all 12 profiles of Hot and Cold must pass this requirement to be considered hyporheic discharge.

For both of the groups, groundwater and hyporheic, there are multiple signal lengths strewn throughout the data that need to be discarded as artifacts of averaging. To eliminate the erroneous signals from the data, each 'cluster' of signal lengths was treated as having one true signal. There were six clusters in the groundwater group and seven clusters in the hyporheic group. There are two tributaries that enter the river within the study reach. The first, Davis creek, is a small creek whose confluence is at river meter 795. The second tributary is Vinegar creek and enters the MFJD at river meter 1505. Any cluster that overlaps with the confluence of these tributaries was disregarded as a valid signal.

To determine which signal length from the analysis is the correct signal length for each cluster, the sum of the absolute temperature difference was calculated. The calculated temperature difference is between the upstream and signal of the river at the respective signal length between 2-100m. The sum of the absolute temperature difference of meters 215-225 and 320-330 for the 11 different signal lengths can be found in Tables 3.8 and 3.9, respectively. The correct signal length corresponds to the largest sum of the absolute temperature difference for each cluster.

This analysis was performed on all four data sets, river left and river right of pre-restoration and river left and river right of post-restoration. Groundwater inflows were found in both of the post-restoration data sets but only in the river right pre-restoration data set. The lengths of groundwater inflows and the average change in temperature associated with the computed inflows are summarized in Table 3.10. Hyporheic flows were only found in the river left post-restoration data set and are summarized in Table 3.11.

Table 3.8 This table represents the sums of the absolute temperature difference for a signal analysis length of 2-100m. The absolute temperature difference was calculated using the temperatures associated with the signal and the section upstream with averaging lengths that correspond to the respective signal analysis (2-100m). The table represents river meters 215-225 which highlight a groundwater inflow at river meter 220 with a groundwater inflow length of 2m (in bold).

Length of Signal for Analysis (m)	River Meter Associated with Signal Analysis (m)										
	215	216	217	218	219	220	221	222	223	224	225
2	0.000	0.000	0.000	0.000	1.777	**8.075**	6.288	0.000	0.000	0.000	0.000
4	0.000	0.000	0.000	0.000	3.781	4.934	4.902	2.753	0.000	0.000	0.000
6	0.000	0.000	0.957	2.831	3.527	3.268	3.140	3.161	1.697	0.000	0.000
10	0.000	1.852	2.344	2.291	2.254	2.216	2.106	1.951	1.864	1.932	0.000
16	1.642	1.606	1.559	1.497	1.454	1.430	1.462	1.482	1.480	1.459	1.420
20	1.294	1.304	1.348	1.400	1.448	1.445	1.425	1.399	1.371	1.345	1.309
30	0.000	0.000	0.000	0.000	0.000	0.000	0.000	0.000	0.000	0.000	0.000
40	0.000	0.000	0.000	0.000	0.000	0.000	0.000	0.000	0.000	0.000	0.000
60	0.000	0.000	0.000	0.000	0.000	0.000	0.000	0.000	0.000	0.000	0.000
80	0.000	0.000	0.000	0.000	0.000	0.000	0.000	0.000	0.000	0.000	0.000
100	0.000	0.000	0.000	0.000	0.000	0.000	0.000	0.000	0.000	0.000	0.000

Table 3.9 This table represents the sums of the absolute temperature difference for a signal analysis length of 2-100m. The absolute temperature difference was calculated using the temperatures associated with the signal and the section upstream with averaging lengths that correspond to the respective signal analysis (2-100m). The table shows river meters 320-330 which highlights a hyporheic discharge at river meter 324 with a hyporheic discharge length of 6m (in bold).

Length of Signal for Analysis (m)	River Meter Associated with Signal Analysis (m)										
	320	321	322	323	324	325	326	327	328	329	330
2	0.000	0.000	0.000	0.000	0.000	0.000	0.000	0.000	0.000	0.000	0.000
4	0.000	0.000	0.000	0.000	0.498	0.387	0.000	0.000	0.000	0.000	0.000
6	0.000	0.000	0.000	0.000	**0.519**	0.423	0.256	0.000	0.000	0.000	0.000
10	0.000	0.000	0.000	0.000	0.000	0.300	0.216	0.107	0.000	0.000	0.000
16	0.000	0.000	0.000	0.000	0.000	0.000	0.000	0.000	0.000	0.000	0.000
20	0.000	0.000	0.000	0.000	0.000	0.000	0.000	0.000	0.000	0.000	0.000
30	0.000	0.000	0.000	0.000	0.000	0.000	0.000	0.000	0.000	0.000	0.000
40	0.000	0.000	0.000	0.000	0.000	0.000	0.000	0.000	0.000	0.000	0.000
60	0.000	0.000	0.000	0.000	0.000	0.000	0.000	0.000	0.000	0.000	0.000
80	0.000	0.000	0.000	0.000	0.000	0.000	0.000	0.000	0.000	0.000	0.000
100	0.000	0.000	0.000	0.000	0.000	0.000	0.000	0.000	0.000	0.000	0.000

Table 3.10 Results of the groundwater inflow analysis. Lengths and locations of the groundwater inflows are summarized along with the average temperature difference associated with the respective groundwater inflow.

Pre - Restoration				Post - Restoration			
River Left		River Right		River Left		River Right	
Areas of GW inflow (m)	Average ΔT (°C)	Areas of GW inflow (m)	Average ΔT (°C)	Areas of GW inflow (m)	Average ΔT (°C)	Areas of GW inflow (m)	Average ΔT (°C)
-	-	85-114	-0.046	32-35	-0.092	272-371	-0.040
-	-	588-667	-0.036	146-235	-0.037	-	-
-	-	-	-	219-220	-0.673	-	-
-	-	-	-	1585-1604	-0.057	-	-

Table 3.11 Results of the hyporheic discharge analysis. Lengths and locations of the hyporheic discharge are summarized along with the average absolute temperature difference associated with the respective hyporheic discharge location.

Pre - Restoration				Post - Restoration			
River Left		River Right		River Left		River Right	
Areas of HY discharge(m)	Average ΔT (°C)	Areas of HY discharge(m)	Average ΔT (°C)	Areas of HY discharge(m)	Average ΔT (°C)	Areas of HY discharge(m)	Average ΔT (°C)
-	-	-	-	162-171	0.072	-	-
-	-	-	-	321-326	0.097	-	-
-	-	-	-	1086-1105	0.031	-	-
-	-	-	-	1651-1730	0.047	-	-
-	-	-	-	1760-1779	0.075	-	-

Google Earth was used to visually compare the temperature signals with locations of ELJs. The groundwater inflows and hyporheic discharges were imported into Google Earth at the respective length for each signal. The ELJs were added specifying which bank they were installed on, see Figure 3.7. Before restoration occurred on this site, three locations of groundwater inflow were identified with two of the three signals occurring within the restoration boundaries. Once restoration was complete five groundwater inflows and five hyporheic discharge locations were discovered, with seven of these ten occurring within the boundaries of the restoration. From comparison of the Google Earth map, five of the post-restoration signals contained at least one ELJ.

To compare floodplain characteristics at the signal locations, LiDAR data were overlaid onto the groundwater and hyporheic results in Google Earth. The historic channels within the floodplain are clear in the LiDAR data and are in the same area as the downstream locations of groundwater and hyporheic, see Figure 3.8. The channel in this area has also been straightened by the historical railroad grade. The upstream locations do not have a distinct historical channel like the downstream locations and the river is more sinuous and not confined by the railroad grade, see Figure 3.9.

The locations of groundwater and hyporheic were identified in the photographs taken during documentation of the cable installation. These photographs allow a rudimentary look into the geomorphic controls of the signal, for example, the area of hyporheic discharge at river meters 1651-1730 is characterized as a riffle pool sequence seen in Figure 3.10. It is typical for geomorphic controls such as riffle-pool or pool-step sequences to be associated with hyporheic exchange (Bencala and Walters, 1983). Within the study site three of the five hyporheic discharge locations occur at riffle-pool sequences. The entire set of photographs can be found in Appendix C.

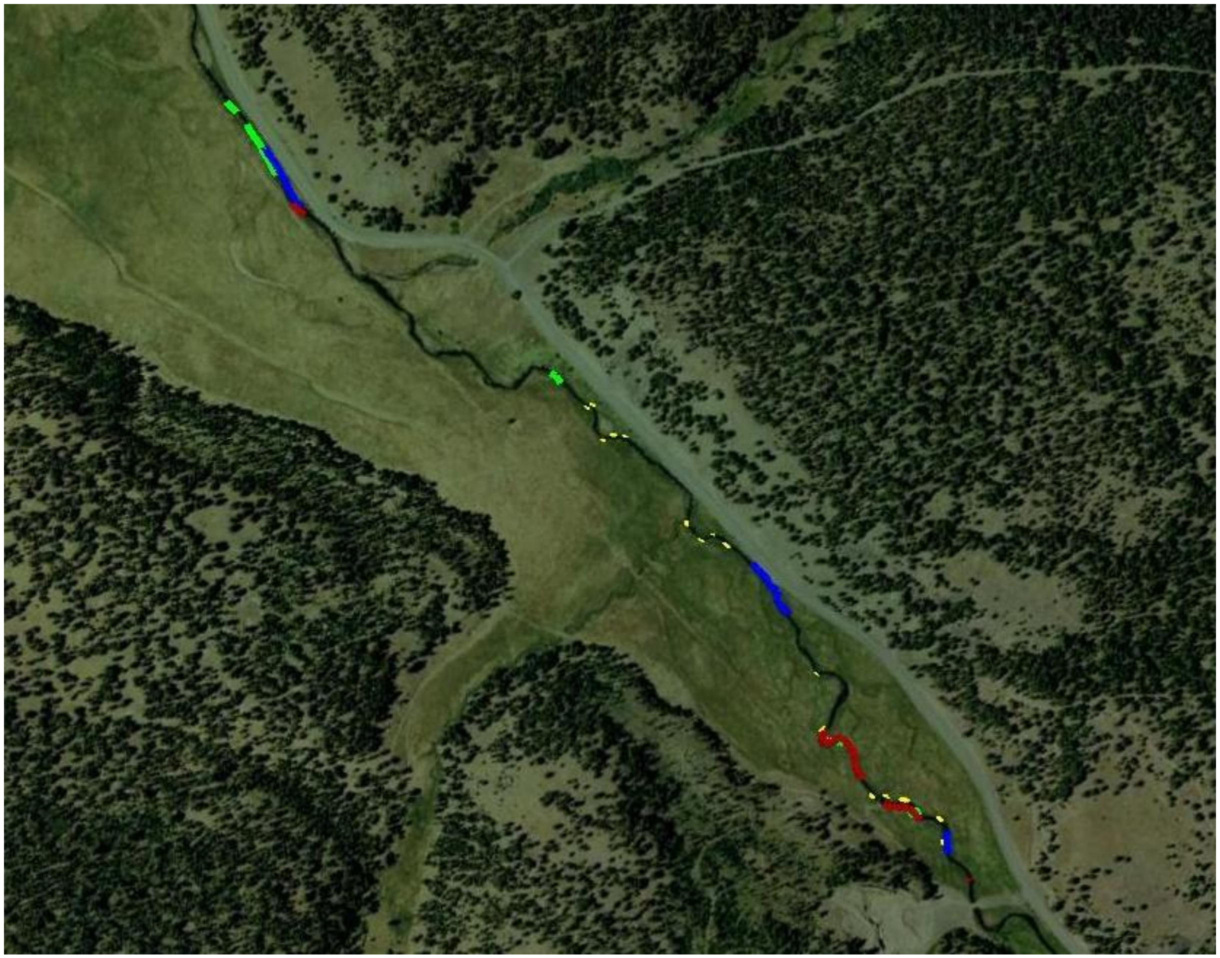

Figure 3.7 Google Earth image of the study site with the ELJs (yellow), the pre-restoration groundwater locations (blue) and the post-restoration groundwater locations (red) and hyporheic locations (green) (*Google Earth*, n.d.).

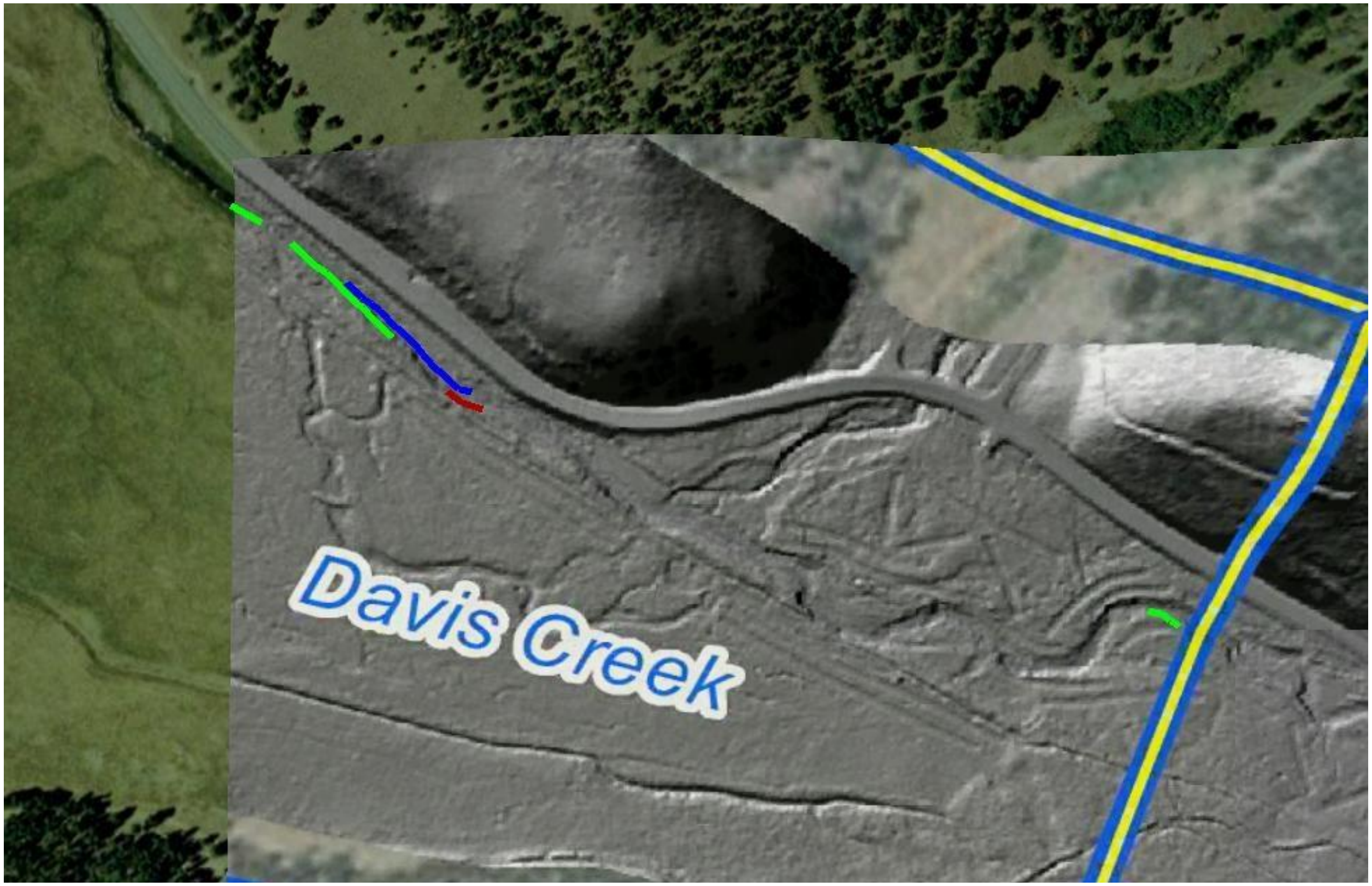

Figure 3.8 Google Earth image with the LiDAR data overlaid on the downstream half of the site. The pre-restoration groundwater locations (blue) and the post-restoration groundwater locations (red) and hyporheic locations (green) are highlighted (*Google Earth*, n.d.).

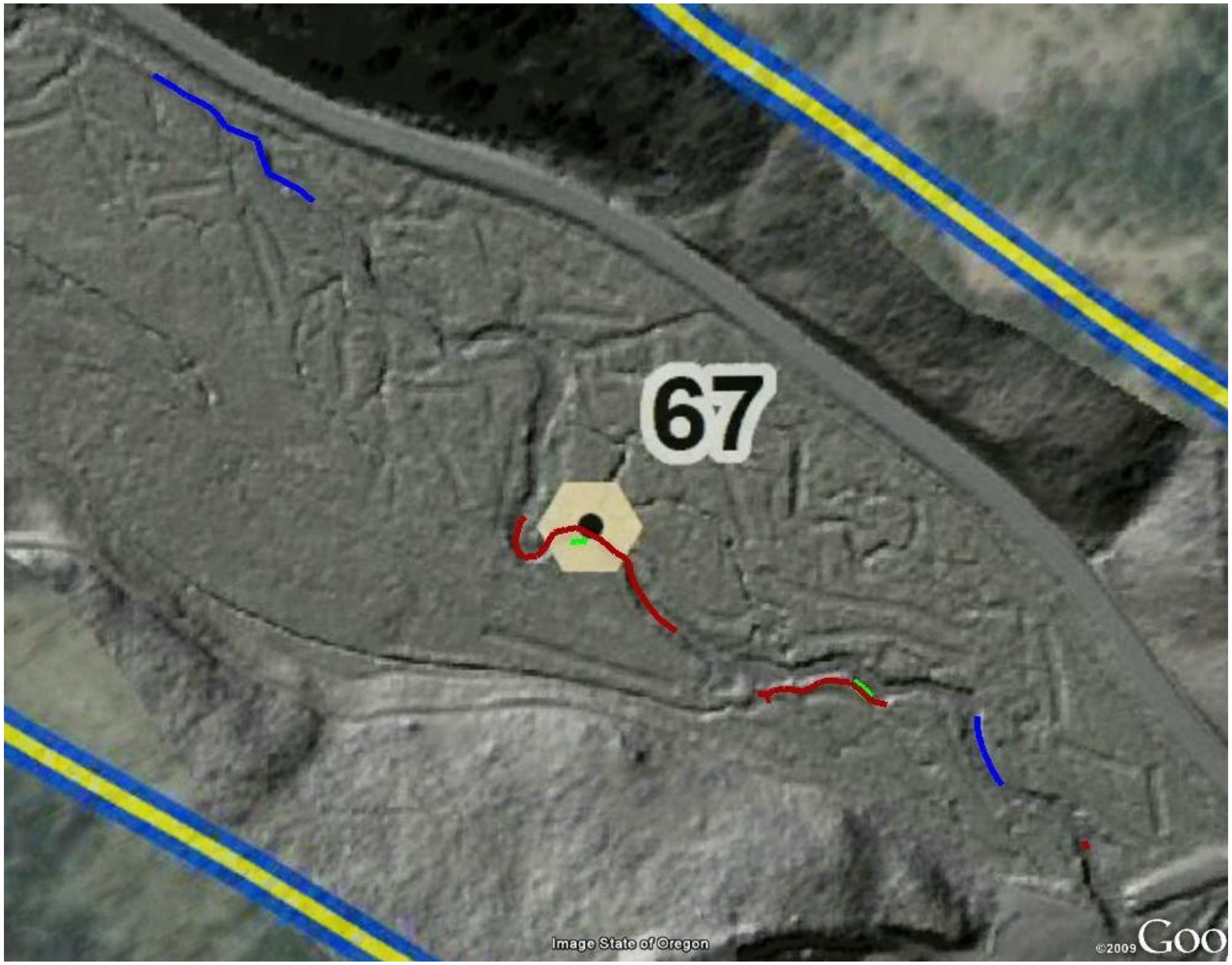

Figure 3.9 Google Earth image with the LiDAR data overlaid on the upstream half of the site. The pre-restoration groundwater locations (blue) and the post-restoration groundwater locations (red) and hyporheic locations (green) are highlighted (*Google Earth*, n.d.).

Figure 3.10 The location of a hyporheic discharge from post-restoration analysis, river meters 1086-1105. The meter on the whiteboard corresponds to the cable meter, not the river meter.

Groundwater Inflow Quantification

To determine how much groundwater inflow is occurring at each site, mass and energy conservation equations are used (see equations 3.3 and 3.4). The upstream flow and temperature as well as the groundwater and downstream temperature are needed to calculate the groundwater flow. The groundwater temperature is assumed to be constant at 6 °C, the mean annual air temperature. The upstream and downstream temperatures are taken from the DTS data described above. The upstream flow is calculated in Chapter 2: Field Measurements and Instrumentation for both pre-and post- restoration. The flow is not constant with time during the pre-restoration period. Therefore, the flow at the upstream boundary is linearly interpolated for the 10 days of groundwater analysis and the results can be found in Table 3.12. The flow is considered to be constant with time for the post-restoration study period with a flow of 0.340 m^3/s at the upstream boundary. For both the pre- and post-restoration analysis the flow increases downstream due to the two tributaries and the cumulative effect of the groundwater inflows. The flows used to calculate the groundwater inflows will incorporate both the tributaries and the upstream groundwater inflows.

At every groundwater inflow location, the flow is calculated for each Hot and Cold period for all analysis days. An example calculation of equation (3.5) for the groundwater inflow at river meters 219-220 of the Cold profile of river left post-restoration Day 1 is:

$$Q_g = 0.327\ m^3/s\left(\frac{11.284℃ - 11.236℃}{11.236℃ - 6.00℃}\right) = 0.003 m^3/s \tag{3.6}$$

For pre-restoration, the 20 flows are then averaged and this averaged flow is the calculated groundwater inflow for each respective location. The post-restoration analysis uses only 6 days, therefore there are only 12 flows that are averaged for each groundwater inflow. The total flow added to the study site from groundwater was calculated as 0.004 m^3/s (0.14 cfs) for pre-restoration and 0.012 m^3/s (0.41 cfs) for post-restoration this equates to 1% and 4% of stream flow, respectively. Although it appears that groundwater increases with stream flow this could be an artifact of groundwater temperature signals being muted by high stream flows. The results can be seen in Table 3.13, with the Matlab script and variables found in Appendix A.

Table 3.12 Pre-restoration flows (m^3/s) for the upstream boundary of the Forrest Property used to calculate groundwater inflows.

Date	Flow (m^3/s)
6/25	0.96
6/26	0.93
6/27	0.90
6/28	0.87
6/29	0.84
6/30	0.81
7/1	0.78
7/2	0.74
7/3	0.71
7/4	0.68

Table 3.13 The quantity of groundwater entering the stream at each location for pre- and post-restoration.

Pre - Restoration						Post-Restoration					
River Left			River Right			River Left			River Right		
Areas of GW inflow (m)	Average Flow (m^3/s)	standard deviation	Areas of GW inflow (m)	Average Flow (m^3/s)	standard deviation	Areas of GW inflow (m)	Average Flow (m^3/s)	standard deviation	Areas of GW inflow (m)	Average Flow (m^3/s)	standard deviation
-	-	-	85-114	0.002	0.001	32-35	0.0002	0.001	272-371	0.002	0.003
-	-	-	588-667	0.002	0.002	146-235	0.005	0.006	-	-	-
-	-	-	-	-	-	219-220	0.004	0.005	-	-	-
-	-	-	-	-	-	1585-1604	0.0003	0.001	-	-	-

Discussion

River temperature is an important component of a healthy salmonid habitat and unfortunately many Oregon Rivers are above Total Maximum Daily Load (TMDL) levels (Brett, 1952; US EPA, 2006). The surface water cooling is controlled by shading from riparian vegetation, evaporative cooling, groundwater inflows and hyporheic exchange. Groundwater inflows and hyporheic exchange are the only two processes that create pockets of cool thermal refugia, an important characteristic for salmonid survival during peak summer temperatures (Torgersen et al., 1999). Restoration of the Forrest property consisted of the addition of ELJs primarily for juvenile salmonid protection from predators and high flows. The objective of this study is to see if the ELJs also created cool thermal refugia through analysis of the DTS temperature profile and determine what cooling processes can be identified with the DTS.

The only temperature signal that can be associated with the restoration effort is the groundwater inflow located at river meter 219-220. This cool thermal refuge is located in the scour pool of the ELJ that was installed during restoration. The other groundwater inflow and hyporheic discharge locations of post-restoration also occur at ELJs but cannot be directly attributed to ELJs like river meter 219-220. The work of Torgerson et al. (1999) has shown that the upper MFJD has many thermal refugia and heterogeneity but the DTS profiles do not support this conclusion. Unfortunately, during the study, the DTS was not running properly which resulted in higher measurement noise than usual. This increase in noise can lead to unidentified locations of cool thermal refugia. This could be the cause for conflicting conclusions between Torgerson et al. (1999) and our study. Other factors that could cause variability in temperature between pre- and post-restoration analysis are flow, tributary temperature and water table levels. Even with increased measurement noise, the DTS was able to detect groundwater and hyporheic locations within the Forrest property for pre- and post-restoration. Groundwater and hyporheic exchange created cool thermal refugia that collectively had a temperature 0.1°C and 1.2°C cooler than the main channel for pre-restoration by for post-restoration.

The current literature is inconclusive as to whether groundwater interactions change with discharge. Some studies have shown there is no change in hyporheic exchange from both low baseflow to high baseflow (Wondzell, 2006) and low baseflow to high flow (Hanrahan, 2008). Other studies state the hyporheic zone decreases with increasing flow (Legrand-Marcq and Laudelout, 1985) while the work of Morrice et al. (1997) exhibits increasing hyporheic with increasing discharge. A change in discharge effects not only hyporheic exchange but groundwater inflows. The detailed work of Käser et al. (2009) relates the water table and an increase with discharge to the quantity of groundwater inflow received by the river. The study demonstrates how groundwater inflow can both increase and decrease during higher discharge. The results of the groundwater inflow suggest that in our study site, groundwater inflow decreases with increasing discharge. Though seen in these data, any extension of this observation would be speculation and beyond the scope of the study. A separate study would be needed to describe the exact relationship between subsurface flow and surface flow.

Although it is difficult to draw strong conclusions on the restoration efforts due to variability in measurement noise, the DTS still gives an interesting perspective of the river. The groundwater inflows within the Forrest reach have very distinct characteristics. The inflow is occurring either in a few meters or over tens of meters, demonstrating direct or diffuse groundwater inflow. Thermal refugia are more likely to occur from direct groundwater inflow because the temperature difference is concentrated in a smaller area than diffuse groundwater inflow.

The LiDAR data give important insight into the signal locations near the downstream boundary. The confluence of a distinct historic channel can be seen in the LiDAR data and is located where the lower four signals are. An historic channel is a common path for groundwater inflow and hyporheic exchange because of the increased porosity and hydraulic conductivity of the material (Stanford and Ward, 1993). Therefore, the lower four groundwater and hyporheic locations are thought to be a result of the historic channel.

Our study shows that DTS can be a useful design tool for river restoration. With knowledge of direct and diffuse groundwater locations, scour pools and log structures can be placed appropriately to create cool thermal refugia. Structures can be placed with knowledge of thermal characteristics and not just flow characteristics.

In addition, the DTS can identify locations of hyporheic exchange ensuring that these locations are not disturbed with restoration activities.

Chapter 4: Conclusions

Conclusions

River temperatures were measured using DTS technology for pre- and post-restoration monitoring on the Middle Fork of the John Day River (MFJD). The river restoration consisted of removing existing rock barbs, installing engineered log jams (ELJs) and excavating scour pools in the upstream half of the study site. The main objective of the restoration was to improve habitat for juvenile salmonids; consequently, CTWS was interested to see how water temperature was affected by the restoration efforts. The physical conditions during pre- and post-restoration sampling were quite different. Pre-restoration measurements were taken in early summer when the snow had just finished melting on the surrounding mountains and the flows of both the MFJD and tributaries were still considerably high. During this time period we also experienced a heat wave driving air temperatures up to 33°C. Post-restoration measurements were taken during typical low flow conditions of late summer. The last few days of the post-restoration were considerably colder with a maximum air temperature of only 20°C. Due to such differing flow conditions of the pre- and post-restoration periods and the hypothesis that reach-scale temperatures would not be affected by restoration efforts, post-restoration conditions were used to calibrate a modified Westhoff stream temperature model. Therefore, it is inconclusive with respect to our modeling results as to whether a change in overall temperature occurred due to restoration efforts. However, the average depth of hyporheic exchange needed to close the energy budget of the calibrated model was calculated for pre- and post-restoration periods. These depths are an indication of the extent to which peak temperatures have been decreased due to hyporheic exchange.

While we were unable to determine whether pre- and post-treatment reach-wide stream temperatures differed, statistical analysis of the DTS temperature profiles allowed us to identify areas of groundwater inflow and hyporheic discharge. The temperature signal associated with groundwater, a cooler maximum, minimum and mean temperature, was utilized to determine location and lengths of both direct and diffuse groundwater inflow. The hyporheic discharge signal, a cooler maximum and warmer minimum, was used to determine location and lengths of hyporheic discharge. Three of the new groundwater inflow locations (those observed only during post-restoration sampling) contain ELJs. Of the three, only one is a direct groundwater inflow within the length of the ELJ. This cool thermal refuge is, clearly, a result of the restoration efforts.

The findings of Chapter 2 and 3 complement each other. Chapter 2 and 3 calculate the majority of hyporheic exchange occurring in the upstream half of the study site. Further analysis and field testing must be carried out to see if the locations match up at a finer scale.

Through our study we have found the data to be inconclusive of a reach-scale temperature change due to installation of ELJs. However, our analysis confirms the increase of localized thermal refugia within the study site due to the placement of the

ELJs and the excavation of scour pools. Thermal refugia are important habitat characteristics for the survival of salmonids during peak temperatures and an increase in locations of thermal refugia is one indication of a successful restoration effort. We have been able to pin-point locations of thermal refugia outside of the restoration segment and this data can be used by the CTWS and the Bureau of Reclamation for future restoration design.

We encountered many problems associated with fiber optics and DTS during installation and data analysis. The main predicament of our study was the poor performance of the Agilent DTS resulting in low accuracy of the temperature data. The Agilent was manufactured in 2006 which is at the start of DTS technology in the ecological field and therefore was not fully developed for our specific needs. Since 2006, DTS technology has been steadily improving creating greater accuracy and precision while producing finer resolution data. For example, Ultima DTS, a DTS expected to be released in 2010 by the Silixia Corporation, will have a resolution of 0.02°C with a ten minute sample time. In addition, another DTS manufacturer, Sensornet, has produced the Oryx DTS that continually calibrates the temperature data removing the need for the tedious calibration procedure experienced in our data. As DTS technology improves, we will be able to locate areas of groundwater interaction at a much finer scale. With this new knowledge, our understanding of river reaches and restoration effects will be greatly advanced.

References

Allen, D., Dietrich, W., Baker, P., Ligon, F., & Orr, B. (2007). Development of a mechanistically based, basin-scale stream temperature model: applications to cumulative effects modeling. *USDA Forest Service Gen. Tech. Rep. PSW-GTR-194*, 11-24.

Anderson, M. P. (2005). Heat as a ground water tracer. *Ground Water*, *43*(6), 951-968.

Arrigoni, A. S., Poole, G. C., Mertes, L. A., O'Daniel, S. J., Woessner, W. W., & Thomas, S. A. (2008). Buffered, lagged, or cooled? Disentangling hyporheic influences on temperature cycles in stream channels. *Water Resources Research*, *44*(9), W09418.

Bartholow, J. (1999). SSTEMP for windows: the stream segment temperature model (Version 1.1.3). *US Geological Survey*, *29*. Retrieved from http://www.mesc.usgs.gov/rsm/rsm_download.html#TEMP

Baxter, C., Hauer, F. R., & Woessner, W. W. (2003). Measuring Groundwater–Stream Water Exchange: New Techniques for Installing Minipiezometers and Estimating Hydraulic Conductivity. *Transactions of the American Fisheries Society*, *132*(3), 493-502.

Bencala, K. E. (2005). Hyporheic exchange flows. *Encyclopedia of Hydrological Sciences*, *3*(Part 10), 1733–1740.

Bencala, K. E., & Walters, R. A. (1983). Simulation of Solute Transport in a Mountain Pool-and-Riffle Stream: A Transient Storage Model. *Water Resources Research*, *19*(3), 718-724.

Bernhardt, E. S., Palmer, M. A., Allan, J. D., Alexander, G., Barnas, K., Brooks, S., et al. (2005). *ECOLOGY: Synthesizing US River Restoration Efforts* (Vol. 308).

Beschta, R. L., & Ripple, W. J. (2005). Rapid assessment of riparian cottonwood recruitment: Middle Fork John Day River, Northeastern Oregon. *Ecological Restoration*, *23*(3), 150-156.

Boyd, M., & Kasper, B. (2004). Analytical methods for dynamic open channel heat and mass transfer: methodology for Heat Source Model Version 7.0. Retrieved from http://www.deq.state.or.us/WQ/TMDLs/tools.htm

Brett, J. R. (1952). Temperature tolerance in young Pacific salmon, genus Oncorhynchus. *Journal of the Fisheries Research Board of Canada*, *9*(6), 265–323.

Brett, J. R. (1956). Some principles in the thermal requirements of fishes. *The Quarterly Review of Biology*, *31*(2), 75-87.

Caissie, D. (2006). The thermal regime of rivers: a review. *Freshwater Biology*, *51*(8), 1389–1406.

Collier, M. W. (2008). *Demonstration of fiber optic distributed temperature sensing to differentiate cold water refuge between ground water inflows and hyporheic exchange* (MA Thesis). Oregon State University. Retrieved from Google Scholar.

Conant, B. (2004). Delineating and quantifying ground water discharge zones using streambed temperatures. *Ground Water*, *42*(2), 243-257.

Cox, M., & Bolte, J. (2007). A spatially explicit network-based model for estimating stream temperature distribution. *Environmental Modelling & Software*, *22*(4), 502-514. doi: 10.1016/j.envsoft.2006.02.011

Crispell, J. K., Endreny, T. A., & Foundation, E. B. (2009). Hyporheic exchange flow around constructed in-channel structures and implications for restoration design. *Hydrological Processes*, *23*(8), 1158–1168.

Evans, E. C., McGregor, G. R., & Petts, G. E. (1998). River energy budgets with special reference to river bed processes. *Hydrological Processes*, *12*(4), 575-595.

Fernald, A. G., Landers, D. H., & Wigington Jr, P. J. (2006). Water quality changes in hyporheic flow paths between a large gravel bed river and off-channel alcoves in Oregon, USA. *River Research and Applications*, *22*(10), 1111–1124.

Fernald, A. G., Wigington, P. J., & Landers, D. H. (2001). Transient storage and hyporheic flow along the Willamette River, Oregon: Field measurements and model estimates. *Water Resources Research*, *37*(6), 1681-1694.

Findlay, S. (1995). Importance of surface-subsurface exchange in stream ecosystems: The hyporheic zone. *Limnology and Oceanography*, *40*(1), 159-164.

Google Earth. (n.d.). . Google.

Gooseff, M. N., Anderson, J. K., Wondzell, S. M., LaNier, J., & Haggerty, R. (2006). A modelling study of hyporheic exchange pattern and the sequence, size, and spacing of stream bedforms in mountain stream networks, Oregon, USA. *Hydrological Processes*, *20*(11), 2443–2457.

Gooseff, M. N., Wondzell, S. M., Haggerty, R., & Anderson, J. (2003). Comparing transient storage modeling and residence time distribution (RTD) analysis in geomorphically varied reaches in the Lookout Creek basin, Oregon, USA. *Advances in Water Resources*, *26*(9), 925-937.

Hanrahan, T. P. (2008). Effects of river discharge on hyporheic exchange flows in salmon spawning areas of a large gravel-bed river. *Hydrological Processes, 22*(1), 127-141. doi: 10.1002/hyp.6605

Harvey, J. W., & Wagner, B. J. (2000). Quantifying hydrologic interactions between streams and their subsurface hyporheic zones. *Streams and Ground Waters*, 3–44.

Hester, E. T., Doyle, M. W., & Poole, G. C. (2009). The influence of in-stream structures on summer water temperatures via induced hyporheic exchange. *Limnology and Oceanography*, *54*(1), 355–367.

Hester, E. T., & Doyle, M. W. (2008). In-stream geomorphic structures as drivers of hyporheic exchange. Retrieved from http://www.agu.org.proxy.library.oregonstate.edu/pubs/crossref/2008/2006WR005810.shtml

Hypothesis Test Assumptions. (2009). *The MathWorks*. Retrieved September 16, 2009, from http://www.mathworks.com/access/helpdesk/help/toolbox/stats/f13914.html

Independent Scientific Advisory Board. (2003). A review of strategies for recovering tributary habitat. *Northwest Power and Conservation Council. ISAB, 2.*

Johnson, S. L. (2003). Stream temperature: scaling of observations and issues for modelling. *Hydrological Processes*, *17*(2), 497–499.

Kasahara, T., & Hill, A. R. (2008). Modeling the effects of lowland stream restoration projects on stream–subsurface water exchange. *Ecological Engineering*, *32*(4), 310-319.

Kobayashi, D. (1985). Separation of the snowmelt hydrograph by stream temperatures. *Journal of Hydrology*, *76*, 155-165.

Kulongoski, J. T., & Izbicki, J. A. (2008). Simulation of fluid, heat transport to estimate desert stream infiltration. *Ground Water*, *46*(3), 462-474.

Lacey, R. W., & Millar, R. G. (2004). Reach scalye hydraulic assessment of instream salmonid habitat restoration. *Journal of the American Water Resources Association*, *40*(6), 1631–1644.

Legrand-Marcq, C., & Laudelout, H. (1985). Longitudinal dispersion in a forest stream. *Journal of Hydrology*, *78*(3-4), 317-324. doi: 10.1016/0022-1694(85)90109-X

Loheide II, S. P., & Gorelick, S. M. (2006). Quantifying stream-aquifer interactions through the analysis of remotely sensed thermographic profiles and in situ temperature histories. *Environ. Sci. Technol, 40,* 3336-3341.

Lowry, C. S., Walker, J. F., Hunt, R. J., & Anderson, M. P. (2007). Identifying spatial/variability of groundwater discharge in a wetland stream using a distributed temperature sensor. *Water Resources Research, 43*(10), 10408.

McCullough, D. A. (1999). *A review and synthesis of effects of alterations to the water temperature regime on freshwater life stages of salmonids, with special reference to chinook salmon* (Project Report). Seattle, WA: U.S. Environmental Protection Agency.

McDonald, L. L., Bilby, R., Bisson, P. A., Coutant, C. C., Epifanio, J. M., Goodman, D., et al. (2007). Research, monitoring, and evaluation of fish and wildlife restoration projects in the Columbia River Basin: lessons learned and suggestions for large-scale monitoring programs. *Fisheries*, *32*(12), 582–590.

Morrice, J., Valett, H., Dahm, C., & Cam, M. (1997). Alluvial Characteristics, Groundwater-Surface Water Exchange and Hydrological Retention in Headwater Streams. *Hydrological Processes*, *11*(3), 253-267. doi: 10.1002/(SICI)1099-1085(19970315)11:3<253::AID-HYP439>3.0.CO;2-J

Neilson, B. T., Stevens, D. K., Chapra, S. C., & Bandaragoda, C. (2009). Data collection methodology for dynamic temperature model testing and corroboration. *Hydrological Processes*, *23*(20).

NOAA. (2009). Pacific Coastal Salmon Recovery Fund Data Website. *Pacific Coastal Salmon Recovery Fund*. Retrieved from http://webapps.nwfsc.noaa.gov/portal/page?_pageid=34,1&_dad=portal&_schema=PORTAL

Pacific Northwest Aquatic Monitoring Partnership. (2005, April 5). Establishing a network of intensively monitored watersheds in the Pacific Northwest.

Palmer, M. A., Bernhardt, E. S., Allan, J. D., Lake, P. S., Alexander, G., Brooks, S., et al. (2005). Standards for ecologically successful river restoration. *Journal of Applied Ecology*, *42*(2), 208-217. doi: 10.1111/j.1365-2664.2005.01004.x

Poole, G. C., O'Daniel, S. J., Jones, K. L., Woessner, W. W., Bernhardt, E. S., Helton, A. M., et al. (2008). Hydrologic spiralling: the role of multiple interactive flow paths in stream ecosystems. *Regulated Rivers: Research & Management*, *24*(7), 1018–1031.

Poole, G. C., & Berman, C. H. (2001). An ecological perspective on in-stream temperature: natural heat dynamics and mechanisms of human-caused thermal degradation. *Enviromental Management*, *27*(6), 787-802.

Roth, T. R., Selker, J. S., Westhoff, M. C., Gabrielli, J., Huwald, H., & Parlange, M. (2008). Small scale stream restoration simulation and response on stream temperature using a physically based temperature model. In *2008 Joint Meeting of The Geological Society of America*.

Roth, T., Westhoff, M., Huwald, H., Huff, J., Rubin, J., Barrenetxea, G., et al. (2010). Stream Temperature Response to Three Riparian Vegetation Scenarios Using a Distributed Temperature Validated Model. *Environ. Sci. and Tech.*

Runkel, R. L. (1998). One-dimensional transport with inflow and storage (OTIS): a solute transport model for streams and rivers. *US Geological Survey Water-Resources Investigation Report*, *98*, 4018.

Runkel, R. L., McKnight, D. M., & Rajaram, H. (2003). Modeling hyporheic zone processes. *Advances in Water Resources*, *26*(9), 901-905.

Selker, J., van de Giesen, N., Westhoff, M., Luxemburg, W., & Parlange, M. B. (2006). Fiber optics opens window on stream dynamics. *Geophys. Res. Lett*, *33*(24), 24401.

Selker, J. S., Selker, J., Gabrielli, J., Gregory, C., Saydec, C., Tufillaro, N., et al. (2008). Taking the temperature of ecological systems with fiber optics. *Eos Trans. AGU*, *89*(20), 187.

Selker, J. S., Thévenaz, L., Huwald, H., Mallet, A., Luxemburg, W., Van de Giesen, N., et al. (2006). Distributed fiber-optic temperature sensing for hydrologic systems. *Water Resour. Res*, *42*, W12202.

Silliman, S. E., & Booth, D. F. (1993). Analysis of time-series measurements of sediment temperature for identification of gaining vs. losing portions of Juday Creek, Indiana. *Journal of Hydrology*, *146*, 131-148. doi: 10.1016/0022-1694(93)90273-C

Sinokrot, B. A., & Stefan, H. G. (1993). Stream temperature dynamics: measurements and modeling. *Water Resources Research*, *29*(7), 2299-2312.

Smith, C. (1998). Pacific Northwest Salmon History Snapshots. Retrieved October 19, 2009, from http://oregonstate.edu/instruct/anth481/fish.html

Stanford, J. A., & Ward, J. V. (1993). An ecosystem perspective of alluvial rivers: connectivity and the hyporheic corridor. *Journal of the North American Benthological Society*, 48–60.

Taylor, S. B. (2007). Watershed assessment, river restoration, and the geoscience profession in Oregon. *Oregon Geology, 68*(1), 27.

Torgersen, C. E., Faux, R. N., McIntosh, B. A., Poage, N. J., & Norton, D. J. (2001). Airborne thermal remote sensing for water temperature assessment in rivers and streams. *Remote Sensing of Environment*, *76*(3), 386-398.

Torgersen, C. E., Price, D. M., Li, H. W., & McIntosh, B. A. (1999). Multiscale thermal refugia and stream habitat associations of Chinook salmon in Northeastern Oregon. *Ecological Applications*, *9*(1), 301-319.

Tufillaro, N., Dorighi, J., Collier, M., & Selker, J. (2008). Measuring Stream Dynamics with Fiber Optics. In *American Physical Society, 10th Annual Meeting of the Northwest Section of APS, May 15-17, 2008, abstract# G3. 001*.

Turo, S. (2009, February). *Habitat Restoration within the Ceded lands of The Confederated Tribes of the Warm Springs Reservation of Oregon*. Presented at the River Restoration NW, Power Point, Skamania Lodge, WA.

Tyler, S. W., Selker, J. S., Hausner, M. B., Hatch, C. E., Torgersen, T., Thodal, C. E., et al. (2009). Environmental temperature sensing using Raman spectra DTS fiber-optic methods. *Water Resources Research*, *45*(null).

US EPA. (2006). 2006 Section 303(d) List Fact Sheet for OREGON | WATERS | US EPA. Retrieved July 1, 2009, from http://oaspub.epa.gov/tmdl/state_rept.control?p_state=OR&p_cycle=2006

Westhoff, M. C., Savenije, H. H. G., Luxemburg, W. M. J., Stelling, G. S., van de Giesen, N. C., Selker, J. S., et al. (2007). A distributed stream temperature model using high resolution temperature observations. *Hydrology and Earth System Sciences*, *11*(4), 1469.

Wohl, E., Angermeier, P. L., Bledsoe, B., Kondolf, G. M., MacDonnell, L., Merritt, D. M., et al. (2005). River restoration. *Water Resources Research*, *41*(10), W10301.

Wondzell, S. M. (2006). Effect of morphology and discharge on hyporheic exchange flows in two small streams in the Cascade Mountains of Oregon, USA. *Hydrological Processes*, *20*(2), 267–287.

Wondzell, S. M., Gooseff, M. N., & McGlynn, B. L. (2007). Flow velocity and the hydrologic behavior of streams during baseflow. *Geophysical Research Letters*, *34*(24), L24404.

Wondzell, S. M., & Swanson, F. J. (1996). Seasonal and Storm Dynamics of the Hyporheic Zone of a 4th-Order Mountain Stream. II: Nitrogen Cycling. *Journal of the North American Benthological Society*, *15*(1), 20-34.

Appendix A

See electronic Appendix

Appendix B

See electronic Appendix

Appendix C

See electronic Appendix